ANTENNA DESIGN AND CHARACTERIZATION FOR MINIATURE WIRELESS OBJECTS

Fabien Ferrero

HABILITATION A DIRIGER LES RECHERCHES

UNIVERSITE DE NICE SOPHIA ANTIPOLIS

ECOLE DOCTORALE STIC

Spécialité : Electronique
Section 63 : Génie électrique, électronique, photonique et systèmes

ANTENNA DESIGN AND CHARACTERIZATION FOR MINIATURE WIRELESS OBJECTS

Présentée et soutenue publiquement par

Fabien Ferrero

A Sophia-Antipolis, le 3 Mai 2016

JURY

Lars Jonsson, Professeur, KTH Royal Institute of Technology	Président
Dominique Baillargeat, Professor, Université de Limoges	Rapporteur
Christophe Delaveaud, Expert Senior au CEA, CEA Leti	Rapporteur
Ronan Sauleau, Professeur, Université de Rennes	Rapporteur
Jean-Yves Dauvignac, Professeur, Université de Nice-Sophia Antipolis	Examinateur
Luc Deneire, Professeur, Université Nice-Sophia Antipolis	Examinateur
Cyril Luxey, Professeur, Université Nice-Sophia Antipolis	Examinateur
Robert Staraj, Professeur, Université Nice-Sophia Antipolis	Examinateur
Philippe Ratajzak, Ingénieur, Orange Labs, La Turbie	Invité

ANTENNA DESIGN AND CHARACTERIZATION FOR MINIATURE WIRELESS OBJECTS

Première partie : Notice HDR

Deuxième partie : Mémoire HDR / HDR Manuscript

PREMIERE PARTIE : NOTICE HDR CURRICULUM VITAE DETAILLE

Nom patronymique : **FERRERO**
Prénom(s) : **Fabien**
Date et lieu de naissance : 29/04/80 à Nice
Nationalité : Française
Situation de famille : Marié, 3 enfants
Situation actuelle: Maître de Conférences 4ème échelon
(Recruté en Octobre 2010)

Adresse Personnelle :

220, chemin des contrebandiers
06160 Juan-les-pins

Unité d'enseignement	**Unité de recherche**
Polytech'Nice-Sophia Département Electronique 930 Route des Colles - 06902 Sophia E-mail : fabien.ferrero@unice.fr	Laboratoire d'Electronique, Antennes et Télécommunications UMR CNRS 6071 930 Route des Colles - 06902 Sophia Téléphone : 04-92-94-28-29

I. Diplômes et Titres universitaires:

2003 - 2007 : Thèse de doctorat en Électronique, - LEAT

Soutenue le 19 Novembre 2007 au LEAT

Directeur de thèse : Pr Gilles JACQUEMOD

Responsables de thèse : Pr Vincent FUSCO, Pr Robert STARAJ ,et Mr Cyril LUXEY

Mention : Très Honorable

2002 - 2003 : D.E.A Propagation, Télédétection et Télécommunication,
Université de Nice-Sophia Antipolis
Mention : Bien

1998 - 2003 : **Diplôme d'ingénieur** Polytech' Nice-Sophia Antipolis (ex ESINSA),
Université de Nice-Sophia Antipolis
Option : Microelectronique

1997 - 1998 : Baccalauréat Scientifique, Lycée Massena (Nice)
Option : Physique - Chimie
Mention : Bien

II. Activités post-thèse

2010 – 2016 : **Maître de Conférences à l'Université de Nice Sophia**
Enseignement à Polytech'Nice Sophia, Département Electronique
Recherche au Laboratoire d'Electronique, Antenne et Télécommunication

2009 – 2010 : **Post Doctorat**: Projet ANR NAOMI

"Conception d'antennes reconfigurables pour récepteurs DVB-H"

2008 – 2009 : Ingénieur de recherche: IMRA Europe SAS

"Conception d'antennes multi-applications pour l'automobile"

2007 – 2008 : **ATER** 63ème section : Polytech' Nice-Sophia Antipolis (192h TD)
Niveaux : 1ère et 2ème année d'école d'ingénieur, cycle préparatoire

III. Thèses encadrées

	Directeur de thèse	**Taux d'encadrement**	**Date de soutenance**
Florian Canneva	R. Staraj (LEAT)	30%	8 Juin 2012
Diane Titz	C. Luxey(EpOC)	30%	20 Septembre 2012
Oumy Diop	C. Luxey (EpOC)	30%	27 Septembre 2013
Marcio Silva Pimenta	J-M. Ribero (LEAT)	30%	14 Novembre 2013
Aykut Cihanghir	C. Luxey (EpOC)	50%	6 Mars 2014
L-H. Trinh	J-M. Ribero (LEAT)	30%	15 Juillet 2015
C. Buey	F. Ferrero (LEAT)	50%	Prévue 2017

IV. Stages Ingénieurs/MASTER encadrées

	Stage	**Taux d'encadrement**	**Date de soutenance**
Madiha El Khattab	Master TRFM	100%	Septembre 2010
Pauline Bouzat	Ingénieur Polytech'Nice Sophia	100%	Octobre 2011
L-H. Trinh	Ingénieur Polytech'Nice Sophia	50%	Septembre 2012
Aimeric Bisognin	Ingénieur Polytech'Nice Sophia	100%	Septembre 2012
Aiouaj Allal	ESEO Angers	50%	Septembre 2013

Cyril Buey	Master 2 MiNT Université de Lille	50%	Septembre 2014
Ouachicha Zayd	Ingénieur Polytech'Nice Sophia	100%	Septembre 2015

V. Distinctions scientifiques

- **LAPC 2012: Best paper prize: First place :**

Diane Titz; Bisognin Aimeric; Fabien Ferrero; Cyril Luxey; Gilles Jacquemod; Claire Laporte; Hilal Ezzeddine; Mario Valente; Patrice Brachat, "60 GHz Patch Antenna Using IPD Technology", LAPC, Loughborough, Nov 2012.

- **LAPC 2013: Best student paper prize : Third place :**

Aykut Cihangir; Fabien Ferrero; Cyril Luxey; Gilles Jacquemod; Emmanuel Larique; Renaud Robin; Patrice Brachat, "**Tunable Antennas Using MEMS Switches for LTE Mobile Terminals".**

- **IEEE APS Design Student contest 2013 : Semi-finalist :**

Trinh Le Huy, Ollivier Loys, Garret, Alexandre, Belleguie Loic and Fabien Ferrero, "**The Lighthouse on Wheel Antenna**"

- **ISSCC 2013 Jack Kilby Award for Outstanding Student Paper**

Jiashu Chen, Lu Ye, D. Titz, F. Gianesello, R. Pilard, A. Cathelin, F. Ferrero, C. Luxey, A. Niknejad, "**A digitally modulated mm-Wave cartesian beamforming transmitter with quadrature spatial combining**,

VI. Production scientifique

Revues internationales avec comité de lecture	49
Papiers invités dans conférences internationales	14
Conférences internationales	64
Conférences nationales	23
Conférence d'ordre pédagogique	4
Journal d'ordre pédagogique	1
Brevet	3

VII. Activités d'animation de la recherche

- Co-directeur du CREMANT (laboratoire commun Orange-Université de Nice-Sophia et CNRS) pour le volet 2012-2016,
- General Chaiman eSAME 2015 (http://www.esame-conference.org/)
- Co-Organisateur du University Booth pour la conférence annuelle SAME 2010-2012, puis Organisateur du University Booth pour SAME 2013 & 2014 ,
- Co-Organisateur de session spéciale à la conférence Eucap 2012, 2015 et 2016,
- Co-Organisateur de session spéciale à la conférence IEEE CAMA 2014

VIII. Activités d'Expertise

- **Reviewer pour les revues internationales** *IEEE Antennas and Propagation, IEEE Microwave Techniques Transaction, IEEE Antennas and Wireless Propagation Letters*

- **Reviewer pour les conférences internationales :** LAPC, Eucap, EuMW
- **Technical Program Chair (TPC) member** pour la conférence EUCAP 2015
- **Membre du jury de 7 thèses Françaises :** F. Canneva-2012, D. Titz-2013, O. Diop-2013, M. Silva Pimenta-2013, A. Cihanghir-2013, I. Dioum-2013, L.H. Trinh-2015.
- **Chairman de session** dans différents congrès internationaux IEEE APS 2013, Eucap 2013-2015, CAMA 2014.
- **Expert pour l'ANRT** pour une thèse CIFRE en 2014 et 2015

IX. Synthèse des enseignements

Année	**Fonction**	**Lieu**	**Volume annuel moyen**
2003-2006	Moniteur	Polytech‟Nice-Sophia	64 h EqTD
2006-2007	½ ATER	Polytech‟Nice-Sophia	96 h EqTD
2007-2008	ATER	Polytech‟Nice-Sophia	192 h EqTD
2000-2010	Post Doctorant - Vacataire	Polytech‟Nice-Sophia	32 h EqTD
2010-2011	Maître de Conférences	Polytech‟Nice-Sophia	409 h EqTD
2011-2012	Maître de Conférences	Polytech‟Nice-Sophia	395 h EqTD
2012-2013	Maître de Conférences	Polytech‟Nice-Sophia	378 h EqTD
2013-2014	Maître de Conférences	Polytech‟Nice-Sophia	384 h EqTD
2014-2015	Maître de Conférences	Polytech‟Nice-Sophia	392 h EqTD

X. Résumé des responsabilités pédagogiques et administratives

- Responsable des stages Ingénieurs de 5ieme année au département électronique de Polytech'Nice-Sophia depuis 2014
- Responsable des salles de travaux pratiques d'électronique analogique du département électronique.
- Membre du comité de pilotage de la plateforme R2lab de l'INRIA

ACTIVITES DETAILLEES EN ENSEIGNEMENTS

J'ai débuté mes activités d'enseignement en 2003 à la suite de l'obtention d'un poste de moniteur au département électronique de l'école Polytch'Nice Sophia. Durant trois années, j'ai effectué 288 heures équivalentes TP (heqTD) sous la forme de Travaux Pratiques en physique, électrotechnique et électronique. Ces enseignements étaient adressés à des élèves de deuxième année de cycle préparatoire et de première année de cycle ingénieur.
J'ai poursuivi les enseignements à Polytech'Nice Sophia par l'intermédiaire d'un poste de demi-ATER en 2006 et d'ATER complet en 2007. J'ai effectué durant ces 2 années 288 heqTD en me focalisant principalement sur des TD et des TP en électronique en cycle préparatoire et cycle ingénieur. J'ai également encadré un projet tutoré de 5 étudiants en 2ième année de cycle ingénieur intitulé « Modélisation d'une chaîne de réception/émission RF Bluetooth en SystemC-AMS ».
Durant mon post-doctorat en 2009, j'ai réalisé 32h de vacation en projet Télécom pour les 3ième année d'école d'ingénieur et en TD de transmission numérique pour les 2ième année à Polytech'Nice Sophia.
A la suite de mon recrutement au poste de Maître de Conférences à Polytech'Nice Sophia en Septembre 2010, j'ai pris la responsabilité de travaux pratiques d'électronique en première et deuxième année d'école d'ingénieur. Durant ces 4 années, j'ai travaillé à faire évoluer les différents sujets et les maquettes pour les rendre plus proches des réalités industrielles et plus didactiques pour les étudiants. J'ai également eu l'opportunité de créer de nouveaux enseignements pour le département Electronique et ITII. Les points principaux sont décrits ci-dessous :

- Cours et TD Objets communicants : J'ai eu l'opportunité à mon arrivée de proposer un nouveau module de 15h (7.5h de cours et 7.5h de TD). Il est destiné aux étudiants de l'option TR sur la conception hardware de système radiofréquence. Il a été étendu à la dernière année de la formation ITII. L'objectif de ce module est de présenter les différentes architectures et contraintes techniques liées à la conception de systèmes radiofréquences. Le contexte des objets communicants est utilisé en trame de fond pour justifier les choix techniques et donner des exemples concrets.
- TP CAO Conception Système sous ADS : Philippe Lorenzini, responsable de l'option Conception des circuits et de systèmes (CCS), m'a demandé de concevoir un module de 18h sur la conception de système assisté par CAO. J'ai proposé d'étudier la conception d'un système « low IF » sur le standard Bluetooth. L'objectif est de voir à partir d'une analyse Top-Down, comment on peut extraire les spécifications de chaque bloc (LNA, mixer, etc,..) en partant des contraintes du protocole et d'un cahier des charges. Différents types de simulateurs d'ADS (Ptolemy, HB, Circuit Enveloppe) sont utilisés durant les travaux pratiques pour explorer l'architecture du système.
- Mini-projet Conception de système radiofréquence : Ce module avait été conçu par Cyril Luxey autour de la conception d'un récepteur LAN FSK sous la forme d'un mini-projet de 15h encadrées et 15h non encadrées. Sur les mêmes bases techniques, j'ai proposé d'ajouter une partie système et packaging à ce module, et d'augmenter les heures non encadrées. Le module se déroule sur un trimestre complet. Différents sujets de projets sont proposés aux étudiants (communication avec une balise en mer, système vidéo dans le casque de pompier …). Les étudiants s'intéressent à la partie technique, protocole, système, packaging et économique du projet. Grace à des cartes

radio-logiciels, des premières mesures peuvent être réalisées. Une séance est également effectuée sur le site d'Orange La Turbie dans le cadre du CREMANT et le matériel spécifique aux mesures radiofréquence du site est mis à disposition pour valider les prototypes des étudiants.
A partir de cette année, une formation sur un nouveau logiciel de CAO 3D « Empire » permet aux étudiants de faire des modélisations plus poussées de leur projet. Les étudiants peuvent ainsi appréhender la complexité d'une conception sur des plateformes hétérogènes.

- TP CAO Microélectronique "Design de LNA en technologie 0.35 µm d'AMS disponible par l'intermédiaire du pôle CNFM PACA. Ce TP a été conjointement créé par Cyril Luxey et Gilles Jacquemod en 2002, j'ai essayé de faire évoluer ce module en ajoutant notamment les simulations process et température sous Cadence Spectre RF. Les meilleurs étudiants peuvent également porter leur design sur la technologie 0.35 µm AMS bi-CMOS pour améliorer les performances de leur LNA.
- TP Electronique RF en première et deuxième année de cycle ingénieur : J'ai développé en collaboration avec un technicien en électronique Franck Perret, une nouvelle maquette d'alimentation à découpage conçue à partir d'un produit du commerce. A partir d'une maquette développée par Cyril Luxey de radar Doppler, j'ai proposé un nouveau TP permettant aux étudiants d'analyser les différents éléments d'une chaîne RF (amplificateur sélectif, VCO, mélangeur). J'ai aussi modifié les différentes maquettes du TP sur les antennes et j'ai ajouté différentes manipulations (Wheeler Cap, Matrice Butler). Suite à la réception de nouvelles maquettes offertes par la société Texas Instruments suite à la demande d'Yves Leduc, j'ai intégré une de ces maquettes pour réaliser un TP sur les filtres universels en première année de cycle ingénieur.
- Je me suis fortement investi dans l'encadrement de projet de deuxième année d'école d'ingénieur: Depuis mon recrutement, j'ai constamment encadré un ou deux projets étudiants de 4ième année. Dans ce cadre, en 2013, nous avons participé au « Student contest IEEE APS » avec 3étudiants de polytech et un doctorant du LEAT. L'équipe a atteint les demi-finales et a réalisé une vidéo de 5mn pour présenter le projet.

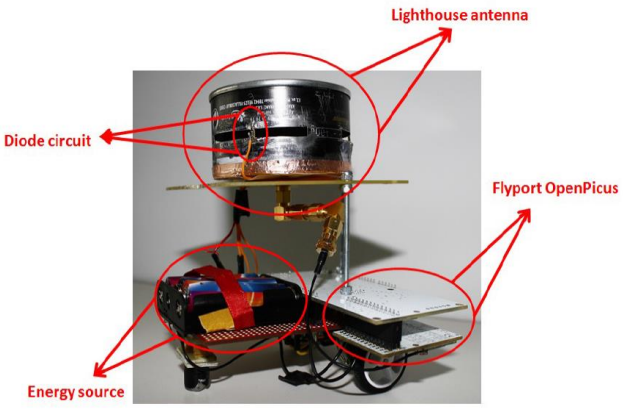

Figure 1: Robot avec antenne reconfigurable pour le contest IEEE

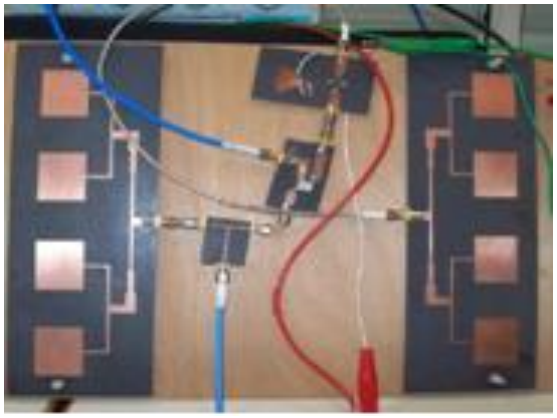

Figure 2: Système Doppler modulaire pour les TP elec 4

- Depuis 2015, je me suis impliqué dans l'enseignement électronique en PEIP2 avec notamment pour mission d'inciter les étudiants à choisir le département électronique pour leur cycle ingénieur. Pascal Masson a proposé d'utiliser des cartes microcontrôleurs de type Arduino comme base d'enseignement pour rendre cette matière plus accessible et didactique. Depuis 2016, je propose des séances de prise en

main d'électronique simple (transistors, AOP) et de modules plus complexes (accéléromètres, transciever Bluetooth). Et les étudiants réalisent, suite à ces séances, un mini-projet de conception d'objet connecté.

Finalement, les différents enseignements que j'ai réalisés durant ces 4 années sont résumés dans le tableau 1.

Enseignements	2010-11	2011-12	2012-13	2013-14	2014-15
Cours électronique MUNDUS (première année cycle ingénieur)	-20h (TD)	-	16h (TD)	-	-
TP Électronique (première année cycle ingénieur)	40h (TP)	33h (TP)	54h (TP)	33h (TP)	-
TD Électronique RF et Traitement analogique du signal (deuxième année cycle ingénieur)	30h (TD)-	30h (TD)-	30h (TD)-	30h (TD)-	32h(TD)
TP Électronique deuxième année cycle ingénieur	73h (TP)-	48h (TP)-	48h (TP)-	93h (TP)-	75h(TP)
TP Électronique en première année cycle ingénieur	32h (TP)	32h (TP)	32h (TP)	32h (TP)	54h(TP) 7.5h(cours)
CAO ADS Troisième année cycle ingénieur option TR et option CCS et cycle ITII	32h (cours) 33h(TP)	32h (cours) 33h(TP)	32h (cours) 33h(TP)	32h (cours) 33h(TP)	32h(cours) 33h(TP)
Mini-projet (Troisième année cycle ingénieur option TR)	18h (TP)	18h (TP)	18h (TP)	18h (TP)	18h (TP)
Cours Radiocommunication deuxième année cycle ITII	20h (cours)	20h (cours)	20h (cours)	20h (cours)	20h (cours)
Cours objets communicants Troisième année cycle ingénieur option TR et ITII	27h (cours) 8h(TD)	31h (cours) 8h(TD)	31h (cours) 8h(TD)	31h (cours) 8h(TD)	31h (cours) 8h(TD)
CAO Spectre RF Troisième année cycle ingénieur option CCS	15h (TD)	15h (TD)	15h (TD)	18h (TD)	15h (TD)
Total heures équivalent TD sur l'année	409 heq	395 heq	378 heq	384 heq	392 heq

Tableau 1 : Récapitulatif des enseignements depuis 2010

ENCADREMENT DE THESE

Depuis 2010, j'ai eu l'opportunité de co-encadrer 7 thèses de doctorat, dont 6 ont été soutenues.

Florian Canneva

Titre de la thèse : ***"Antennes miniatures reconfigurables en fréquence, polarisation et rayonnement"***
Financement : **Bourse Européenne**
Date début : **Oct. 2008** Date de soutenance : **8 Juin 2012** Encadrement : **30 %**
Directeur de thèse : **Robert Staraj 40 %, Co-encadrant : J-M Ribero 30%**
Publications : J11MO-J11MO2-J13MO
Situation actuelle du diplômé : **Ingénieur chez Ethertronics, Sophia Antipolis**

Diane Titz

Titre de la thèse : ***" Design and Characterization of Antenna-on-Chip and Antenna-in-Package solutions for 60 GHz communications and beyond "***
Financement : **Bourse Normale**
Date début : **Oct. 2009** Date de soutenance : **20 Septembre 2012** Encadrement : **30 %**
Directeur de thèse : **Cyril Luxey 40 %,** Co-encadrant : **Gilles Jacquemod 30%**
Publications : J12MO-J12RE-J12AW-J12MO3-J12AM-J12AW3-J13AP-J13CP-J13EL-J13AP3-J13AP4-J14MO-J14AW-J14AW3-J14CP-J14AW
Situation actuelle du diplômé : **Professeur agrégé en CPGE au Lycée Jules Ferry, Cannes**

Oumy Diop

Titre de la thèse : ***" Etude et Minimisation du Facteur de Qualité d'Antennes Miniatures conçues pour de Petits Objets Communicants "***
Financement : **Bourse MESR**
Date début : **Oct. 2010** Date de soutenance : **27 Septembre 2013** Encadrement : **30 %**
Directeur de thèse : **Cyril Luxey 40 %,** Co-encadrant : **Aliou Diallo 30%**
Publications : C12IW2 C12SA
Situation actuelle du diplômé : **Ingénieur chez Epcos-TDK à Sophia Antipolis**

Marcio Silva Pimenta

Titre de la thèse : ***" Antennes souples à bases de métamatériaux de type conducteurs magnétique artificiels pour les standards de systèmes de géolocalisation "***
Financement : **Bourse ANR Metavest**
Date début : **Oct. 2010** Date de soutenance : **14 Novembre 2013** Encadrement : **30 %**
Directeur de thèse : **Jean-Marc Ribero 40 %,** Co-encadrant : **Robert Staraj 30%**
Publications : J12MO4
Situation actuelle du diplômé : **Ingénieur chez Insight SIP à Sophia Antipolis**

Aykut Cihanghir

Titre de la thèse : ***" Antenna designs using matching circuit for 4G communicating devices "***

Financement : **Bourse Projet ARTEMOS**

Date début : **Dec. 2010** Date de soutenance : **6 Mars 2014** Encadrement : **50 %**

Directeur de thèse : **Cyril Luxey 50 %**

Publications : J13EL-J13AW-J14AW2-J14FE-J15FE

Situation actuelle du diplômé : **Ingénieur chez TDK**

Le Huy Trinh

Titre de la thèse : ***" Conception d'antennes reconfigurables pour les systèmes radios logicielles "***

Financement : **Bourse MESR**

Date début : **Oct. 2012** Date de soutenance : **15 Juillet 2015** Co-direction **: 30 %**

Directeur de thèse : **Jean-Marc Ribero 30 %,** Co-encadrant : **Robert Staraj : 30%**

Publications : J12EL-J15AW3-J15IJ-C15EU3

Cyril Buey

Titre de la thèse : ***" Conception/Développement du système antennaire reconfigurable d'une Small/Femto Cell 5G "***

Financement : **Thèse CIFRE Orange**

Date début : **Nov. 2014** Date de soutenance : **Nov. 2017** Co-direction **: 50 %**

Co-encadrant : **Leonardo Lizzi : 50%**

Publications : I14CA

ENCADREMENT DE STAGES

Entre 2009 et 2015, j'ai participé à l'encadrement de 7 stages de niveau master 2 de 6 mois. Le stage de Le Huy Trinh, Aiouaj Allal et Cyril Buey était financé par Orange dans le cadre du CREMANT. Le stage d'Aimeric Bisognin était financé par l'équipe EpOC de l'Université de Nice dans le cadre d'une collaboration sur la conception d'antennes millimétriques au sein du CREMANT. Les autres stages étant financés par le LEAT.

Madiha El Khattab

Titre du stage : ***" Antennes miniatures multistandards actives à base de nouveaux matériaux et métamatériaux"***
Financement : **Fond propre LEAT**
Date début : **Fev. 2010** Date de fin : **Juillet. 2010** Encadrement **: 100%**
Situation actuelle : Test Analyst chez Median Technology

Pauline Bouzat

Titre du stage : ***" Conception d'une antenne combinée GPS / Iridium "***
Financement : **Fond propre LEAT**
Date début : **Fev. 2011** Date de fin : **Juillet. 2011** Encadrement **: 100%**
Situation actuelle : Business analyst chez Amedeus

Le Huy Trinh

Titre du stage : ***" Conception d'antennes reconfigurables pour les systèmes radios logicielles "***
Financement : **Stage Orange**
Date début : **Fev. 2012** Date de fin : **Juillet. 2012** Encadrement **: 50%**
Nom et % du co-encadrant: **P. Brachat** (50%)
Situation actuelle : Thèse MESR au LEAT

Aimeric Bisognin

Titre du stage : ***" Conception et caractérisation de structures antennaires in-package pour applications millimétriques WLAN indoor à 60GHz et 120GHz "***
Financement : **Fond propre EpOC**
Date début : **Fev. 2012** Date de fin : **Juillet. 2012** Encadrement **: 100%**
Situation actuelle : Thèse ST Microéléctronique

Aiouaj Allal

Titre du stage : ***" Mise en place d'un banc de mesures MIMO 2x2 pour des applications LTE "***
Financement : **Stage Orange**
Date début : **Avril. 2013** Date de fin : **Aout. 2013** Encadrement **: 50%**
Nom et % du co-encadrant: **J-P. Rossi** (50%)
Situation actuelle : Ingénieur Télécoms à SIAE Montpellier

Cyril Buey

Titre du stage : ***" Dimensionnement et évaluation d'un routeur à 8 antennes WiFi"***
Financement : **Stage Orange**
Date début : **Avril. 2014** Date de fin : **Septembre. 2014** Encadrement **: 50%**
Nom et % du co-encadrant: **J-P. Rossi** (50%)
Situation actuelle : Thèse Orange

Zayd Ouachicha

Titre du stage : ***" Mesure de système miniature à 868 MHz"***

Financement : **Stage CREMANT**

Date début : **Avril. 2014** Date de fin : **Septembre. 2014** Encadrement **: 100%**

Situation actuelle : Ingénieur Sopra

Part 2 : Research activities

I will try in this part to retrace my research activities from the start of my PhD until now. I will use this manuscript as an opportunity to disclose complimentary or un-published work.

I have started my research activity more than 10 years ago, and the writing of this HDR is coming at the right time, when a flashback on your past research will help you to get into position for the next 10 coming years.

My different research topics were mainly driven by Master and PhD student supervision, thus i have divided the different section of this manuscript in relation with the students who were involved in the studies.

In 2010, I was recruited on a "Maître de conference" position at the Polytechnic school of the University of Nice Sophia-Antipolis to teach electromagnetics, Telecommunication and RF microelectronics. I'm continuing my research activities within the "Laboratoire d'Electronique, Antennes et Télécommunications (LEAT)" (Director is Jean-Yves Dauvignac) in the CMA team (antenna design and modeling). An important part of my research presented in this manuscirpt has been realized in colloboration with EpOC laboratory (Director is Gilles Jacquemod). The majority of my work has been done in the frame of the CREMANT, joint lab between University of Nice Sophia and Orange Company.

My research interests concerns the design and measurement of circuits and antennas for telecommunication system. The first section of this part will be dedicated to my PhD studies on the design of passive and active antennas. Then, I will present in the section II my research work during my ATER position in 2008. My research as research engineer in *IMRA Europe* Company will be described in the section III. In section IV will be dedicated to my Post-Doc realized in the LEAT in the frame of the NAOMI ANR project in 2010.

The three last sections will be dedicated to my research studies as a "Maître de conference" from 2011 in the frame of multiple MASTER and PhD studies that I Supervised or co-supervised.

I. Introduction

From the past 20 years we have experienced a large change in people relationship, and telecommunication technologies have been a key enabler of this evoluation.

The first industrial revolution began in Britain in the late 18th century, with the mechanisation of the textile industry, printing and transportation using steam power. Tasks previously done laboriously by hundreds hands were replaced by a single cotton mill: the factory was born. Communication through journals and books enabled a mass alphabetization for the first time in history. Public school in Europe and North America from 1830 to 1890 provided a skilled workforce, able to lead complicated operation needed for the industry and railway development based on steam power.

The second industrial revolution came in the early 20th century with electricity and combustion engine. Electricity in factories and at home opened the mass production era. With Henry Ford creating the moving assembly line, cars became accessible and the road network spread in the countries. In a few decades, horses were replaced by cars in city and by tractors in fields. New materials made from petrol appeared. Telephone lines, radio and television changed the social life toward new communication models and trades.

The first two industrial revolutions made people richer and caused urbanization. A lot of people consider that a third revolution is under way and, like all revolutions, it will be disruptive.

A number of remarkable technologies are converging: digital systems, novel materials, robotics, drones new fabrication processes, telecommunication, renewable energy and a whole range of web-based services.

In my opinion, we can define four different sectors that are going to disrupt the world in this third industrial revolution: Additive manufacturing, Robotics, Renewable energy and Digital communication.

1. The Third revolution disruptive sectors

a) Additive manufacturing: 3D printing technology revolution

The factory of the past was dedicated to the fabrication of (x)illions of identical products: H. Ford was used to say that car-buyers could have any colour they liked, as long as it was black. Steve Jobs has allowed the consumer to choose between 5 colors, but inner material of an IPhone is identical. We have seen with the automotive market (Citroen DS3, Fiat 500, Mini) that the cost of producing much smaller batches of a wider variety, with each product tailored to each customer's expectations, is now possible. The factory of the future will focus on mass customization.

This revolution will change the way things are fabricated, but also where they are made. Factories have moved to low-salary countries to drop labour costs. First labour costs have a less and less important part in the final product cost: a $499 first-generation iPad included only about $33 of manufacturing labour, of which the final assembly in China accounted for just $8 [ECO12]. Production is going to move back to rich countries in order to have the fabrication closer to the customers, to respond more quickly to changes in demand.

However, even if the production is going local, the design part will be completely digital and the market will be worldwide. App Store and Android Market are the first exemple of Worlwide open market directly connected to consumers.

3D printing is at an inflection point, and is about to shake most of the mainstream processes. The first step of this technology was dedicated to prototyping, rapid tooling, trinkets, and toys. But upcoming Additive manufacturing will create durable and safe products for sale to real customers in moderate to large quantities. More and more materials can be used beyond the classical ABS plastic, from ceramic [SCI16] to metal [ACC13].

Fig I.1 : 3D printing gears

b) Robotics : The Smart machines challenge

Boston Consulting Group has predicted that up to a quarter of jobs will be replaced by either smart software or robots by 2025 [BBC15].

In France, Taxi drivers are actually fighting against Uber on-demand services, but a more lethal threat is arriving with autonoumous car. Google announced in 2015 that their vehicles have driven over 2,000,000 km without any traffic accident caused by the autonomous car.

Amazon plans to use unmanned aerial drones to deliver packages by air. Drones with 2.3 kg package carrying capacity would be able to carry 83% of all of the items that Amazon delivers.

In the manufacturing sector, most of the jobs will not be on the factory floor but in the offices nearby, which will be full of designers, engineers, IT specialists, logistics experts, marketing staff and other professionals. The manufacturing jobs of the future will require more skills. Most of the repetitive tasks will become obsolete.

Fig I.2 : Amazon aerial drones for package delivery

c) Renewable energy

The increased energy efficiency and accompanying productivity gains that come with the shift into a Third Industrial Revolution infrastructure, prepare the way for a sustainable circular economy. Using less of the earth's resources more efficiently and productively and making the transition from carbon based fuels to renewable energies, is a defining feature of the Collaborative Age. In 2014, renewable energies such as wind, geothermal, solar, biomass and burnt waste provided 19% of the total world final energy consumption, roughly 50% of it traditional use of biomass [CHE16]. EU countries have agreed on a new framework for climate and energy, claiming that at least a 27% share of renewable energy consumption is expected for 2030.

We do not expect really disruptive technologies in this area, but the optimization of the process and mass-production is going to drop the price of the existing technology. In parallel, dispite the fact that energy price is quite low in 2016, we are expecting a continuous growth of energy price in the next 20 years, thus naturally pushing for renewable energies.

If you consider the (xillion of new "cool" connected objects which require electrical power to work, recharging them will quickly become a nightmare for all users, pushing for the development of power efficient devices harvesting their energy from their environment.

d) Digital communication

The Internet of (every)Thing will connect everyone and everything in a seamless network. People, smart machines, renewable resources, 3-D printers, logistics networks, consumption habits, and every other aspect of economic and social life will be connected via sensors, actuators and softwares to the cloud. The huge amount of data extracted from these sensors, will be analyzed with advanced analytics, transformed into predictive algorithms, and programmed into automated systems, to improve productivity, and reduce the production cost.

In order to integrate in a small volume the processing unit, the transceiver and the sensors, dedicated electronic platform are emerging. As an exemple, Intel is currently developing a System-on-Chip (SoC) named Curie including a microcontroller unit (MCU), flash memory, a DSP for sensor pattern matching, an accelerometer and a Bluetooth Low Power Transciever with a coin-battery form factor. ST Microelectronics has just announced the development of a SoC including a STM 32 MCU and a LoRa transceiver.

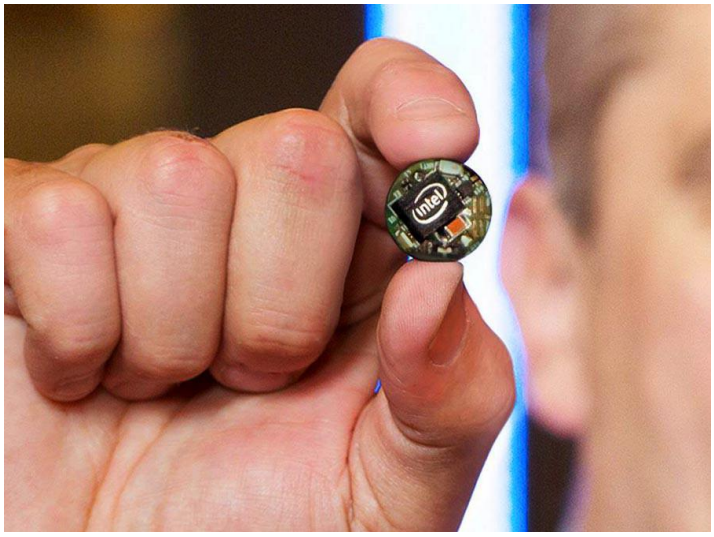

Fig I.3 : Intel wearable Curie™ electronic platform

This is the disruptive sector closer to my research topic and my perspectives will be largely matched to the different need for efficient and smart IoT networks.

2. Research and Education perspectives

I can conclude that from an academic point of view, this (r)evolution is a fantastic opportunity for research and education. Of course in this prospective view, telecommunication technologies are in the heart of this revolution. Electromagnetic waves are essential to suppress all the distance limits, to create smarter environments. Our future research has to pave the way to this revolution. Due to the need of flexilility, support of multi-standard, flexibile concept are needed.

On the education part, our teaching activity has also to evolve in order to give to the future generation the required skills to accommodate themselves to this change. The impact of the third revolution on learning will be profound. Any student has already infinitely more information on any given subject with a simple click of a button than could ever be disseminated by any teacher.

Therefore, we should shift from traditional notions of a teacher-student relationship, to one with the responsibility on educators to facilitate flexible learning by becoming catalysts, enablers and inspirers of this mass of information.

References

[ECO12] “The third industrial revolution”, The Economist, Apr 21st 2012

[SCI16] Additive manufacturing of polymer-derived ceramics, Zak C. Eckel, Chaoyin Zhou, John H. Martin, Alan J. Jacobsen, William B. Carter, and Tobias A. Schaedler, Science 1 January 2016: 351 (6268), 58-62.

[ACC13] Anzalone, G.C.; Chenlong Zhang; Wijnen, B.; Sanders, P.G.; Pearce, J.M., "A Low-Cost Open-Source Metal 3-D Printer," in Access, IEEE , vol.1, no., pp.803-810, 2013

[BBC15] Jane Wakefield “Intelligent Machines: The jobs robots will steal first”, BBC, Sept. 2015.

[CHE16] Nicola Armaroli, Vincenzo Balzani: Solar Electricity and Solar Fuels: Status and Perspectives in the Context of the Energy Transition. In: Chemistry – A European Journal 22, (2016), 32-57, doi:10.1002/chem.201503580.

II. PhD studies (2003-2007)

Just after my master thesis in Engineering diploma in 2003, Gilles Jacquemod, Full professor at the University of Nice, proposed me to continue my studies through a PhD thesis funded by the French government (MESR). The subject of my research was focused on reconfigurable circuits and antennas. Under the supervision of Gilles Jacquemod, Robert Staraj, Cyril Luxey from the LEAT, and Pr. Vincent fusco from the Queens University of Belfast, I had the task to design reconfigurable antenna in polarization and directivity. I started my studies in October 2003 and I defend my thesis the 19th of November 2007. The title and members of my jury are stated below:

« Reconfiguration dynamique d'antennes imprimées en directivité et polarisation »

Pr Yann DEVAL, IMS de Talence, Président de jury

Pr Christian PERSON, GET/ENST de Bretagne, Rapporteur

Pr Philippe BENECH, IMEP ENSERG de Grenoble, Rapporteur

Mr Patrick PONS, LAAS de Toulouse, Examinateur

Mme Andreia CATHELIN, ST/Minatec de Grenoble, Examinateur

Pr Gilles JACQUEMOD, Université Nice Sophia-Antipolis, Directeur de thèse

Pr Robert STARAJ, Université Nice Sophia-Antipolis – LEAT, Responsable de thèse

Mr Cyril LUXEY, Université Nice Sophia-Antipolis – LEAT, Responsable de thèse

A. Motivation

The nineties have seen a rapid development of the mobile phone technology, in less than 10 years; a "wireless" revolution has established a new era in the telecommunication area.

Considering the constant increasing of wireless objects, features and data rates, more and more complex technologies have to be integrated to support these developments. Fast-Fading and shadowing effects in multi-propagating channel degrade strongly transmission signal to noise ratio. To counter these parasitic effects, polarization and directivity diversity has been proposed as shown on Fig. 1. Designing reconfigurable antenna is a major challenge and it start with the development of active devices reliable, efficient, with low insertion loss and low cost. Up to now, radiofrequency industry has mainly used semi-conductor device which are able to meet most of customer needs. At the start of my PhD, micro mechanical system for radiofrequency application was a very hot topic in the antenna community, and the high potential of this novel technology was highly attractive. It was also full of sense to start this

activity at the LEAT at this time as this research topic was merging electromagnetic skills with micro-electronic technology. Considering the increasing of carrier frequencies, and linearity issues, these components (MEMS) offers interesting solutions (Fig. 1).

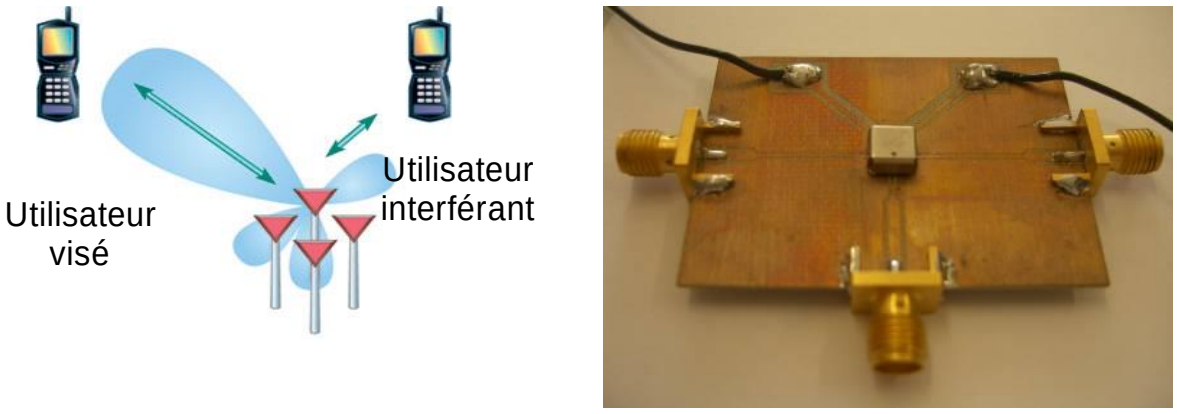

(a) (b)

Fig. 1 (a) Directivity diversity applied to mobile phone, (b) Magfusion magnetic MEMS

Studies realized in this PhD concerns, on one hand, one the design and fabrication of efficient RF MEMS device, on the other hand, on the design of antenna topology with suitability for polarization and directivity reconfiguration.

B. Design of RF MEMS devices

The semi-custom MEMS processing *MetalMUMPS PLUS* from *MEMSCAP* Company was selected because it was part of Europractice program. Some process problems were encountered due to diffusion of the copper layer in the gold layer which created a dielectric isolation between the gold and the polysilicon layer. The biasing of the MEMS electrodes was not possible and therefore, only passive measurements were presented.

To perform minimum insertion loss for the phase shifter, we adopt switched line type architecture. Each phase shifter is composed of two cascaded phase cell and each cell can switch between three different delay lines. The key element of the phase shifters is then the switch.

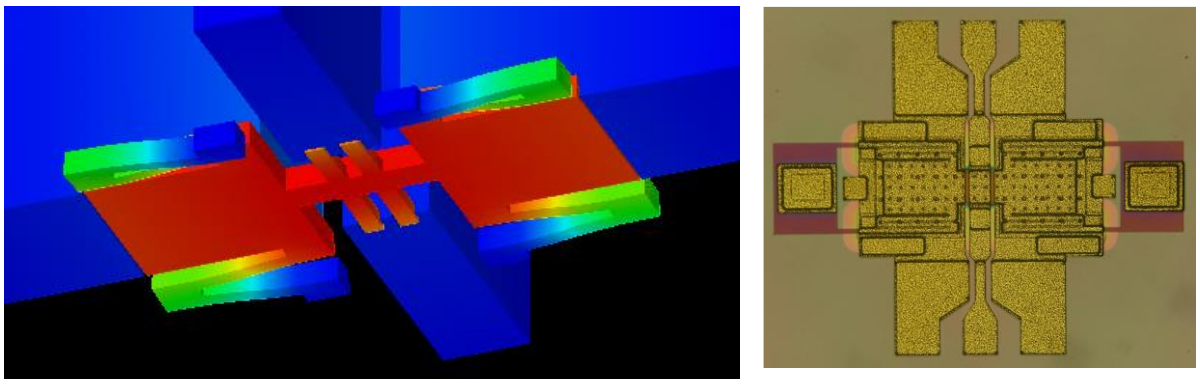

(a) (b)

Fig. 2 (a)Mechanical simulation with Coventor, (b) Picture of a shunt MEMS (size 300*200 um^2)

The movable membrane is made of a 2-µm thick polysilicon conductor layer placed between two 0.35-µm thick silicon nitride layers and is situated under the 7-µm thick gold CPW lines. This original topology was intended to simplify the packaging of the MEMS. The switches are electro-statically actuated and use the upper silicon nitride layer as a dielectric. The second silicon nitride layer allows polysilicon discontinuity on the same membrane. Moreover, both silicon nitride layers ensure a perfect compensation of the residual stress in the moveable structure. Two silicon dioxide layers are used as sacrificial layers. The mechanical behavior of the structure was simulated with Coventor Software (Fig. 2). To reduce actuation voltage, serpentine springs were used to connect the mobile membrane to the substrate. The switches were design to have a collapsing voltage of V_c=24 V.

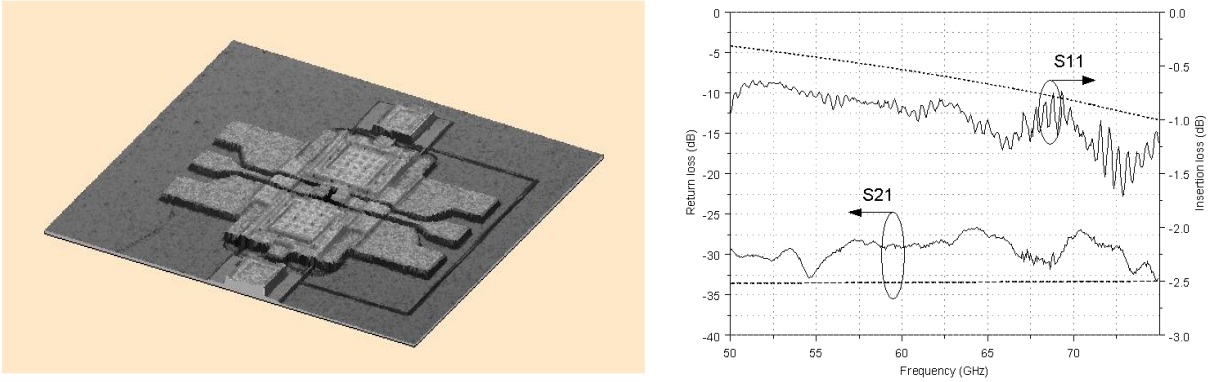

(a) (b)

Fig. 3 (a) 3D scanning using confocal optical sensor of the series MEMS switch, (b) S11 and S21 for the series MEMS switch

Photography of the MEMS switch using confocal optical sensor is proposed in Fig. 3. First results for the MEMS are presented here. Fig. 3shows the results for the measurement and simulation of the series type MEMS. The isolation between the two ports is higher than 25 dB. The return loss is measured to be better than -0.8 dB at 60 GHz. The level simulated are quite close to the data measured. Measurements of the shunt MEMS are presented in Fig. 4. The insertion loss is lower than 0.5 dB at 60 GHz and the return loss is lower than -20 dB at 60 GHz.

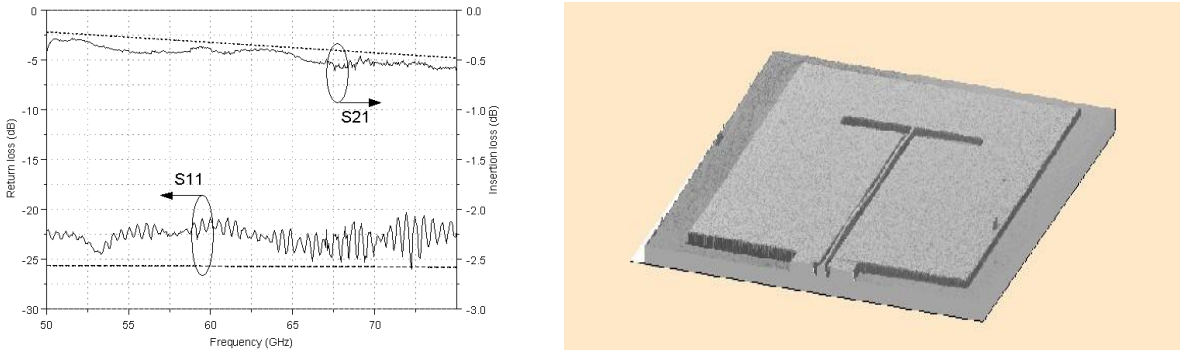

(a) (b)

Fig. 4 (a) S11 and S21 for the shunt MEMS switch, (b) 3D scanning using confocal optical sensor of rectangular slot antenna

A full beam-steering system including antenna and phase shifters was designed. In order to have an array as compact as possible with minimal losses, the whole antenna is built using a MEMS process. A photograph using confocal microscope is presented in Fig. 4. Thanks to the short guided wavelength in Silicon at 60 GHz (λ_{Si}=1.46mm), it becomes possible to integrate the whole MIMO array, including radiating elements and phase shifters, on a silicon die of 1cm². In order to direct the beam in only one direction, a metallic plane reflector is added under the substrate. a CPW lines were used to reduce mutual coupling between closely spaced lines. The final layout and a picture of a part of the antenna system is presented in Fig. 5. This work was presented in [C06IC].

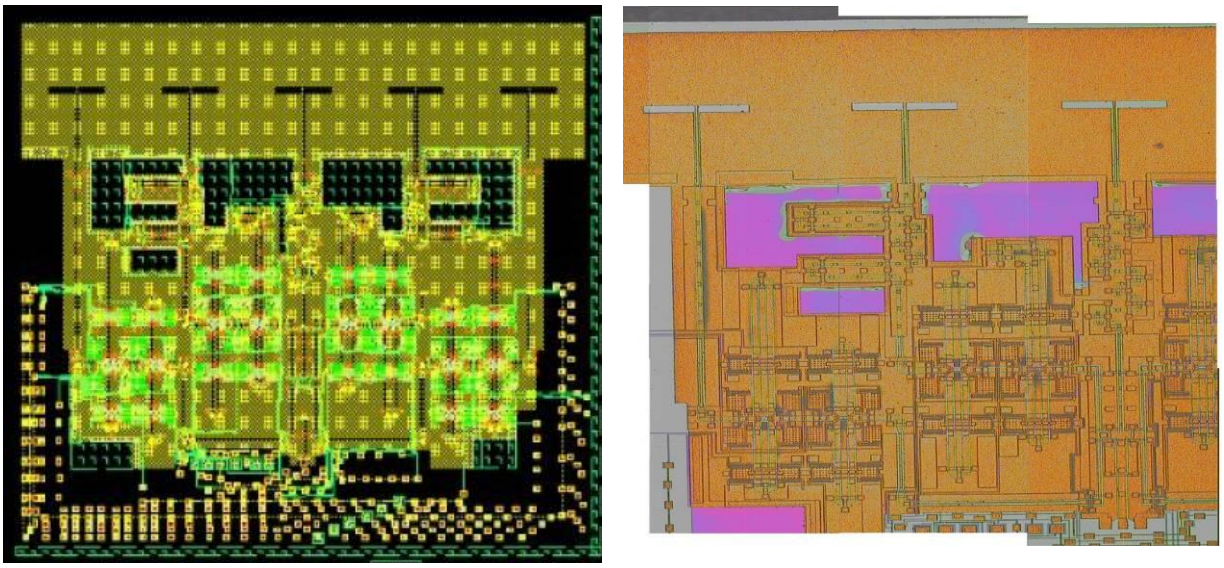

(b) (a)

Fig. 5 **(a) Layout of the beamforming antenna system, (b) Photograph with microscope**

C. Reconfigurable hybrid coupler

For fifty years, considerable effort has been devoted to the study of tunable directional couplers for reconfigurable microwave systems.

Our goal was to design a reconfigurable coupler able to alternatively provide the 3-dB Hybrid mode (90° phase difference between the direct and the coupled port) or the uncoupled-line mode (very low coupling between the direct and the coupled port). For this purpose, we proposed the modification of a Quasi-Lumped Quadrature Coupler (QLQC) [FUS89]. A frequency-tunable QLQC structure has been proposed in 1991 using ganged capacitors as the vertical lines of a classical 3-dB hybrid circuit [FUS91]. For a given capacitance, this QLQC is able to operate over a 5% bandwidth with adequate performance. When tuning the ganged capacitors, the same 3-dB hybrid performance is maintained over a 120% bandwidth. This foregoing research predicted a varactor diode implementation but such components with suitable tunable capacitance values were not at that time available. However, such a QLQC cannot meet our requirements; and further theoretical investigation is needed in order to anticipate if the QLQC may be modified to achieve our operational requirements.

1. Theory and design of the tunable QLQC

The QLQC is a circuit with the vertical printed branches of a classic hybrid coupler are both replaced by a lumped component with a suitable admittance. In this way the size of the

classical 3-dB hybrid can then drastically reduced. The structure consists of two parallel horizontal transmission lines with characteristic impedance Z_1 (Fig. 6). The complete analysis of this structure has been presented in [J09MO].

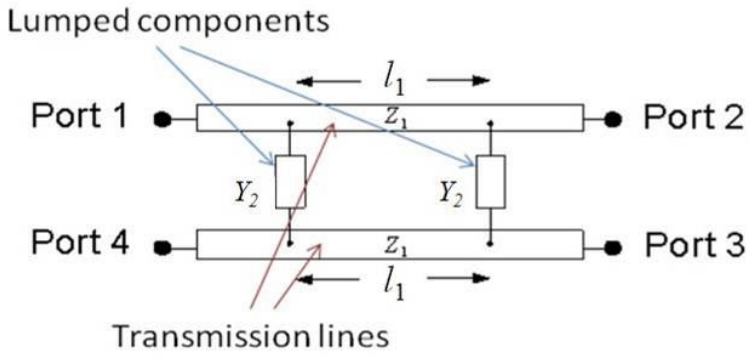

Fig. 6 Schematic of a Quasi-Lumped Quadrature, QLQC, Coupler.

2. Tunable QLC and the uncoupled-line mode

In order to add some reconfigurability to this coupler, we substitute the lumped capacitors by varactor diodes to get tuning capability versus DC bias. With a QLQC, the biasing circuit will be really simple to implement thanks to the fact that the two horizontal transmission lines are electrically isolated: one of these lines can be set to the high DC voltage while the other can be forced to the DC ground. The analytical equations of the voltage amplitudes at port1 and emerging trough port4 from port1 versus the admittance Y_2 are given by (5). In addition, the theoretical coupling ratio k versus the admittance is given by (6).

$$A_{11} = -A_{41} = \frac{-Y_2 - jY_2^2}{1 + 2Y_2 + j(1 + 2Y_2 + 2Y_2^2)} \qquad \text{(Equ.1)}$$

$$k = \frac{A_{21}}{A_{31}} = \frac{1 + Y_2 + j(1 + Y_2 + Y_2^2)}{Y_2 + j(Y_2 + Y_2^2)} \qquad \text{(Equ.2)}$$

The magnitude in dB and the phase of the coupling k as well as the matching at port 1 (magnitude of the S_{11} obtained by taking 20 log (equation 5) and the port4-to-port1 isolation (same equation) are plotted versus the admittance (and thus the capacitor C_{hyb}) in Fig. 7.a. When the capacitance is tuned from $0.1*C_{hyb}$ to $1.2*C_{hyb,}$ k is varied from -3dB to +21dB and the phase difference between S_{21} and S_{31} is maintained between 86° and 90°. At the same time, the return loss and the isolation are both always higher than 15.5 dB. These curves demonstrate that the QLQC can effectively operate as a quadrature tunable power splitter and thus perform well for both the 3dB hybrid mode and the uncoupled-line mode at the same frequency. A picture of the prototype is presented in Fig. 7.b.

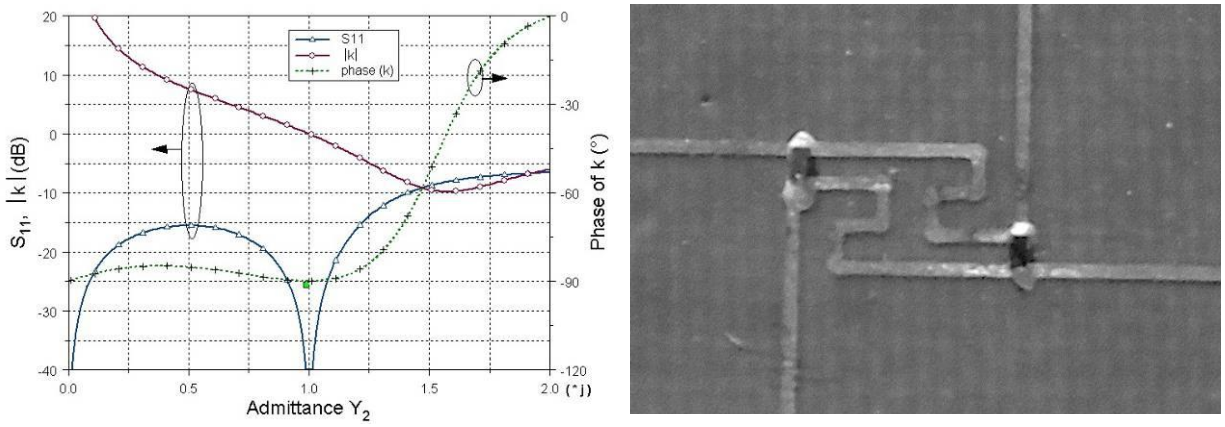

Fig. 7 (a) Matching, coupling and output phase of the Quasi-Lumped Coupler when the capacitor is tuned, (b) Picture of the fabricated tunable QLQC

We measured this hybrid circuit at 3.5 GHz for reverse voltages V_r ranging from 0V to 15V (Fig. 5). For capacitances lower than 0.2pF (V_r>11V), it can be seen that the four-port network can be considered as two parallel uncoupled transmission lines. For a capacitance of 0.920 pF (V_r=0.96V), the system operates like a 3-dB hybrid coupler. In Fig. 8.a, we present the simulated and measured S_{ij} parameters versus frequency of the tunable QLC when V_r=0.96V (3-dB hybrid mode). These curves are in very good agreement. The feeding signal is evenly divided between port2 and port3 at 3.5 GHz. The return loss at port1 and the port4-to-port1 isolation are both better than -25dB. In the uncoupled line mode (i.e. reverse voltage equals to 15V), good isolation levels are obtained between port1-port3 and port1-port4 as well as a good match. The insertion loss between port1-port2 is found to be -0.45dB at 3.5 GHz.

From this reference structure, cascaded structures were proposed to enhance bandwidth and reconfigurability as shown in Fig. 8.b [J07EL]

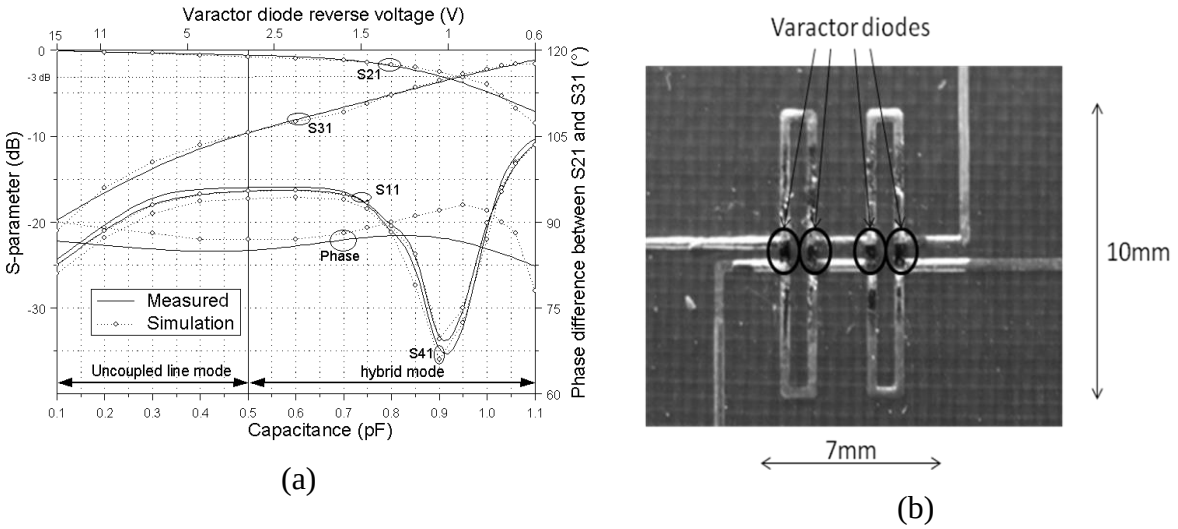

Fig. 8 (a) S-parameters versus capacitance, (b) Cascade QLQC coupler

D. Application of reconfigurable couplers

Based on this reconfigurable microwave structure, we propose several antenna topologies for polarization agility.

1. Quad polarization microstrip antenna

We proposed a novel design of a reconfigurable quad-polarization microstrip antenna. This has been presented in [J09AP]. Special emphasize is put on overcoming the bias complexity and reducing the occupied space to avoid repercussions on the antenna's performance. The radiating patch is fed via two orthogonal slots etched in its ground plane. These slots are excited by a tunable Quasi-Lumped Coupler (QLC) used in two different operating modes: namely, classical 3-dB hybrid mode and, uncoupled-line mode (i.e. directional coupler with very low coupling). The coupler can be simply reconfigured by switching the bias of two varactor diodes via a simple DC circuitry where no additional capacitors or inductors are required. This coupler is fed by a Single Pole Dual-Through (SPDT) switch as shown in Fig. 9.a. The linearly polarized or circularly polarized radiated waves are simply selected when changing the operating mode of the QLC. The SPDT switch allows selection of the horizontal or vertical polarization mode in the first case while the right-hand or left-hand polarization mode is selected in the second case by choosing which input of the coupler is fed. A prototype is fabricated with a 0.762-mm-thick upper layer substrate for the radiating element and a 0.130-mm-thick layer substrate for the coupler circuit, both of the same dielectric material with a relative permittivity of 2.22 (Fig. 9.b).

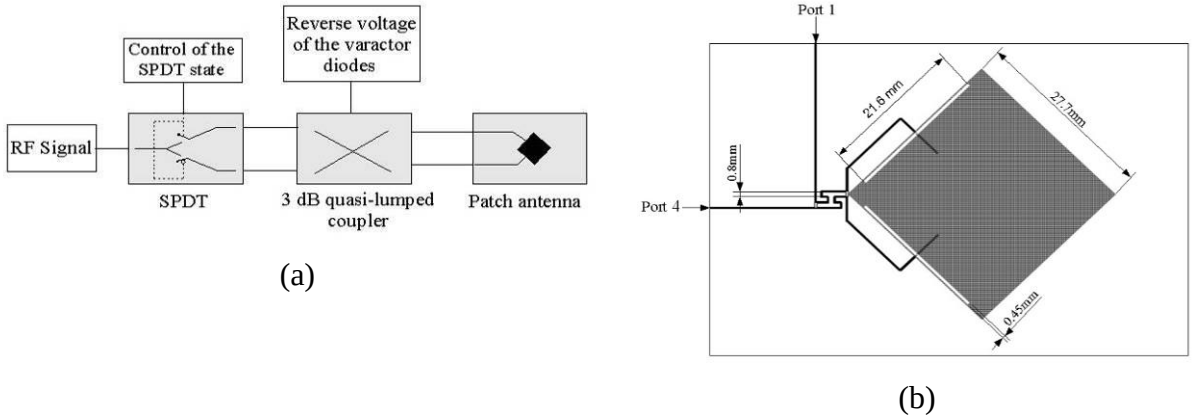

Fig. 9 (a) Topology of the polarization-agile antenna, (b) Layout of the polarization-agile antenna (top-view)

The CP axial ratio (V_r = 0.96V) and cross-polarization level (V_r = 15V) versus frequency are presented in Fig. 10.a in the broadside direction of the antenna. In CP mode, the 3dB axial ratio bandwidth is 3.8% (134MHz). The cross-polarization levels in the uncoupled line mode (radiated linear polarization) are always greater than 20dB over the greater bandwidth of 300 MHz. The measurements of the x-z plane far-field radiation pattern at 3.5GHz are shown in Fig. 10.b for the hybrid mode. With the antenna configured for CP, the axial ratio is less than 3 dB over the entire half plane around the zenith. The pattern shape of the antenna in the uncoupled line mode shows a good linear radiation with a cross-polarization level always superior to 12 dB. A maximum gain of 6.2 dBi in the broadside direction is measured.

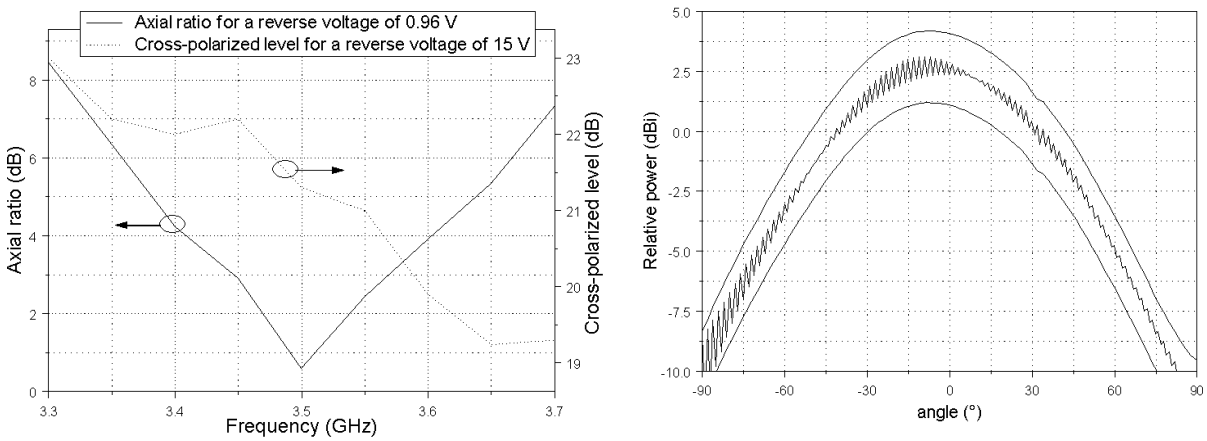

Fig. 10 **(a) Axial ratio in the hybrid mode and cross polarized level in the uncoupled line mode versus frequency of the antenna, (b) Measured CP radiation pattern of the antenna for V_r=0.96V at 3.5 GHz (3-dB hybrid mode)**

2. Linearly-Polarized Tunable Antenna

Many solutions have been investigated to rotate linear polarization without any mechanical systems. Our proposed solution allows a dynamic rotation of the angle of the linearly-polarised electrical field over a 90° angle: each direction can easily be achieved. It was presented in [J11EL].

The principle of our antenna is shown in Fig. 11.a. Two orthogonal linearly-polarized antennas are fed by a tunable power divider. The port 2 of the power divider is feeding the vertically-polarized antenna with a power level P_V (y direction). The port 3 of the power divider is connected to the horizontally-polarized antenna with a power level P_H (x direction). By changing the power level of the outputs of the power divider, it is therefore possible to change the rotation of the linearly-polarized wave over a 90° angle (Fig. 11.a). The phase difference between the two outputs of the power divider has to be kept null to ensure a high level of axial ratio i.e. high polarization purity. In addition, to keep the gain of the antenna constant when changing the direction of the polarization, the addition of Pv and PH has to be kept constant.

The gain radiation pattern in the normal direction of the antenna (broadside) for a 360° rotation of the emitter is presented for three different voltages in Fig. 11.b. These measurements show that a 93° rotation of the linearly-polarized wave is possible by changing the reverse voltage from 0.9V to 15 V. During this rotation, the deviation of the gain in the maximum direction is only ± 0.2 dB. Moreover, the cross-polarization level is kept higher than 25 dB for all the different voltages.

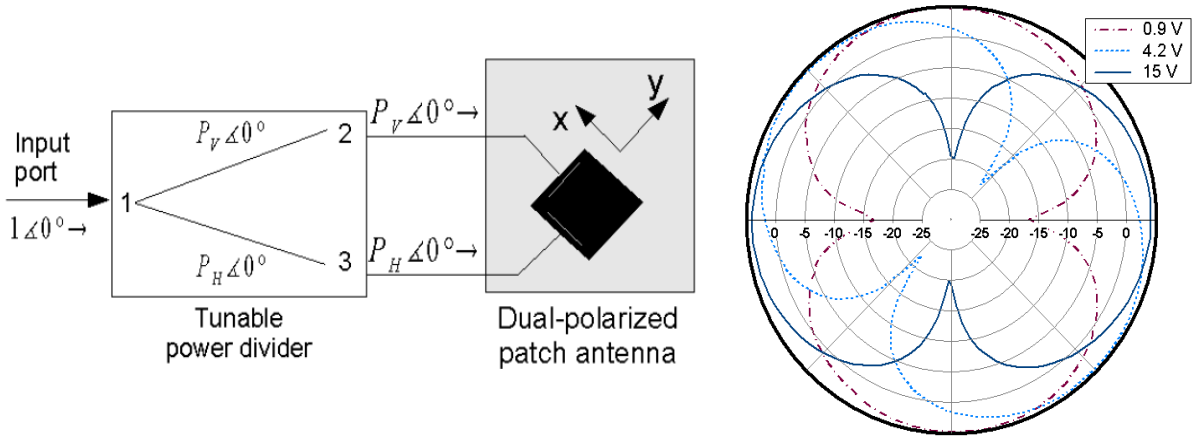

(a) (b)

Fig. 11 **(a) Topology of the linearly-polarized tunable antenna, (b) Gain radiation pattern in the broadside direction of the antenna for a 360° rotation of the emitter @ 3.5 GHz**

E. References

[FUS89] S.B.D. O'Caireallain, V.F. Fusco, "Quasi-Lumped Element Quadrature Coupler Design", Microwave and Optical Technology Letters, Vol. 2, No. 6, pp. 216-218, June 1989.

[FUS91] V. F. Fusco, "Tunable Quasilumped Element Quadrature Hybrid", IET Electronics Letters, vol. 27, No. 24, pp. 2246-2248, 21st November 1991.

III. Temporary assistant professor (ATER 2007-2008)

Following my PhD defense, I focused my work, in collaboration with Benjamin Nicolle who was a PhD student at the LEAT, on high level modeling of complex system. Our objective at the time was to develop a start-up able to propose engineering services for industrial project. The modeling was based on VHDL-AMS modelling. This technique was applied to two different areas: RF telecommunication and Biological system.

A. RF chain modeling using VHDL-AMS

Traditionally, analog and RFIC designers use a Bottom–Up design methodology based on the use of elementary components (transistors, diodes, capacitors) in order to create electrical functions. Then, these functions are assembled within more and more complex blocks until the complete analog system design is reached. Thus, the obtained system is an association of elementary blocks, generally described at the transistor level. The major disadvantage of this description level is the extremely long simulation time that it takes to simulate the complete system. It also makes difficult system verification because of the number of iteration needed to find and correct an eventual error.

The efficiency of the Top–Down design flow depends directly on the performances of the simulation environment. With systems becoming more complex and heterogeneous, the ability of modeling both digital analog and RF parts within the same environment is of major concern. For all those reasons, HDLs as Verilog-AMS and VHDL-AMS seem to offer good mixed-signal capabilities and multi-abstraction level modeling solutions in order to optimize the major phases of a complex system design flow. This study was focused on the advantages of such a modeling solution compared to the generally used modeling habits, within the RFIC design flow. A test case is proposed based on an RFIC satellite receiver design, and the non-linear parameters are evaluated and compare with measurement as shown on Fig. 12. Results show that the behavioral approach permits fast and accurate estimations (0.7 dB error average for 8-channel composite-triplebeat inteference at 950MHz). This study was presented in [J09MJ].

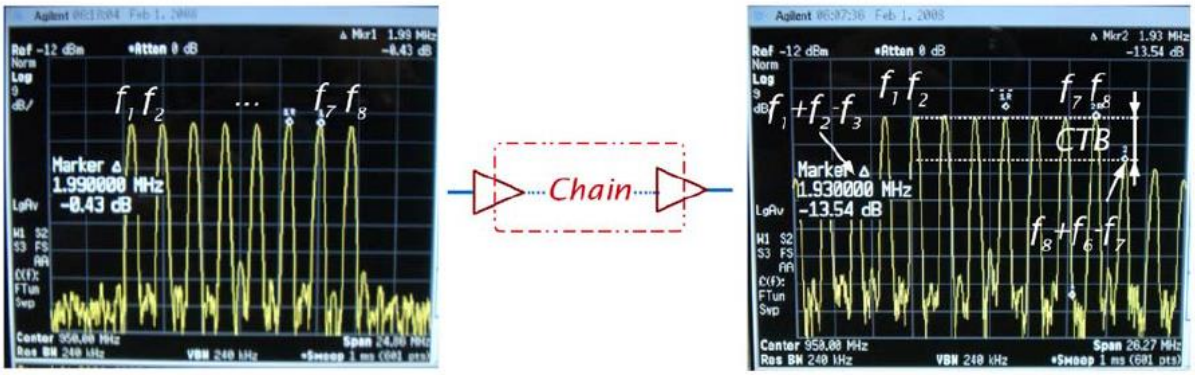

Fig. 12 CTB measurement on a RF chain

B. Virtual Skin model

The behavioural methodology was also applied to a very different area, a biological model of the skin for sun burn prevention. VHDL-AMS allows to model discrete time behavior (as VHDL) and continuous time behavior with differential algebraic equations (DAEs). Sunlight (especially UVA penetrating deeper into the skin) has a profound effect on the skin causing skin aging. We have been able to create a complex functional skin model and its environment and to simulate it dynamically taking a part of the sunlight spectrum as the chain reaction initiator. Therefore, we have divided the whole system in three blocks as explained figure 1 for complexity management purpose: sun UV spectrum, skin interaction and chemical reactions in the skin (Fig. 13.a). We focused our study on the mitochondrial cell as it one of the best-described entity in the literature. The previous generic sensitizer model has been refined for Riboflavin species. When the excited sensitizer interacts with an oxygen, it creates a reactive oxygen species (ROS) which can initiate a lipid chain reaction upon sun radiance. Human skin defenses are included in the model as E vitamin, glutathione, etc. We implemented as a first step, 96 chemical reactions using a 1st order approximation. We use a species dictionary and a code generator based on chemical equations. Therefore, this model can evolve easily to introduce more reactions. First results have confirmed assumption of a lipid chain reaction in the skin initiated by the UVA radiance. 20 Ks real time was simulated in 1 min on a standard PC. After 1Ks UVA radiance, the chain reaction initiates and we measured a lipid half-lifetime of 14 Ks (Fig. 13.b). This result was very promising [C08HS] and this work was continued by System VIP Company.

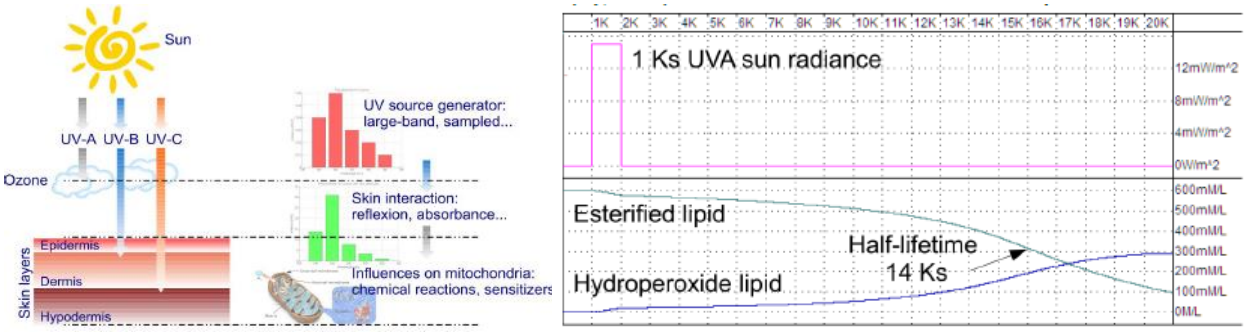

(a) (b)

Fig. 13 **(a) Virtual skin and its environment system architecture, (b) Lipid peroxidation simulation**

IV. Research engineer in IMRA Europe SAS

I worked between September 2008 and September 2009 as a research engineer for IMRA Europe SAS Company. IMRA is an advanced research center in signal processing, image processing and solar cell. It is funded exclusively by the Japanese consortium Aisin Seiki, parts manufacturer of Toyota. I work on several subjects during this year. A first part of my study was focused on the measurement of field over a hybrid car body; a second was focused on the design of integrated antenna for cars.

A. Hybrid car field measurement

Hybrid car exhibit a high level of interference which can corrupt RF receptor. The purpose of this field measurement is to identify the frequency band which can propagate along the Prius body and to find the main current path. 23 different points were measured on the Prius body for electric and magnetic near-field. A spectrum analyser acquires data point between 500 KHz and 20 MHz. For the magnetic field, it was possible to estimate the direction of the surface current by performing two orthogonal measurements on each point.

Thanks to these measurements, we indentify that a propagation channels was present on the Prius body between 6 MHz and 15 MHz. The surface current is mainly flowing by the edge of the metal parts of the car. R&S HZ-11, E and H near-field probe set were used (Fig. 14.a). The H-field probes have the directivity of loop antennas and can be use to determine the current direction on the body. We use a 6 cm loop which offers an E field rejection of 41 dB.

The E-field probes are designed for omnidirectional signal reception over a wide frequency range. On approaching a radiation source, the probe is capacitively coupled with the field. The 3.6 cm spherical probe offers a 30 dB H-field rejection. For each measurement, the probe was placed perpendicular to the body surface. The car was placed on a travelling crane as shown on Fig. 14.b and we test the Prius up to 110 km/h.

(a)

(b)

Fig. 14 (a) Probe field, (b) Probe measurements method

The near field signal is amplified using a 38 dB gain preamplifier. A spectrum analyser records the signal from 500 kHz to 20 MHz for each measure points. Then, measurements are stored in a file with 501 different frequencies and the associated power measurement in dB µV (Fig. 15.a). We intended with this analysis to understand the surface current path on the car body. To help the understanding of this effect, a 3D Prius was modeled with the local surface current value (Fig. 15.b).

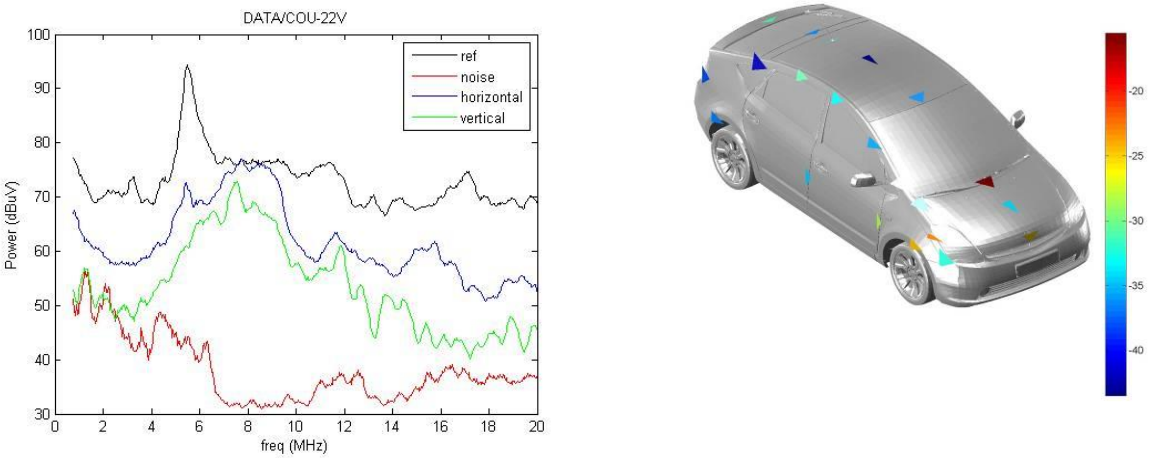

(a) (b)

Fig. 15 **(a) H-field measurement versus frequency, (b) Surface current on Prius body @ 6MHz**

Thanks to these measurements, we indentify that a propagation channels was present on the Prius body between 6 MHz and 15 MHz. The surface current is mainly flowing by the edge and the slot of the Prius body. The whip antenna is well isolated from these current. The electric field is maximal on the slots of the body and exhibits some frequency peak close to the whip antenna.From this measurement, we clearly understand that the next generation of hybrid car will have to take into account electrical motor interference in the AM receptor design.

B. Integrated antenna for cars

The main part of my activity in IMRA Europe was dedicated to antenna design for automotive application. Antenna system are essential in automotive area to receive different electromagnetic wavelengths as radio AM and FM, television, cellular phone, etc … Classical solutions are the whip antenna mounted vertically on the vehicle. The radiation efficiency of this type of structure is good (>70 %) but it reduce the aerodynamic characteristics and obstruct the external appearance of the vehicle. The whip antenna can be broken and stolen, moreover, it produce a wind break noise at high speed. Finally, this antenna has a reduced bandwidth (<30% bandwidth with a return loss < - 6dB).

A second solution is the printed on screen window antenna. These antennas are integrated in the vehicle and imply a low visual obstruction. However, due to their low metal thickness, the efficiency is very low (<10 %) and active element as amplifiers are needed.

Last solution is to use small whip antenna (< 20 cm) with a matching active circuit. The whip height reduction increases its impedance and worsens the obtainable bandwidth. To obtain correct performances, active antenna principle is needed. The antenna feed point is directly connected with an amplifier. This amplifier is optimized for a high input impedance in order to pick up as much as possible from the antenna voltage and to act like an impedance converter. The output of this amplifier is matched to 50 ohm and connected to the coaxial

cable. Antennas for automotive application have to support various bands which are described in Tab. 1.

During my year in IMRA, we developped two different solutions for integrated antenna, and the two topologies were patented. This first one was a wide band antenna integrated in the spoiler of the car; the second one is a monopole with a shark fin shape placed in the top of the roof.

Applications	**Europe (MHz)**	**United State (MHz)**	**Japan (MHz)**
FM radio	88 - 108	88 - 106	70 - 90
DAB	174 - 237	88 - 106	470-770
TV	175 - 862	175 - 806	170 - 770
Car to car	5900	5900	700
WIFI	2400 - 5800	2400 - 5800	2400 - 5800
Cellular	900 – 1800	700-2170	810 - 2170

Tab. 1 Target applications with the UWB antenna

1. Spoiler antenna

Our proposal is to integrate the planar radiating element directly in non metallic part of the vehicle like the air spoiler and the side mirror. This antenna combine a good efficiency (>50%) in a large bandwidth (S11 < -6 dB on a band larger than one decade) and an invisible shape. Air spoiler and mirror are usually made of thermoplastic resin, thus integration of electromagnetic radiating element is possible.

Thanks to the size of the spoiler, usually at least 1 m wide and 20 cm length, it is possible to integrate several antennas for spatial and directional diversity.

Currently, ultra-wide band technologies target applications in the 3.1 GHz to 10.6 GHz band for pulse coded communication. Most recent applications target sensor data collection, precision locating and tracking applications. To fulfil these specifications, specific antennas have been developed with monopole and dipole structure. In addition to the ultra-wide band capabilities, the radiation pattern of these antennas has to be omnidirectional as main applications target mobile devices. Our proposal is to adapt the monopole concept developed for the 3.1 GHz -10.6 GHz band in the 170 MHz-6 GHz band considering the vehicle body , this frequency bandwidth is valuable for the automotive applications (DAB, TV, cellular phone, DSRC, WIFI, …). Concerning the FM radio, a modification of the UWB structure is performed to enable the reception of the FM frequency band.

To cover the FM frequency band, a hole is etched in the monopole and a gap is created near the feeding point. This hole and the gap form a bend monopole, to control the resonance frequency of this bend monopole, a lumped capacitor is inserted in the gap (Fig. 16.a). The capacitance controls the resonance frequency and the bandwidth can be tune on the FM frequency band.

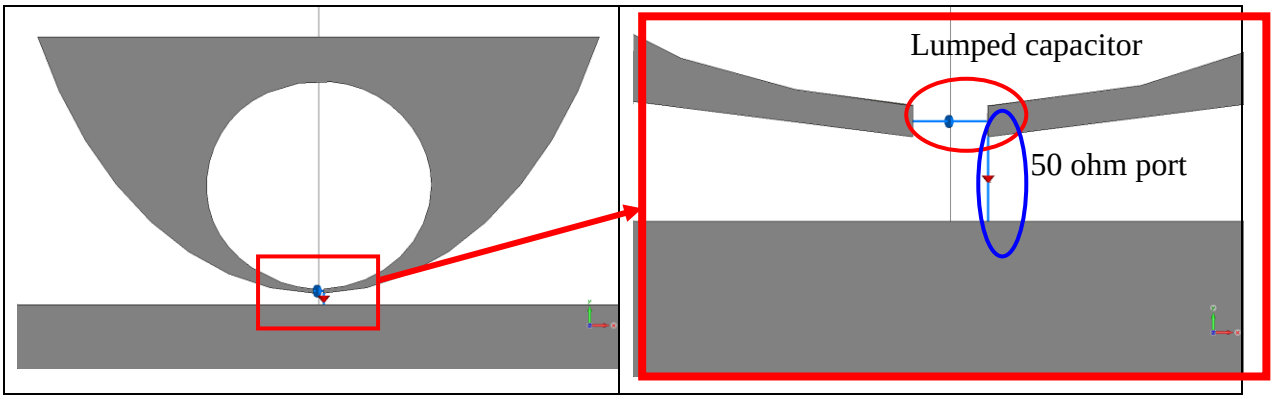

Fig. 16 Figure 1 : UWB antenna with hole and lumped capacitor

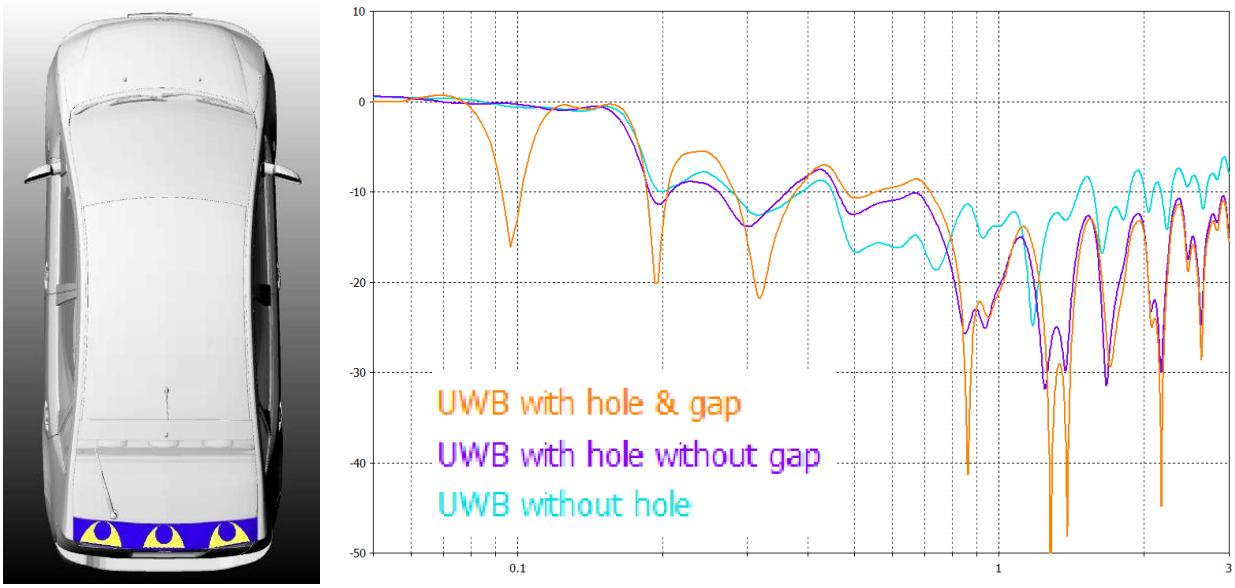

(a) (b)

Fig. 17 (a) Integration of 3 UWB antennas in a air spoiler, (b) Return loss with and without the gap

To confirm the importance of the gap, a simulation is done with the hole but without the gap. The simulation is presented on Fig. 16.b and show that no resonance appears in the low frequency. This effect can be used to optimize the FM reception for the different country, as shown on Tab. 1.

All presented antennas can receive and broadcast several automotive applications in several part of the world as describe in table 1. A synthesis on the two original antennas, the UWB antenna with the hole and the half UWB antenna with the hole, is presented on the Tab. 2.

Concerning the fabrication of this antenna and the integration with the spoiler, a metallic tape (copper) with the shape of the antenna can be set on the spoiler before the painting.

Design parameters	Europe	United State	Japan
Antenna 1 size (m^2)	0.36*0.15	0.36*0.15	0.36*0.15
Lumped capacitor (pF)	60	60	87

UWB band (S11<-6dB)	170 MHz – 6 GHz	170 MHz – 6 GHz	170 MHz – 6 GHz
Low frequency resonance (S11<-6dB)	85-110 MHz	85-110 MHz	69-90 MHz
Antenna 2 size (m^2)	0.15 * 0.19	0.15 * 0.19	0.15 * 0.19
Lumped capacitor (pF)	75	75	110
UWB band (S11<-6dB)	170 - 360 MHz 560 MHz – 6 GHz	170 - 360 MHz 560 MHz – 6 GHz	170 - 360 MHz 560 MHz – 6 GHz
Low frequency resonance (S11<-6dB)	87-108 MHz	87-108 MHz	73-88 MHz

Tab. 2 Synthesis of the antenna dimensions and performances

A prototype was realized and measured (Fig. 18). A mechanically tunable capacitor (10 – 100 pF) was used. This work was patented in [B09IM].

Fig. 18 Figure 2 : Prototype UWB antenna

2. Shark Fin Whip antenna

This second proposal is to use a new shape for the monopole which combines a double resonator for the FM and DAB band, and a UWB monopole for all applications upper than 470 MHz.

Our proposal is to adapt the monopole concept developed for the 3.1 GHz -10.6 GHz band in the 470 MHz-6 GHz band, this frequency bandwidth is valuable for the automotive applications (TV, cellular phone, DSRC, WIFI, …). Concerning the FM radio and DAB, a modification of the UWB structure is performed to create two resonators which are tunable using two capacitors.

The current invention is a multi-service antenna which can be positioned on a roof vehicle. The antenna type is a monopole. It is using the metallic part of the roof as a ground plane. Thanks to a specific design, a size reduction and good performances (gain, bandwidth) are obtained for a small size antenna.

Our solution integrate in a small area (85*120*10 mm) a double resonator for FM and DAB band and an ultra wide band monopole which is matched to 50 ohm (S11 < -6dB) from 470 MHz to 6 GHz (shape on the antenna is shown on Fig. 19.a).

The proposal radiating element is smaller, exhibit a more aerodynamic shape, and provide more applications.

The radiating element is composed by two bended monopole connected together. At the end of the two monopoles, a capacitor is used to increase the electrical length of the monopole and to match it to their specific application (FM and DAB). The position of these capacitors is presented on Fig. 19.b.

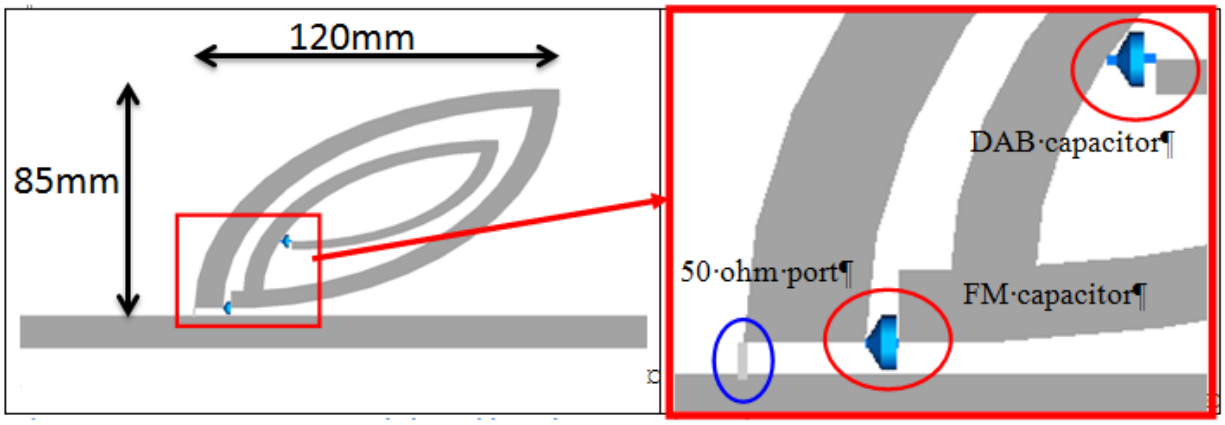

Fig. 19 (a) UWB antenna on a ground plane for shark fin form factor (b) 50 ohm port and capacitors position

For FM and DAB, the two resonances can be tuned by adjusting the value of two capacitors. Simulations presented on Fig. 20.a show the tuning of the FM resonance when the FM capacitance is changed from 3 pF to 1.1 pF. This specificity can be used to tune the FM resonance to the local region band (70-90MHz for Japan and 87-107 MHz for EU and US).

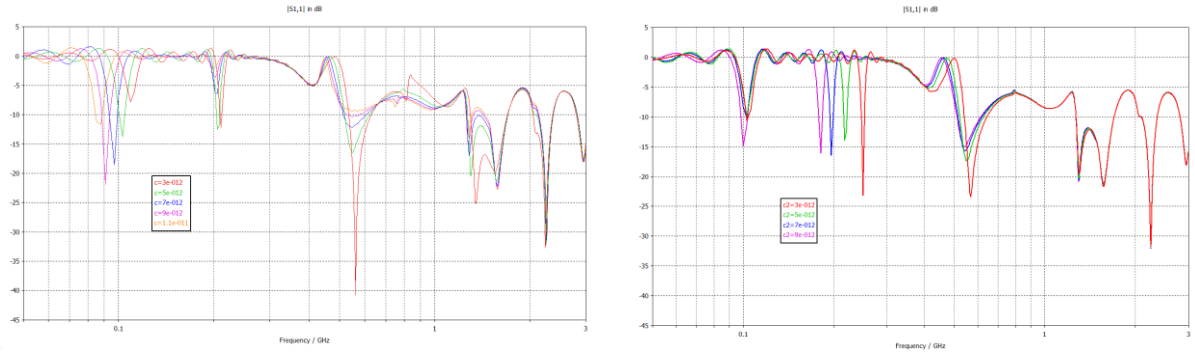

(a) (b)

Fig. 20 (a) Return loss for different FM capacitances, (b)Return loss for different DAB capacitances

Fig. 20.b presents the simulation of the return loss for different DAB capacitance (from 3 pF to 9 pF). Results show that the DAB resonance is tuned while other frequencies remain stable.

This characteristic facilitates the design of the antenna, as the system can be quickly optimised. It is also possible to use varactors instead of classical capacitors, and to obtain an active tuning to optimize dynamically the reception.

For FM and DAB, the size of the resonator increases its impedance and worsens the obtainable bandwidth. To obtain correct performances, active antenna principle is needed.

The topology of the active circuit is presented on Fig. 21, with 3 separate channels for AM, FM/DAB and TV/GSM/etc applications.

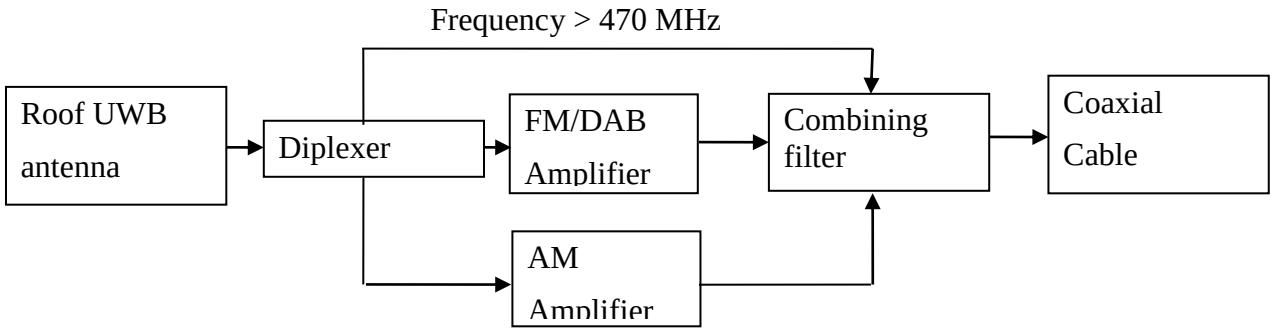

Fig. 21 Topology of the active circuit

For FM and DAB, the small size of the resonator increases its impedance and worsens the obtainable bandwidth (impedance is typically higher than 1 kΩ on the band). To obtain correct performances, active antenna principle is needed.

The topology of the active circuit is presented on Fig. 21, with 3 separate channels for AM, FM/DAB and TV/GSM/etc applications. To separate the signal between these three channels, classical diplexer and combining filter is used (passive filter) as shown on Fig. 22.a.

For the FM/DAB channel, the antenna feed point is directly connected with an amplifier. This amplifier is optimized to get high input impedance and output matched to 50 Ω. This circuit pick up as much as possible from the antenna voltage and act like an impedance converter, then the 50 Ω output is connected to the coaxial cable through the combining filter. The amplifier is design for optimal performances for FM and DAB band. The FM and DAB amplifier consists of one amplifying stage equipped with a GaAs HEMT transistor. This type of transistor has excellent noise-figure and transconductance, achieves good linearity and high input impedance (> 1 MΩ). The voltage gain of the stage is a trade-off between sensitivity, noise level and linearity.

This structure was patented in [B09IM2].

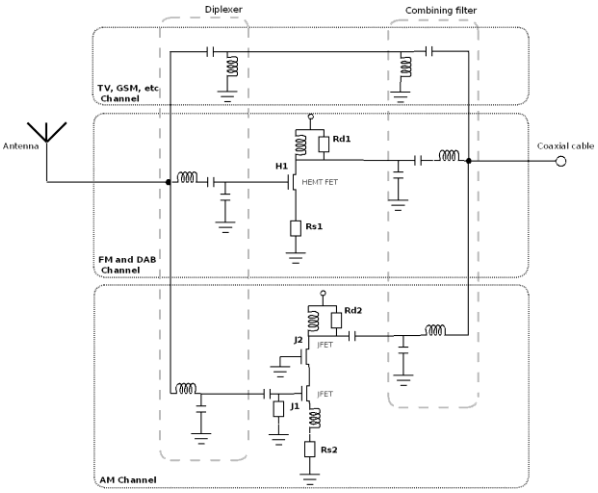

(a)

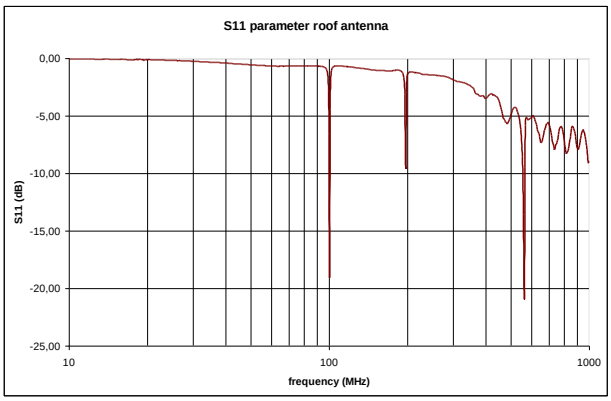

(b)

Fig. 22 (a) Example of schematic for the active circuit, (b) Measurement of the return loss of the passive antenna

For AM channel, impedance matching is not needed due to the high external noise. AM amplifier is built around a JFET cascode stage as shown of Fig. 22.a. JFET technology is used as it presents a high immunity to flicker noise. Thanks to the cascode configuration, the Miller effect upon the J1 transistor is avoided and a low input capacitance is provided. As for the FM/DAB amplifier, the gain is a trade-off between sensitivity, noise level and linearity.

V. Postdoc on NAOMI project (ANR)

In September 2010, I started a one-year Post-Doc in the frame of NAOMI ANR project. The main goal of the NAOMI project was the antenna miniaturisation using innovative material for DVB-H application.

Digital video broadcasting for handheld terminal (DVB-H) is emerging as a new service for mobile multimedia device. The operating frequency is ranging from 470 MHz to 702 MHz (relative bandwidth 40 %). The free-space wavelength at the lower end is large (λ_0=64cm) compared to the typical size of handheld devices which implies to miniaturize the radiating element. However, miniaturization of antennas is well known to reduce the bandwidth and to decrease efficiency. DVB-H standard is based on the use of 8 MHz tunable narrow channels selected over the whole DVB-H bandwidth. Narrow band tunable antennas have the potential to exhibit higher efficiency, smaller size and lower return losses. The purpose of our study was to develop small antennas placed on a 230*130mm² PCB ground plane for a tablet PC or portable TV handset.

A. Tunable DVB-H antenna

1. Design

For this type of application, the size of the screen occupies the main part of the chassis and only a small volume can be dedicated to antennas. As folded monopole structure was chosen for its good tradeoff between bandwidth, size and efficiency, a small clearance zone in the corner of the PCB (30 *8 mm²) is realized. The monopole (total length 12 cm) is folded in a 2.7 mm3 volume (30*8*8). A view of the antenna is given on Fig. 23. The antenna center frequency without the varactor diode is 979 MHz. Monopole usually exhibits an impedance of 33 Ω at the resonance frequency. However, when the internal monopole antenna is placed closer to the PCB, the resistive part of the antenna impedance collapses. In our study, using HFSS microwave EM simulator, the resistive part of the impedance is found to be equal to 9 Ω, which is rather small. To add some tunability on the resonance frequency, a varactor diode is positioned between the top of the monopole and its basis. To simplify the study, an analytical model is determined. An equivalent series resonance circuit can be used to model the monopole antenna behavior. The varactor diode is modeled using a capacitor and a resistor in series. The varactor diode is shunting a large part of the resonator inductance (3/4) and a small part of the resistance (1/10). These ratios were determined by fitting the simulated curves with the circuit model using Agilent ADS simulator. An equivalent circuit model of the whole radiating structure is proposed on Fig. 24.a. However, due to the small resistive part of the impedance, a matching circuit is also required. The matching circuit is implemented by using an open stub which is more convenient to match a series resonator on a wide band. The stub is placed closed to the ground plane as shown in Fig. 23. The Smith chart for a varactor capacitance of 2.35 pF for several lengths of the stub is presented in Fig. 24.b. Comparison is made between the model and the EM simulation and a good agreement is found. Optimum stub has to match the antenna on all the DVB-H coverage. As bandwidth is narrower at low frequency, stub length has to be chosen to enlarge the -10 dB bandwidth at 474 MHz. The optimal bandwidth is obtained for a length of 29.4 mm.

2. Prototype and experimental results:

A prototype was realized. The bended monopole was fabricated in nickel silver using micromachining technique. The monopole is then soldered on the FR4 substrate. A surface-mount GaAs hyperabrupt varactor from MACOM (MA46416) was used. A 50 Ω-microstrip line across the ground plane is used for the RF feeding and for the DC biasing of the varactor. As the monopole is folded on itself, a 100 pF capacitor acting as a DC block and an RF short circuit is introduced in the metallic strip just after the varactor, allowing a part of the monopole to be DC isolated. This part is then connected to the DC ground potential by using a thin line including a choke inductor to block the RF signal. The details of the biasing circuit are shown on the Fig. 23.

Return loss measurements of the antenna with varactor reverse bias voltages between 2.5V and 10.5V are presented in Fig. 25.a. The operating frequency was continuously tuned over the DVB-H band. Concerning the bandwidth, the narrowest -6 dB return loss bandwidth (10MHz) was measured at 470 MHz. At 700 MHz, the bandwidth was 20 MHz. Thus, the antenna fulfils the DVB-H specifications. The efficiency of the antenna was measured using Wheeler cap method [WHE59]. A metallic box of 23*23*40 cm3 was used to perform measurements. Fig. 25.b presents the simulated and measured efficiency and DVB-H specification for 5 different frequencies. A good agreement is found between the EM simulation and the Wheeler cap method. Due to cavity mode in the Wheeler cap, efficiency measurement for frequency higher than 650 MHz was not possible but simulation shows that efficiency continue to increase. Thus, a comfortable safety margin is obtained from ETSI specifications. This work was presented in [J10MO].

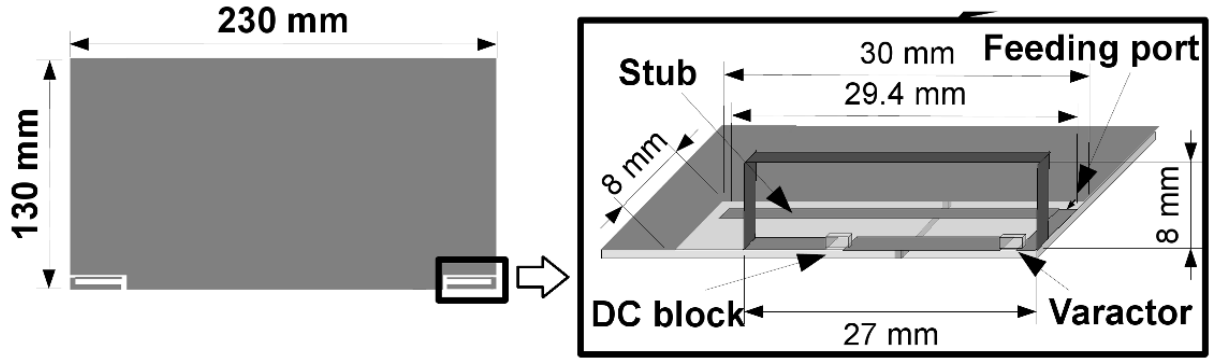

Fig. 23 Antenna geometry

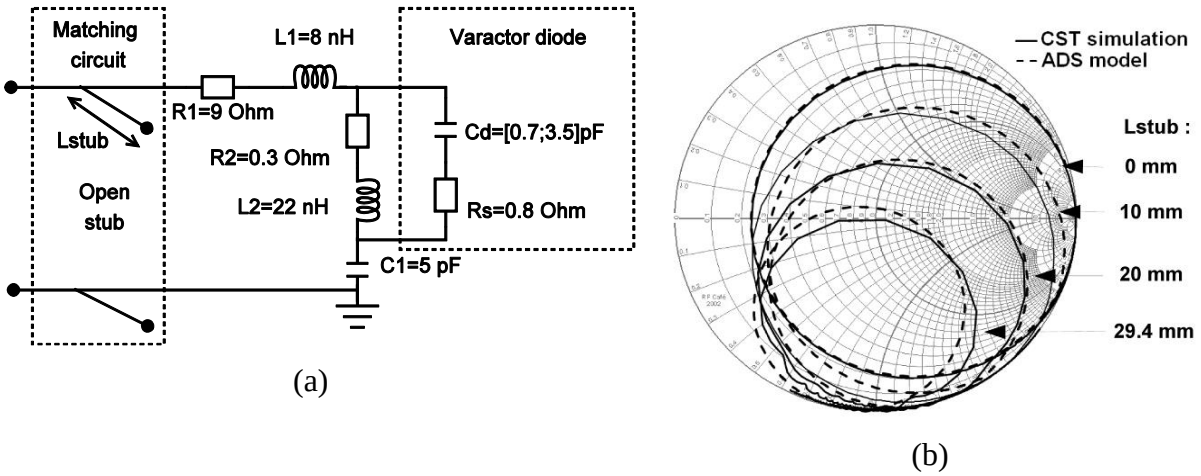

Fig. 24 Equivalent circuit, (b) Smith chart comparison

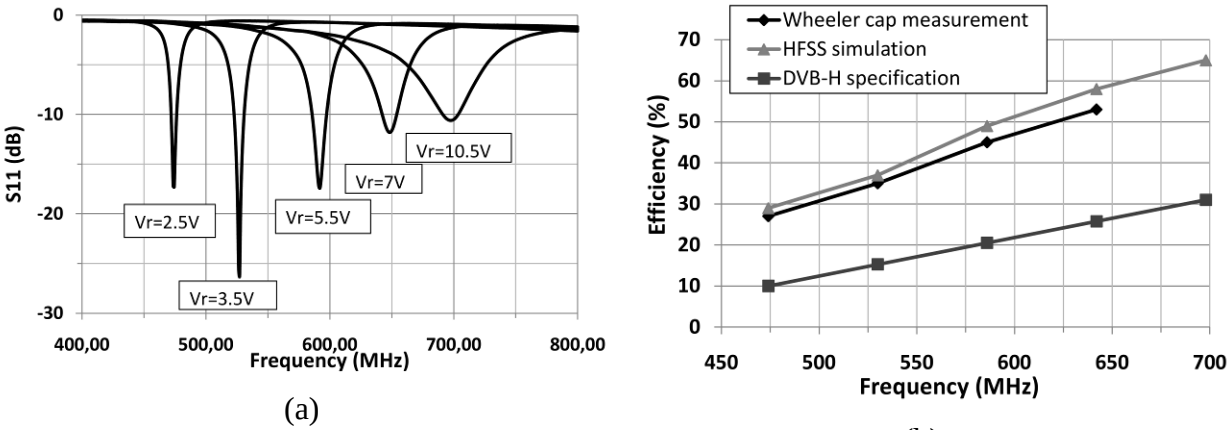

(a) (b)

Fig. 25 (a) S_{11} for 5 different voltages, (b) Simulated and measured efficiency

B. Magneto-Dielectric Tunable UHF Antenna

The second part of my Post-Doc was focused on the use of Magneto-Dielectric material for antenna miniaturization. Compared to high permittivity dielectric, high permeability materials have the capability to reduce the size of the antenna without decreasing the relative bandwidth and total efficiency [SOU10]. However, such magneto-dielectric material get higher losses than classical substrate, thus an accurate study has to be realized to quantify the real impact of such resonators on miniature antenna. This work was presented in [J10AW].

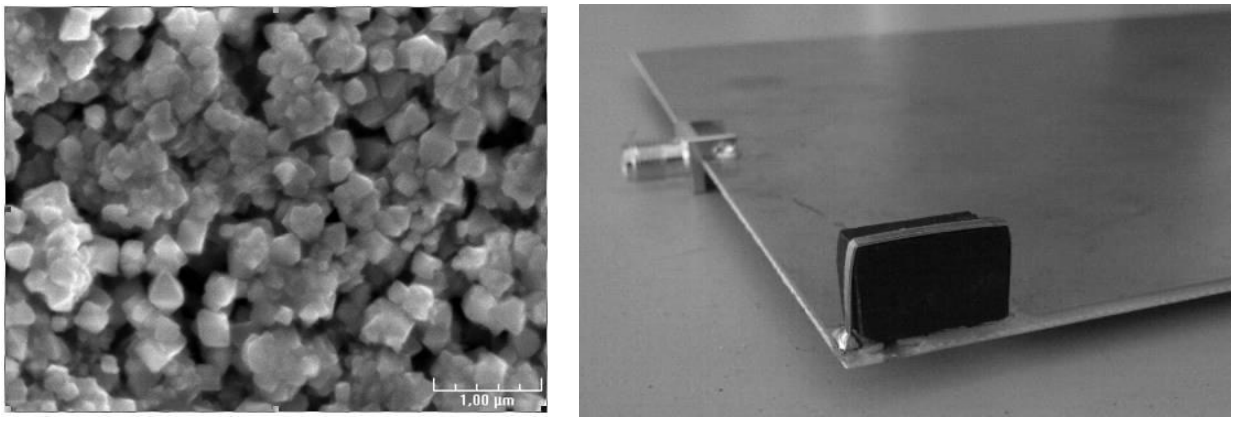

(a) (b)

Fig. 26 (a) Magneto-dielectric porous ceramic, (b) Picture of antenna B prototype

1. Magneto-dielectric material

The purpose of our study was to develop small antennas placed on a 230*130mm² PCB ground plane for a tablet PC or portable TV handset. In this work, a new iteration of magneto-dielectric material used in [SOU10] and [PIN10] was implemented. Thanks to a hot isostatic pressing technique, the average magnetic losses were reduced by a ratio of 13 % on the DVB-band. To evaluate the interest of this material, two different antennas were designed with and without the magneto-dielectric resonator. Two separate prototypes have been realized and measured to compare their radioelectric performances.

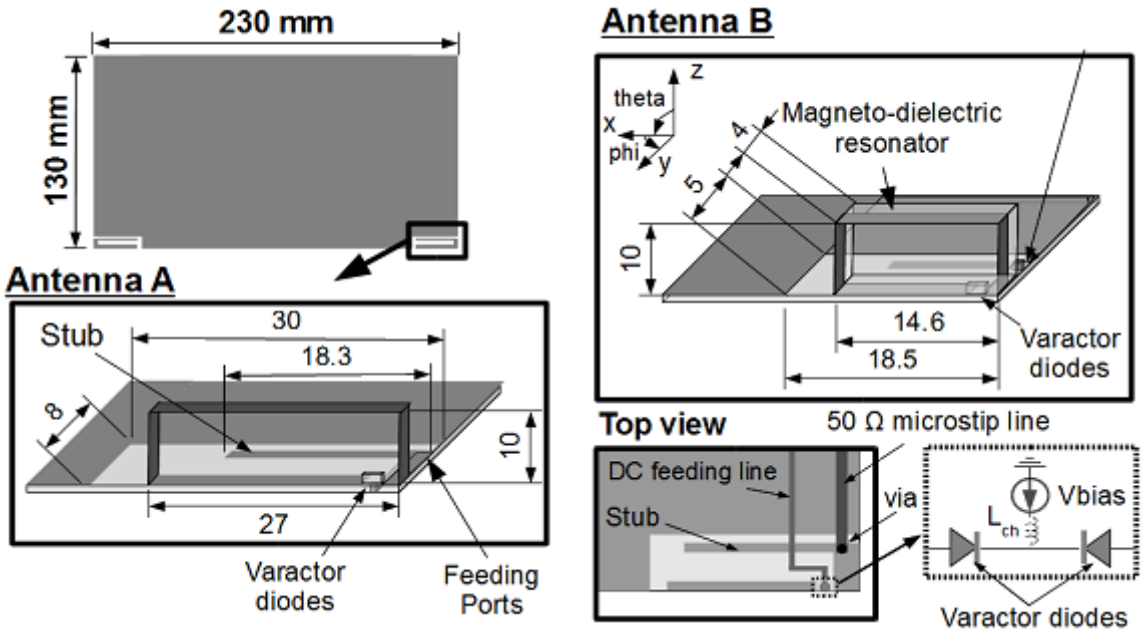

Fig. 27 Antenna A and B dimensions (all dimensions are in mm)

For last year, a new type of magneto-dielectric material composed by a $Ni_{0.5}Zn_{0.3}Co_{0.2}In_{0.02}Fe_{1.98}O_4$ nanopowder has been developed by LabSTICC laboratory. After shaping and appropriate thermal treatments, a porous ceramic is obtained. A picture of the porous ceramic is presented on Fig. 26.a. Its unusual electromagnetic properties come mainly from the nanometric size of the magnetic particles, and from the controlled porosity of the substrate.

From measurements, a magnetic permeability ranging between 4.8 and 5.8, and a dielectric permittivity of 4.5 were found. Losses were measured to be in the 10^{-3} and 10^{-2} ranges for dielectric and magnetic losses respectively. Magnetic permeability, dielectric permittivity and losses are relatively constant versus frequency. However, magnetic losses increase quickly from frequency of 700 MHz. Therefore, porous materials made of nanosized particles have been used, to overcome problems of fully sintered magneto-dielectric materials. The obtained material shows electromagnetic properties suitable for antenna miniaturization up to 800MHz.

2. Antenna structure

The antenna structure is very similar to the one presented previously. Two different antennas were optmized using CST electromagnetic solver. The first antenna is not using any resonator (antenna A) and the second is using the magneto-dielectric ceramic as a resonator (antenna B). Because of the radioelectric characteristic of the magneto-dielectric material, the size of the second antenna is reduced in volume by a ratio of 2.6 in comparison to the first antenna (Antenna A is 2.4 cm^3 and Antenna B is 0.925 cm^3). All dimensions of both antennas are described in Fig. 27. A tunable capacitor (MA46416) is then positioned between the top of the monopole antenna and its base. Two separate prototypes are realized for antennas A and B.

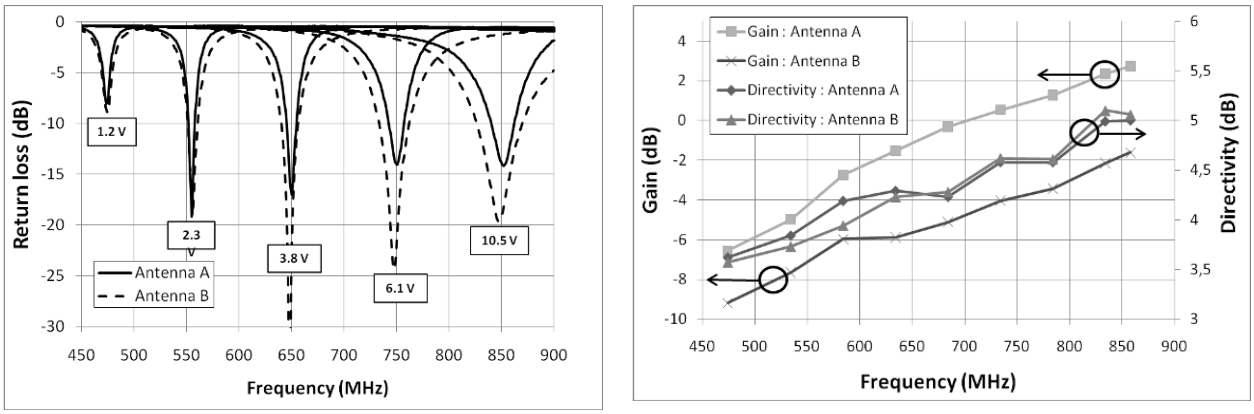

(a) (b)

Fig. 28 **(a) Return loss for antennas A and B for different reverse voltages, (b) Gain and directivity of antenna A and B versus frequency**

3. Measurements

Return loss measurements of antennas A and B versus frequency for varactor reverse bias voltages varying between 1.2V and 10.5V are presented in Fig. 28.a. The operating frequency was continuously tuned over the DVB-H band. Measurements show that for both antennas, resonance frequencies correspond to the same reverse voltage on the varactor diodes, thus they add equivalent losses to both antennas. Concerning the bandwidth, the narrowest -6 dB return loss bandwidth (9MHz) was measured at 474 MHz for antenna A. Despite the fact that antenna B is smaller than antenna A, antenna B has a wider bandwidth for all the different voltages. At 850 MHz, -6 dB return loss bandwidth is 50 MHz for antenna A and 80 MHz for antenna B. This effect is mainly due to the losses in the magneto-dielectric material, and the bandwidth enlargement is greater at higher frequencies where magnetic losses are stronger. Eventually, both antennas fulfill the return loss DVB-H specifications. Radiation measurements were performed on a Stargate-24 measurement station with SATIMO facilities. Measured directivity and realized gain are presented for both antennas on Fig. 28.b. Directivity for both antennas is quite similar on the DVB-H band and naturally increases with frequency. However, the directivity remains low on the DVB-H band (< 5 dB). Furthermore, the gain is lower for antenna B compare to antenna A. At 470 MHz, the gain of Antenna A is 1.8 times larger the gain of Antenna B, while the volume ratio between them is 2.6. These results confirm that magneto-dielectric material can help to maintain a correct efficiency when the size of the antenna is reduced. However, the gain difference between both antennas increases versus the frequency (2.6 dB @ 470 MHz and 4.2 dB @ 860 MHz) which confirms that losses in magneto-dielectric material increase with frequency. The European Telecommunications Standards Institute (ETSI) recommends a gain of -10dB at 470 MHz [ETS05], and this specification is respected for both antennas.

C. References

[SOU10] D. Souriou, J. L. Mattei, S. Boucher, A. Sharaiha, A. C. Tarot, A. Chevalier, P. Queffelec: "Antenna Miniaturization and Nanoferrite Magneto-Dielectric Materials", ANTEM 2010, Ottawa, July 2010.

[PIN10] J.-F. Pintos, A. Louzir, P. Minard, J. Perraudeau, J.L. Mattei, D. Souriou, P. Queffelec, “Ultra-Miniature UHF Antenna using Magneto-dielectric Material”, ANTEM 2010, Ottawa, July 2010.

[WHE59] H. A. Wheeler, “The radiansphere around a small antenna,” Proceedings of the IRE, vol.47, pp. 1325-1331, August 1959.

[ETS05] “Digital Video Broadcasting (DVB), DVB-H Implementation Guidelines”, ETSI TR 102 377 v1.2.1, Nov. 2005.

Research activities as " Maître de conférences" (2010-2014)

I was recruited in October 2010 as a "Maître de conferences". I've divided my research activities into three main parts: the first one concern the design reconfigurable antenna in UHF band. The second part is dedicated to the optimization of miniaturized, multi-band and multi-antenna system, and the last part deals with design and characterization of millemeter waves communcation systems.

VI. Reconfigurable antenna

From the really beginning of my research career, I've been strongly involved in reconfigurable activity. First, because I've a strong background in electronic and micro-electronic and it was obvious for me to try to mix my education with my research topic. Secondly, when I start my PhD, MEMS for RF was at the really beginning, and there was a feeling in the antenna community that this new type of component was going to revolution the antenna market. 10 years after, MEMS are still an interesting axis of research, but no successful application to massmarket has been demonstrated so far. Then, most of my work has been done using PIN diodes and varactors, and more recently CMOS Digital Tunable Capacitor (DTC).

A. Motivation

In recent years, telecommunication technologies have witnessed exponential growth, especially in the cellular communications and wireless sensor networks segment. To meet the demand for increasing transmission capacity, improving the signal to noise ratio of cellular communication channels and expanding the operating band of the equipment is necessary. For example, when LTE standard was designed and deployed, several new bands were added. Moreover with latest LTE realease, Multiple Input Multiple Output (MIMO) schemes and aggregation have been implemented. Moreover, additional feature have been added to mobile phone terminal as DVB-H for video broadcasting. The expansion of the operating band poses a huge challenge, especially in the low frequency band, because of the large wavelength.

Some new frequency ranges are proposed for the future deployment of 5G systems, such as 410-430, 470-790, 1000-1700, 2025-2110, 2200-2290, 2700-5000, 5350-5470, and 5850-6425 [ITU13] as shown in Fig. 29. For each frequency band, the strategies and utilizations are different such as the lower frequency bands (for example 470-790 MHz) are suitable for providing coverage for both indoor and outdoor due to its great propagation characteristics. And higher frequency bands (for example 3400-3800 MHz) are most suitable to provide high capacity and performance for small coverage, etc. In [HUA13], White paper from Huawei proposed a tentative spectrum for WRC-15, accompanied by the detailed analysis and the summaries for each frequency band. This document mainly discussed about possible candidate bands such as 470-694 MHz, 694-790 MHz, 1350-1525 MHz, bands around 2 GHz, 3600-4200 MHz, and 4400-4990 MHz. The design of a wireless system that has one or more multi-standard antennas integrated in a mobile device is very difficult. Passive antenna has reached a limit, and the use of frequency reconfigurable antenna to extend operational bandwidth is a promising solution. Besides, in wireless sensor networks application, directional reconfigurable antenna has the potential to reduce collisions, increase communication distance and optimize consumption, when compared with traditional omnidirectional antenna. The main objective of this part was to design and optimize the reconfigurable antenna for cellular communications and wireless sensor network.

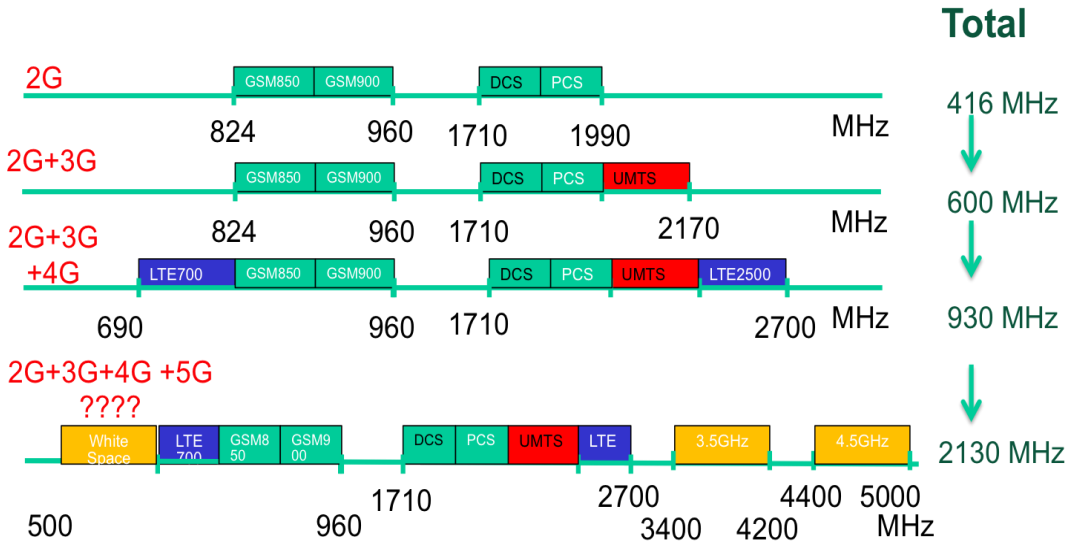

Fig. 29 Frequency spectrum requirements for future standard antenna

B. DVB-H reception system

This study has been done in the frame of Florian Canneva PhD and ANR NAOMI project. I start to supervise this work during my Post-doc, and i simply continue it with my MCF position. Jean-Marc Ribero was the main supervisor and Robert Staraj contributes to this study. This research worked was dedicated to frequency reconfigurable antenna using PIN diodes or Varactor diodes. Many solutions were developed during this PhD, I will focus on two different work: a PIFA reconfirable antenna and an active system for improvement of antenna isolation.

1. Reconfigurable PIFA

The antenna consists in a Printed-Inverted-F-Antenna (PIFA) of dimensions 30x30 mm^2, 5 mm above a printed circuit board of dimensions 230x130 mm^2. The geometry of the structure and its position on the ground plane is given on Figure 1. The antenna is loaded by a varactor diode, connected to the upper metallic plate by a 3-mm width metallic strap of also 2-mm height, which will allow to choose the desired channel in the DVB-H band. Indeed, as the frequency behavior of the PIFA can be modeled by a RLC shunt resonator, by changing the capacitance C the varactor diode allows to select the desired resonance frequency. The RF/DC decoupling of the reverse bias voltage applied to the varactor is obtained by a slot etched in the ground plane. An extra 100 pF CSM capacitor is placed across the slot to increase its capacitance and to keep the antenna matched. The ground plane is designed on a 0.8-mm thick FR4 substrate with a dielectric permittivity er = 4.7. Dimensions and position of the decoupling slot are shown on Fig. 30. The width of the slots is 0.2 mm. This work was preented in [J11MO2]

To simulate the varactor diode, a simplified equivalent circuit made up of a resistor in series with a variable capacitor was used. Return losses for different values of the capacitor have been simulated using Ansoft high frequency structure synthesizer (HFSS) solver. A prototype has been realized using a surfacemount GaAs hyperabrupt varactor from MACOM (MA46416). For reverse biasing voltage values Vb from 0 to 20 volts, the varactor diode capacitance varies from 6 to 0.6 pF. Simulation and measurements for four different biasing voltages of the varactor are given on Fig. 31.a. Measurements agree with the simulation. As we can see, for a biasing voltage between 1.55 and 8.06 V, the proposed radiating element reaches to cover the whole DVB-H band, with for each frequency, a _10- dB bandwidth equal or superior to 8 MHz. Simulations of the efficiency have been done for four different frequencies (474,590, 690, and 874 MHz) using HFSS electromagnetic simulator.

Furthermore, the efficiency satisfies the specification required for the DVB-H standard. For example, radiation efficiency, total efficiency and return loss at the lower channel of the DVB-H standard, (channel 34, from 470 to 478 MHz) are given in Fig. 31.b. In this channel, the total efficiency is upper than 25%, whereas the specification is only 10%.

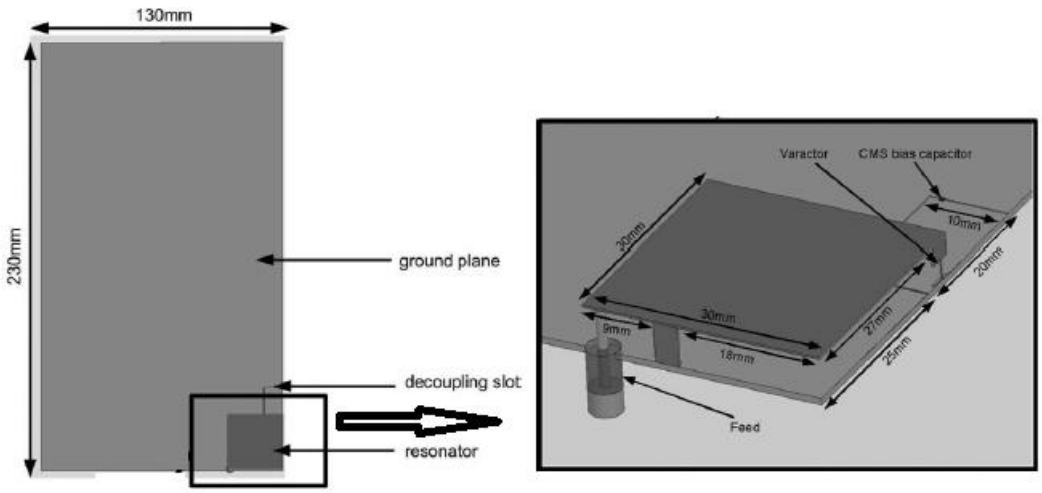

Fig. 30 Antenna geometry

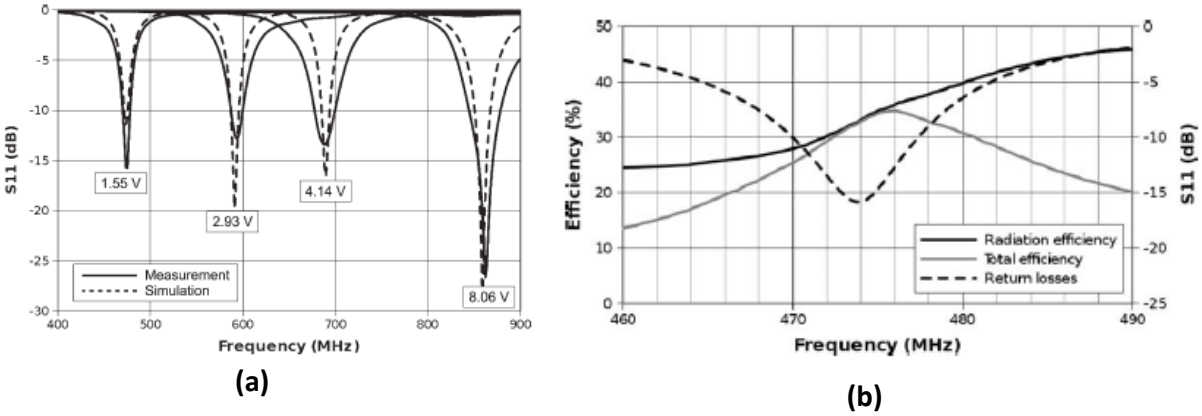

Fig. 31 (a) Measurements and simulations of the return losses for different bias voltage, (b) Measurement of S11, total efficiency, and radiation efficiency at 474 MHz

2. Active system for improvement of antenna isolation.

A modified version of the previous antenna was used in this study. Two PIFA have been placed on a ground plane of 100*60 mm^2. It has been shown that the performance of the antennas can be improved by a good coupling with the ground plane. Then, to have the best electromagnetic performance than we can we place the antennas at the position given Fig. 32.a.

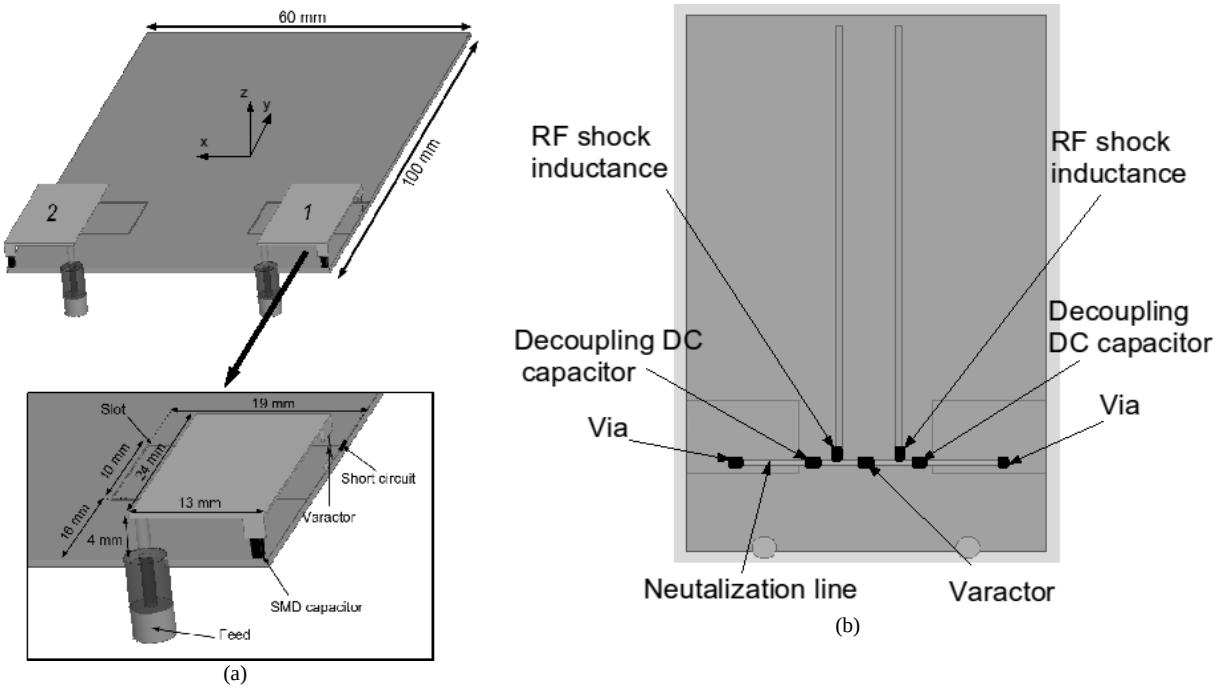

Fig. 32 (a) Position of the resonator on the PCB, (b) Active neutralization line

The Fig. 32.b presents position and dimensions of the active neutralization line. The principle is to use a line to change the equivalent impedance between the two ports and then to reduce the transmission throw. Unfortunately this technique is too narrow band to cover the band needed for the DVB-H standard. By changing the value of the equivalent capacitor of the varactor, we will change the equivalent impedance between the two ports. The varactor choose in order to decoupling the two antennas in the wanted frequency range is the MACOM 46418 which has a range of equivalent from 3 to 0,3 pF for a bias voltage from 1 to 9 V. To decoupling the RF/DC tension, we use SMD (Surface Mounted Device) stock inductance of 4,7 µH and lying capacitor of 100 nF.

The system has been realized using micro-machining techniques. The S parameters of antennas have been measured for different configurations at 400 and 500MHz. Measurements have been also compared with simulation in each case. Fig. 33 a & b represent respectively the S parameters of the system when the antennas work at 400 MHz in a non-optimal case (a) and in an optimal case (antennas are well-matched and decoupled). In the first case, the bias voltage for antennas 1 and 2 are respectively 1,11 V and 1,63 V and the varactor on the neutralization line is not biased. For the second case, the bias voltage for antennas 1(V_1) and 2 (V_2) are respectively 1,11 V and 1,56 V and the bias voltage for the neutralization line V_{bias} is 4.2 V. By adapting the neutralization line we reduce the S_{21} from -7.5 to -27 dB.

We can easily observe that, by adjusting the good bias voltage and so adjusting the good value of the equivalent capacitance of the varactor, we can dramatically reduce the coupling between the two elements. Furthermore, the reduction of the coupling between the two antennas improve the matching of it. Then the S_{11} decreases from -7 to -22 dB. Fig. 34 a and b show respectively the results of the measurement that have been done for other working frequencies, when the antennas resonate at 506 MHz when the line is not biased (V_1 = 2.06 V, V_2 = 2.34 V, V_{bias} = 0V) and when the line is optimized (V_1 = 1.96 V, V_2 = 2.22 V, V_{bias} = 5,6 V). The adjustment of the bias voltage reduces the S_{21} from -9 dB to-35 dB and S_{11} from -5 dB to -17 dB.

We can observe a small difference between measurements and simulations. This should be due to the biasing wire. Indeed at low frequency the wave length is more important, then, in

spite of the decoupling RF/DC component using, the wire will have an influence on an influence on input impedance. In addition, the technical datasheet of varactors claim an error on the value of the capacitance of 10%.

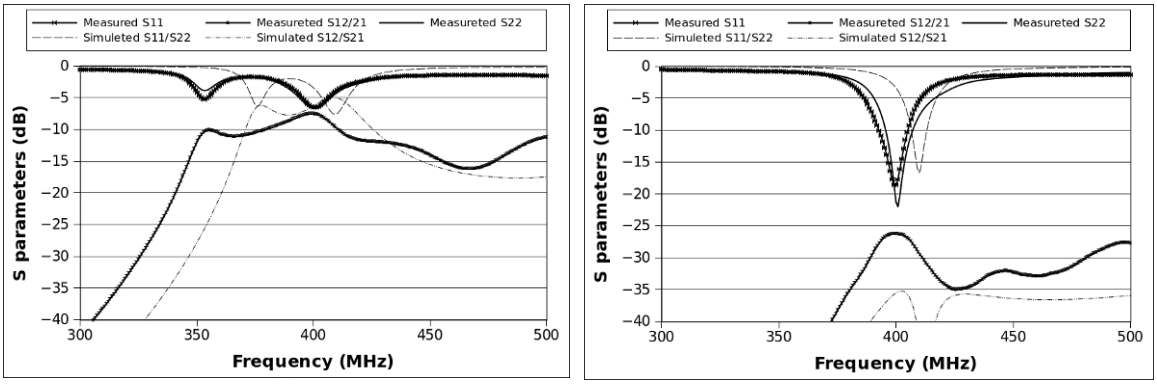

Fig. 33 Measured S parameters when the two antennas work at 400 MHz for the case the reconfigurable line is not optimized (a) and the reconfiguration line is well-optimized (b)

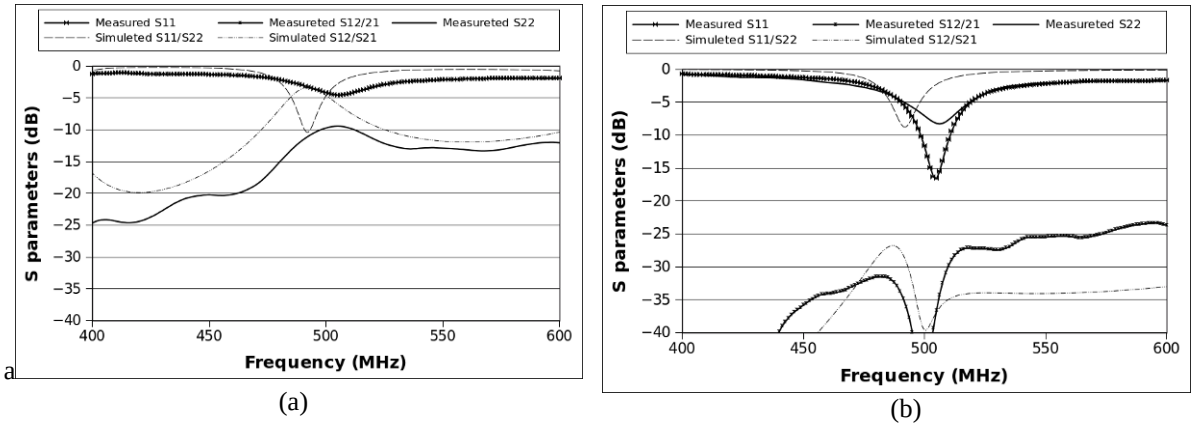

Fig. 34 Measured S parameters when the two antennas work at 500 MHz for the case the reconfigurable line is not optimized (a) and the reconfiguration line is well-optimized (b)

C. Tunable Antenna designs using MEMS switch for 4G communicating devices

This study was realized in the frame of the ARTEMOS project, whose objective whose main target is to design tunable architectures for the RF front ends in future mobile handheld terminals. This work was realized in the frame of Aykut Cihanghir PhD, under the main supervising of Cyril Luxey and Gilles Jacquemod. This study was presented in [C13LA]

With the introduction of the fourth generation (4G) of cellular mobile communications, there has been an increase in the frequency bands that a generic mobile phone should be able to operate. This requirement poses some challenges in the design of the transceiver modules of the device as well as the RF front-end and the antenna.

From the antenna design point of view, the newly added frequency bands especially LTE bands 12-13-17 which goes down to 700MHz creates the main design challenge: covering

700-960MHz (30% bandwidth) in the low-band, considering also backward compatibility with the former technologies like GSM850/900. Since the space reserved for the antenna is electrically small in this frequency range and tends to decrease, special design techniques are necessary to obtain the required bandwidth for a generic mobile terminal antenna.

In this work, a reconfigurable designs for 4G coverage in mobile terminals have been proposed. Different antenna topologies are evaluated consisting of tunable antennas as well as single/multi-feed structures.

1. MEMS switch component

With the new functionalities continuously being added to mobile handheld devices, the necessity of covering more and more frequency bands from the antenna design perspective has arisen. Since the dimensions of the space reserved for the antenna has been kept almost the same although the necessity to be more broadband and also with the introduction of the LTE frequency bands going down to 700MHz, the challenge has even become harder for the antenna designer. One of the methodologies to overcome this challenge is using reconfigurable (or tunable) antennas using tunable components like MEMS switches. This components can be used directly in the antenna structure (for example to tune electrical length of a strip) as well as at the antenna feed to tune the input impedance. An antenna design using a MEMS switch was realized to switch between the operating bands, which are selected as low-band (LB; 700-960MHz) and high-band (HB; 1.7-2.7GHz).

The MEMS switches that are to be used are designed and manufactured by DELFMEMS [DEL13].

The mechanical principle is based on two main innovations: the fact the movable membrane has no anchors and that both states are forced states. The membrane used for the electro-mechanical function is an anchorless membrane. It is just simply supported over two pillars so the degree of freedom are not the same compared to classical cantilevers (clamped-free membrane) or bridges (clamped-clamped membrane) based structures. Two sets of electrodes combined with two pillars create a lever effect which enables a push pull effect.

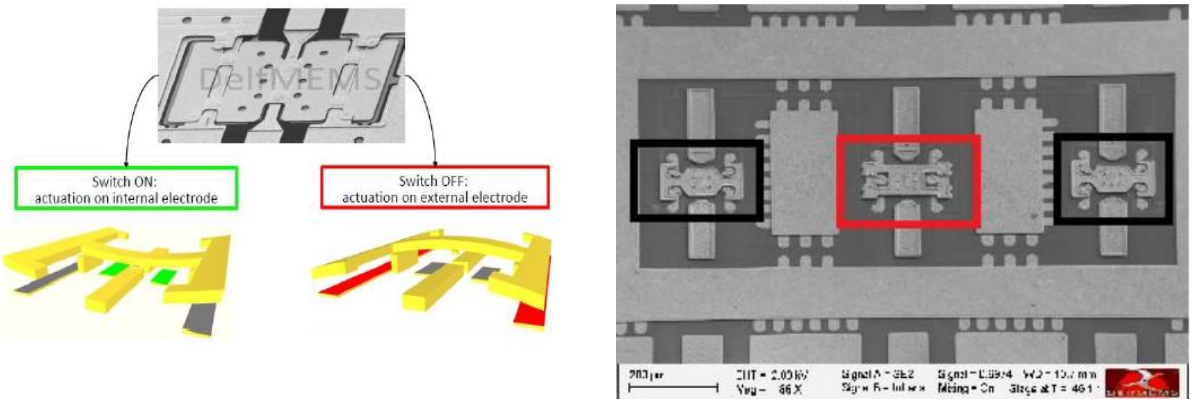

Fig. 35 (a) Schematic view of the two forced states, (b) SEM view of a SPST cell including 3 SPST

On state and off state are performed respectively when internal or external set of electrodes is actuated as illustrated Fig. 35.a, on state is provided when internal actuation is performed (voltage applied on inner electrodes); forced OFF state is provided when external actuation is performed (voltage applied on outer electrodes). The main drawback of such design is that a dual command is necessary in order to properly drive the device. A SEM view of the SPST cell is presented in Fig. 35.b.

Insertion loss (IL) was measured on several devices with values at 2GHz between 0.25dB and 0.28dB and below 0.42dB at 5GHz (Figure 3.a). One of the major contributors to the insertion loss is the parasitic capacitance created by the horizontal feed-through when crossing the sealing ring of the packaging. For the next run the width of the sealing ring will be highly reduced thus decreasing the capacitance. Hence, the IL will be automatically decreased.Concerning the reflection coefficient, a matching below 15dB is obtained up to 5GHz.

2. Reconfigurable Antenna Design

The antenna design use MEMS component for band-switching between the LB and HB. The antenna excitation methodology is based on the selection between two driven strips. The proposed antenna layout can be seen in Fig. 36.a. The antenna is directly printed on the FR4 substrate having dimensions of 115mm X 60mm X 0.8mm, with a ground clearance of 15mm for the antenna. The antenna consists of two driven strips, one for LB coverage and one for HB coverage. To increase the bandwidth potential in the LB, a parasitic element (printed under the substrate) was again used, which is capacitively excited by the LB driven strip and connected to the ground plane over an SMD inductor (18nH) on the other end. The inductor used in the ground connection helps to increase the electrical length of the parasitic strip, thus arranging the resonance frequency created by the parasitic strip. One SPDT MEMS switches is used to direct the excitation current either through the LB path or the HB path as seen in Fig. 37.a. When the LB driven strip is excited, the parasitic strip is also capacitively excited, enabling a higher bandwidth potential in the LB.

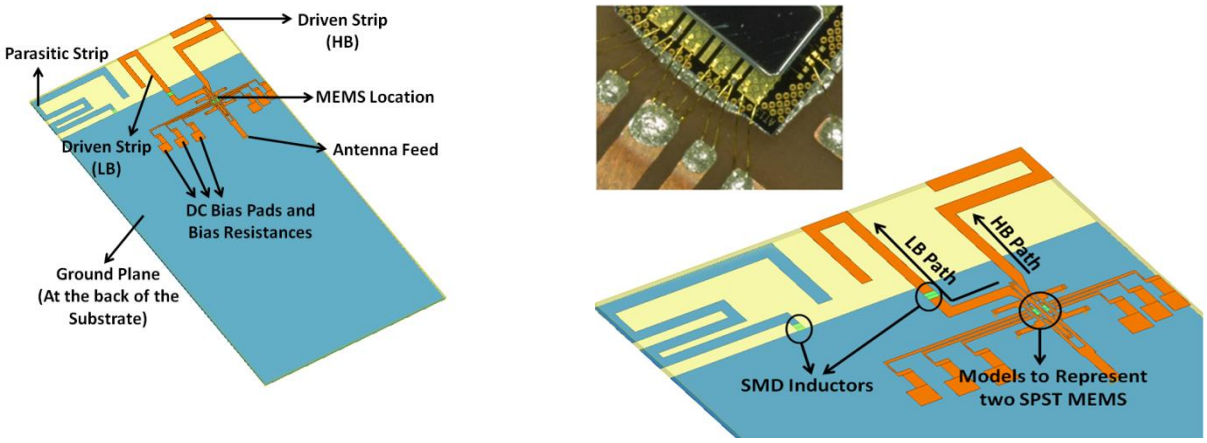

Fig. 36 Simulation Model of Tunable Antenna (General View) and soldering of the MEMS Switch using bonding wires

The S-parameter measurements of this prototype could be measured both with real MEMS devices and with passive prototypes. In passive measurements, to represent the ON state of the MEMS, a simple wire was soldered bypassing the MEMS and the connection was left open to represent the OFF state. The measured reflection coefficient for the antenna in the LB and HB states can be seen in Fig. 37.b. The target bands can be covered with a reflection coefficient below -6dB in both passive measurements and measurements with real MEMS devices, using the band-switching topology. Simulations are also presented and a good agreement is observed with measurement.

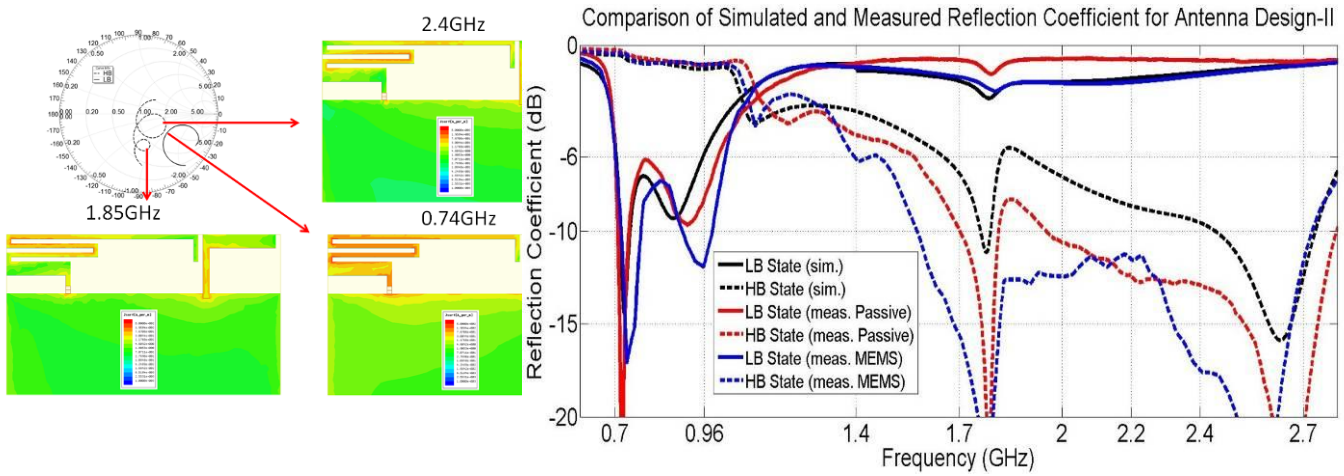

Fig. 37 (a) Swith chart and Currents on the Antenna for Different Frequencies, (b) Simulated Reflection Coefficient with the Switchable MN

The total efficiency of the antenna was also measured (for passive prototypes only, due to reliability issues) for LB and HB cases and presented in Fig. 38.There is an efficiency of higher than -3dB except around 700MHz in the LB and an efficiency higher than -2.5dB in the HB.

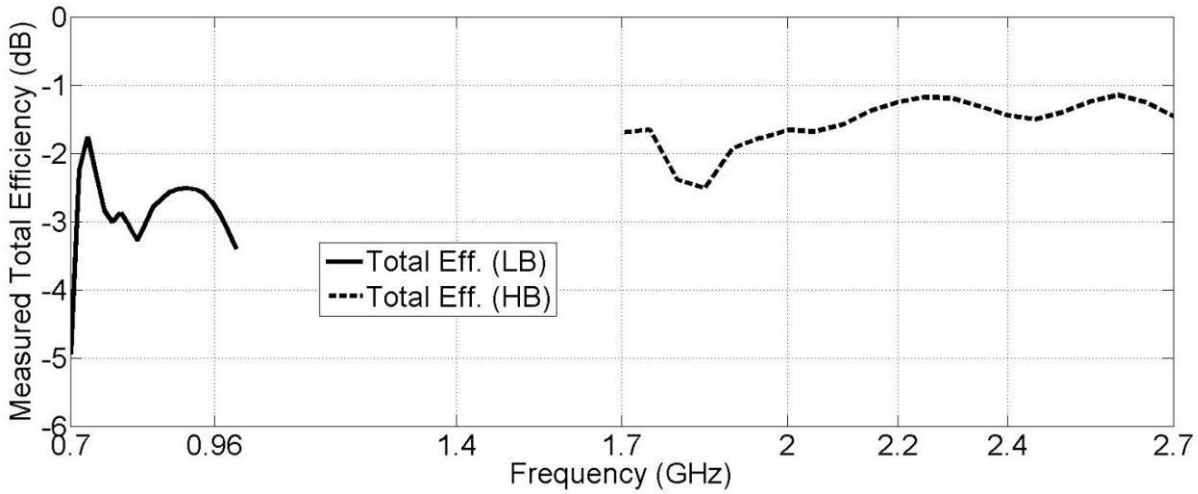

Fig. 38 Measured Total Efficiency for Antenna Design I

D. Reconfigurable antenna for extension of lte operational mode over tv white spaces

This part presents a reconfigurable antenna for mobile terminal and TV white space communications, using a Digitally Tunable Capacitor (DTC). This study was realized in the frame of Trinh Le Huy PhD, J-M Ribero was the main supervisor, and Robert Staraj collaborates to this work.

The antenna structure is matched permanently over the high frequency bands including DCS/PCS, UMTS, LTE 1800/2600, and 3.5GHz bands. Concerning the sub-GHz bands, several reconfigurable states enable a full coverage of LTE 600/700 and GSM 850/900 standards, as well as future applications on TV White space (TVWS). With dimensions of $40\times10\times6$ mm^3 for the antenna and $130\times70\times0.8$ mm^3 for the whole PCB, this structure can be easily integrated in any mobile terminal.

As tunable component, CMOS DTC are used, it combines high power handling (34 dBm), low power consumption (150 µA) and a good capacitance scale (7.7:1) in a compact packaging. It is controlled with I2C or SPI protocol and has 32 different states [DTC15]

1. Antenna design

The geometry of the proposed antenna (Fig. 39) is based on the capacitive coupling principle between a fed monopole and parasitic elements. The antenna has a compact design (40 mm ×10 mm × 6 mm) and it is placed on top of a FR4-Epoxy substrate with a size of 130 mm × 70 mm × 0.8mm, relative permittivity 4.4, and loss tangent 0.02.

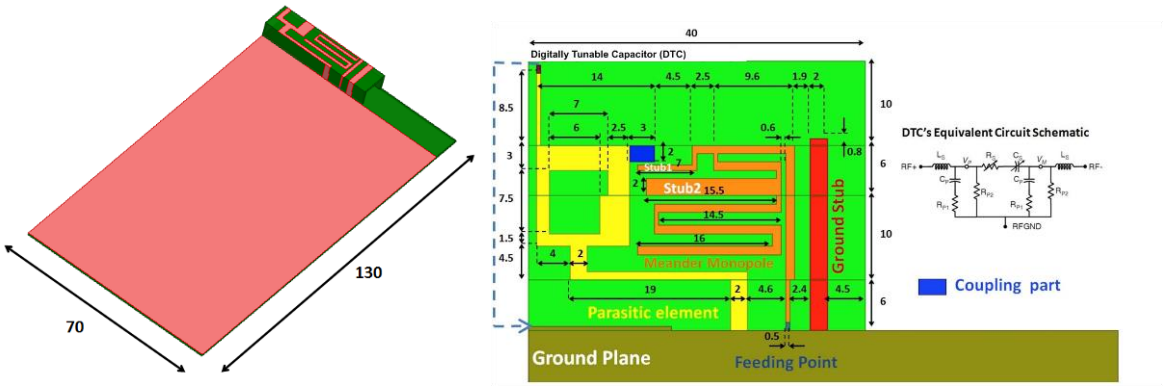

Fig. 39 The geometry of proposed antenna and chassis dimension.

The proposed antenna consists of three different elements (Fig. 39). The center element is a meandered monopole fed by a 50Ω microstrip line (orange). The monopole has an overall length of about 84 mm, which creates a resonance around 900 MHz. In the middle of this branch, two strips (pink) are used to provide two resonances at 1750 MHz and 3500 MHz. Moreover, the shunt capacitance effect between the meander monopole and the shorted parasitic element (yellow) generates an additional resonance for the lower band. By tuning the dimension of the "coupled part" (red), the impedance matching in the low-band can be optimized. This shorted parasitic element is connected to the ground plane through a variable capacitor. By tuning its capacitance C_{Tot}, a narrow band can be reconfigured to cover the 630-860 MHz frequency range. On the right side, a ground strip (blue) is used to cover the 2.5 GHz band. Finally, a new resonance is obtained at 2.7 GHz thanks to an optimization of the shape of the meander monopole. The combination of these two different solutions enables the correct matching of the antenna over the middle frequency band. The simulated reflection coefficient for different capacitance is presented in Fig. 40 for (a) low band and (b) high band.

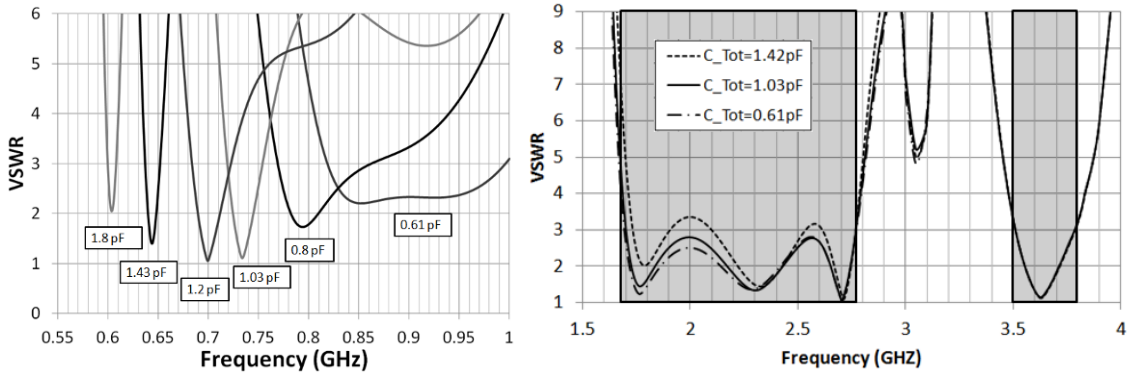

Fig. 40 simulated reflection coefficient (a) LB (b) HB

2. Results and discussion

The VSWR curves in the lower frequency bands are presented in Figure Fig. 40.b. When the capacitance value of DTC is tuned between 0.6 pF to 1.8 pF, the reflection coefficient of the antenna is modified. For the 0.6pF capacitance, a bandwidth a 100 MHz between 860 MHz and 960 MHz is obtained. For higher capacitance values, a narrow band with a 3:1 VSWR can be tuned from 600 MHz to 850 MHz with an instantaneous bandwidth always higher than 10 MHz. This modification has a small impact on the high frequency band, and the antenna is constantly matched between 1.6 GHz to 2.7 GHz and 3.3 to 3.6 GHz with a 3:1 VSWR (Fig. 40.b).

Figure Fig. 41 shows the prototype of the proposed antenna. The unwrapped radiating structure shown in Figure 3.24 has been printed on the FR4 substrate and successively folded thanks to the mechanical milling of the edges to be bent. The tunable capacitor used to reconfigure the antenna is the Peregrine PE64905 DTC. On the back of the PCB, an I2C system used to control the DTC is placed. It consists of a Mbed NXP LPC 1768 microcontroller and three AA batteries which are placed in the holder. In shunt configuration, the DTC can provide capacitance values from 0.9 pF to 5.6 pF (measured values). Consequently, in order to achieve the needed 0.61 pF capacitance value (Fig. 40.a), a series capacitor C_s = 1.9 pF is connected to the DTC. The resulting measured capacitance values ($C_{Tot}=C_{DTC}C_s/(C_{DTC}+C_s)$ as well as the bandwidths of the antenna obtained in the different DTC configurations are summarized in Table 3.1. As it can be noticed, the antenna enables continuous coverage with high frequency resolution control in the low band.

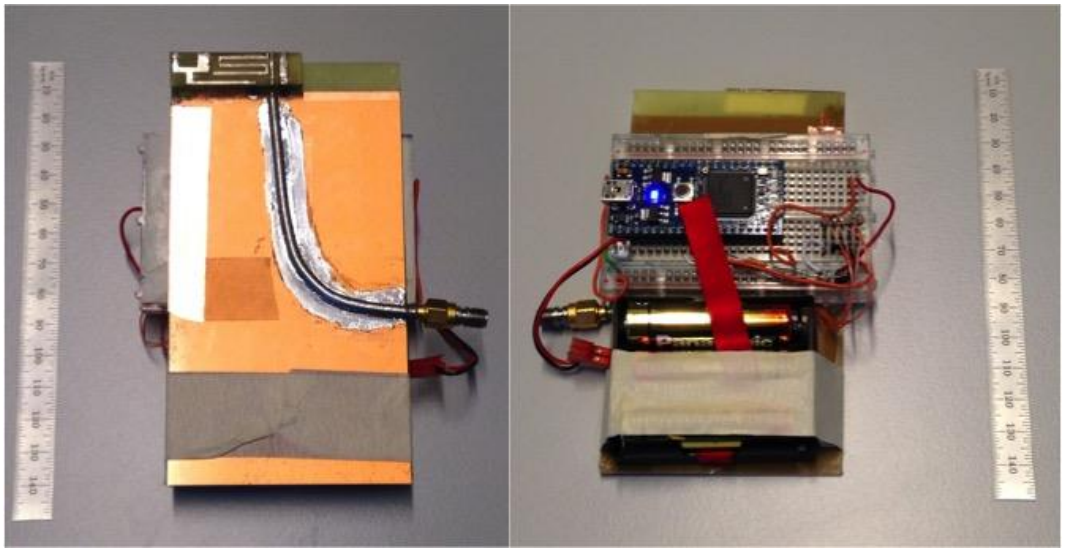

Fig. 41 The fabricated prototype and the control unit.

DTC State	C_{DTC} (pF)	C_{Tot} (pF)	BW (MHz)	DTC State	C_{DTC} (pF)	C_{Tot} (pF)	BW (MHz)
0	**0.90**	**0.61**	**790-980**	16	3.35	1.21	663-680
1	1.29	0.77	760-840	17	3.49	1.23	660-677
2	1.42	0.81	742-805	18	3.63	1.25	657-673
3	1.56	0.86	734-792	19	3.80	1.27	655-670
4	1.70	0.90	725-778	20	3.94	1.28	652-667
5	1.83	0.93	721-762	21	4.08	1.30	650-664
6	1.96	0.96	716-751	22	4.26	1.31	647-661
7	2.10	1.00	710-740	23	4.39	1.33	645-659
8	**2.24**	**1.03**	**704-730**	24	4.54	1.34	643-656
9	2.37	1.05	697-721	25	4.68	1.35	641-654
10	2.59	1.10	690-713	26	4.85	1.37	639-652
11	2.65	1.11	683-705	27	4.99	1.38	638-650
12	2.78	1.13	677-698	28	5.13	1.39	636-648

13	2.92	1.15	674-692	29	5.27	1.40	634-646
14	3.05	1.17	670-688	30	5.46	1.41	632-644
15	3.19	1.19	666-684	31	**5.60**	**1.42**	**631-643**

Tab. 3 Measured antenna matching for different CTot

The measured VSWR values of the prototype in the different frequency bands are shown in Figures Fig. 42(a) and (b). The results in LB show a slight shift in the resonance frequencies with respect to the simulated data, which can be ascribed to fabrication imperfections. A better agreement between simulations and measured is obtained in the higher bands.

In the low frequency band, the proposed antenna can operate from 630 MHz to 960 MHz by changing the DTC value with VSWR lower than 3. In the middle frequency band, VSWR is slightly modified when DTC value is tuned, but it is always lower than 3 for capacitance values (C_{Tot}) higher than 1.03 pF. Consequently, the frequency bands from 1700 MHz to 2700 MHz and from 3500 MHz to 3800 MHz are also covered.

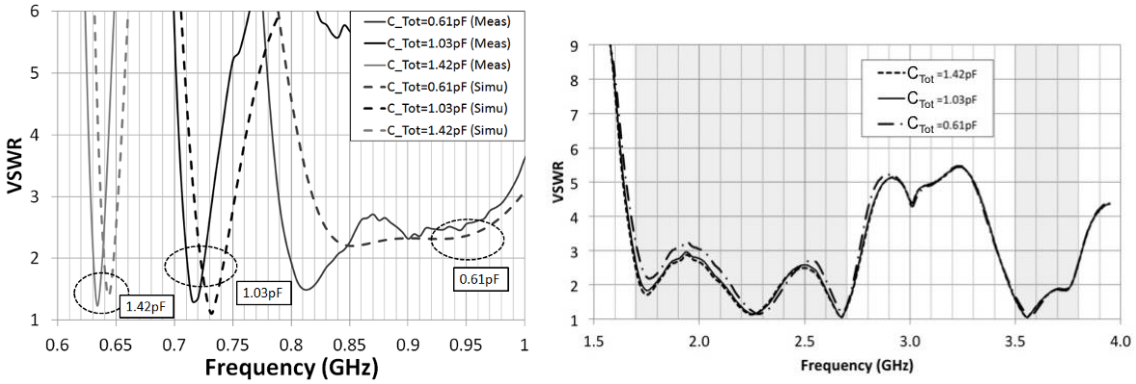

Fig. 42 Measured antenna VSWR in (a) the low frequency band and in (b) in the middle and high frequency bands

The total efficiency of the antenna has been measured by using a StarLab-Satimo chamber and is presented in Fig. 43. Since the lower frequency limit of the Starlab-Satimo chamber is 700 MHz, the total efficiency of antenna has been measured only for frequencies above this value. Some slight differences between simulations and measurements are visible in the lower frequency band. However, the agreement is quite fair considering the 1 dB accuracy of the Starlab-Satimo station. The total efficiency level is sufficient for mobile handset applications. It varies from -4 dB at 730 MHz to -2 dB at 860 MHz, from -6 dB to -0.5 dB in the 1710-2700 MHz band and from -2.5 dB to -1.5 dB in the range 3500-3800MHz.

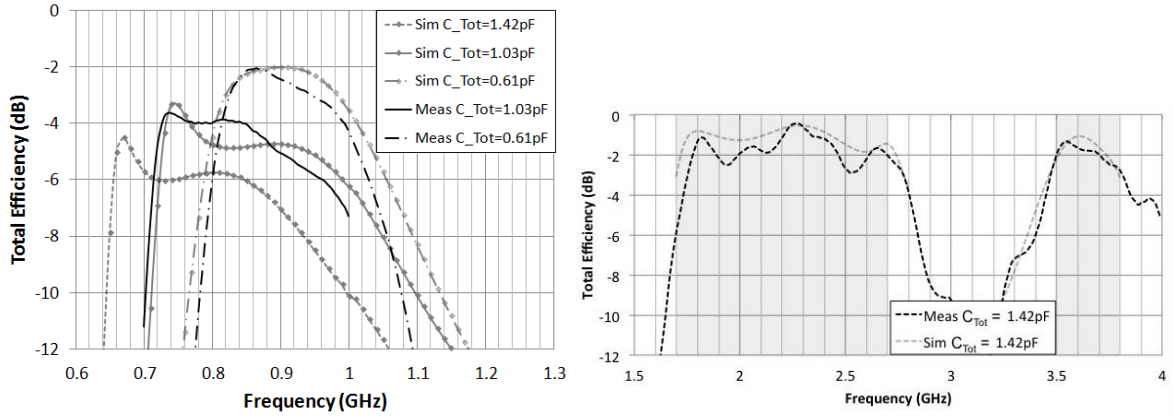

Fig. 43 Measured and simulated antenna total efficiency in the low frequency band

Finally, Fig. 44 illustrates the simulated and measured radiation patterns of the proposed antenna at 920, 2100, and 3500 MHz, respectively. The measured results fairly agree with the

HFSS simulation. The radiation behavior at the different frequencies is quasi-omnidirectional, thus being suitable for mobile terminal scenarios.

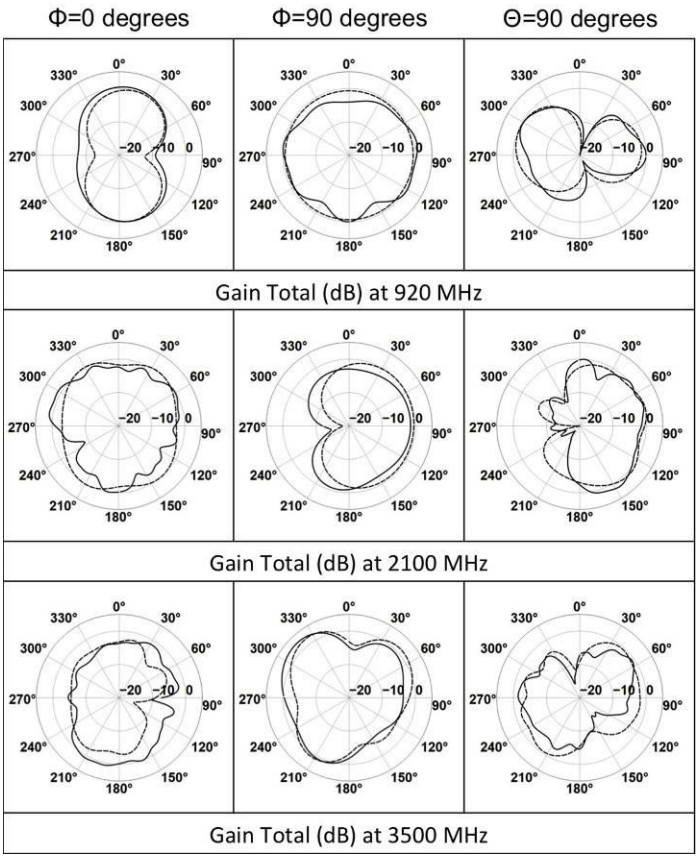

Fig. 44 Simulated (dotted line) and measured (solid line) radiation pattern of the proposed antenna

E. References

[ITU13] TU-R Joint Task Group, "Annex 3 to joint task group 4-5-6-7 chairman's report working document towards preliminary draft CPM text for WRC- 15 agenda item 1.1," Tech. Rep. Document 4-5-6-7/393-E, Oct. 30, 2013.

[HUA13] Huawei. (2013, February). Whitepaper On Spectrum [Online]. Available: http://www.huawei.com/ilink/en/download/HW_204545

[DEL13] Delfmems, http://www.delfmems.com/

[DTC15] Peregrine Semiconductor Corp., "UltraCMOS Digitally Tunable Capacitor (DTC) 100-3000 MHz", Document No. 70-0335-06, 2012.

VII. Multi-band and miniature antenna

From the start of telecommunication history, antenna designer have tried to miniaturize radiating elements, because antenna are always too large. Being an antenna designer is really complicated task, considering that nobody want to add any cents for the antenna, but the specification and bands are always increasing, thus leading to impossible tradeoff. This consideration can explain the constant decrease of the antenna performance reflection coefficient criteria (-6dB of reflection coefficient in mobile phone). Moreover, new applications for wireless connectivity as biomediacal or wearable system require antenna miniaturization. Moreover, in order to maintain acceptable radiation efficiency, isolation techniques from humain body impact are needed.

A. Motivation

The popularity of small communicating objects as mobile phones are become a mainstream is today life. However, more and more standards are needed to be covered in a unique terminal, leading to the development of multi-band and wide band communication device.

A fundamental and intrinsic parameter of an electrically small antenna is its Quality Factor (Q), which is defined as the ratio of 2π times the energy stored in the near fields excited by the antenna to the energy radiated plus dissipated per cycle. The potential bandwidth of an antenna is inversely proportional to its quality factor, which results in low bandwidth potential for a high-Q antenna. The lowest obtainable radiation quality factor can be calculated from Equ. 3 which is known as the Chu limit for electrically small antennas.

$$Q_r = \frac{1}{(ka)^3} + \frac{1}{(ka)} \qquad \text{(Equ.3)}$$

where k is the wavenumber (2π/λ) and a is the radius of the smallest sphere that can enclose the antenna. It is necessary to note that this value is an optimistic theoretical value considering a linearly polarized antenna radiating only in one (TE or TM) mode.

$$FBW = \frac{1}{Q}\sqrt{\frac{(TS-1)(S-T)}{S}} \qquad \text{(Equ.4)}$$

The obtainable frequency bandwidth can be calculated from Equ. 4 as also presented in [HOL11], where S is the maximum target VSWR and T is the coupling coefficient as given in [PUE89]. For a value of T=1, Equ. 4 reduces to:

$$BW_{cc} = \frac{1}{Q}\frac{(S-1)}{\sqrt{S}} \qquad \text{(Equ.5)}$$

This situation is called the "critically coupled" case, where the input impedance of the antenna is matched exactly to Z_0 (generally 50Ω) at a single frequency point.

For the calculation of the Q-factor of an antenna from its input impedance, Equ. 6 was proposed in [YAG05], which proposes a fast and reliable calculation method.

$$Q(\omega) = \frac{\omega}{2R(\omega)}\sqrt{[R'(\omega)]^2 + \left[X'(\omega) + \frac{|X(\omega)|}{\omega}\right]^2} \qquad \text{(Equ.6)}$$

with ω being the angular frequency point, R(ω) and X(ω) stands for the real and imaginary parts of the impedance at angular frequency ω, and R'(ω) and X'(ω) are the first derivates of R(ω) and X(ω) according to the frequency. This formula is valid for a single resonant antenna close to its resonance frequency but it has proven reliable performance so far.

B. Antenna miniaturization for bio-medical applications

This work was realized in the frame of Oumy Diop PdD, under the main supervision of Cyril Luxey and supervision of Aliou Diallo. When I join this PhD, it was already in progress and i do not participate to the first study on miniaturisation limits, but i contribute to the second part on the design and fabrication of small antenna. This second axis was focused on 2.4GHz antenna for biomedical implant and handheld device. Several configurations were studied and fabricated using various type of technology. Especially IPD process, which has the potential to co-integrate antenna and RF circuit, was studied.

Communicating objects in the 2.4 GHz ISM band are becoming smaller and smaller, then entire radiofrequency front-ends need to be co-integrated to miniaturize and optimize the performance. A further improvement consists in co-designing those two elements in terms of impedance conjugate match. Today transceiver solutions are mainly integrated on monolithic silicon using system-on-chip technology. However, some parts of the system cannot be integrated as silicon technology exhibits a low quality factor for inductors, baluns and circulators and therefore low performance. The IPD^{TM} process developed by STMicroelectronics Tours [STM12] has been especially created to design lossless passive devices like resistors, capacitors or inductors. Therefore, designs of passive circuits (baluns, transformers), diplexers and filters UHF frequency already on the market, show a promising trend for this IPD^{TM} process [CHI11-ART11]0. A co-integration of the active circuit and a circulator or a transformer has been presented in [SHI11] but the antenna was still an external component on the Printed Circuit Board (PCB). However, the IPD technology is also potentially highly interesting for a full integration of the passive front-end including the antenna device.

A simplified side view of the BEOL of this process in presented in Fig. 45.a. This study is of special interest as IPD^{TM} technology from ST Microelectronics, Tours has been fully characterized in the ISM band, and offer very high quality factor for inductors in this frequency band.

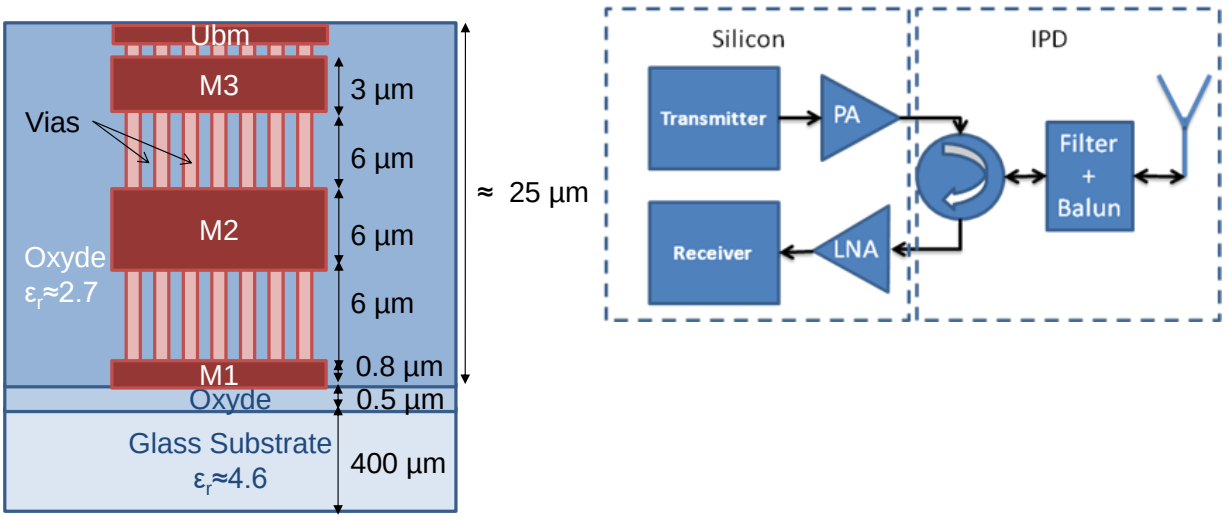

Fig. 45 (a) IPD^{TM} Process build-up (not to scale), (b) Co-Integration of the active and passive circuits

Moreover, antenna directly integrated in silicon would have a very low efficiency and will increase hardly the cost of the final solutions. An elegant solution is to obtain a good trade-off between integration and performance in realizing the front-end passive circuit using the IPD technology. A schematic example of this integration scheme is shown in Fig. 45.b with circulator, balun, filter and antenna integrated on a IPD^{TM} susbtrate.

To connect the transceiver (RFIC) and the IPD, several solutions exists as wire bonding and solder bumps. In the second case, the IPD^{TM} superstrate is flip-chipped on the PCB. In the ST technology, two bump diameters are available, 140 µm and 240 µm, respectively called micro and macro bumps. We choose here to use the macro bumps to enhance the matching bandwidth. The general AiP strategies developed and presented in Fig. 46 has the potential to deliver a low-cost solution for 2.4GHz communication.

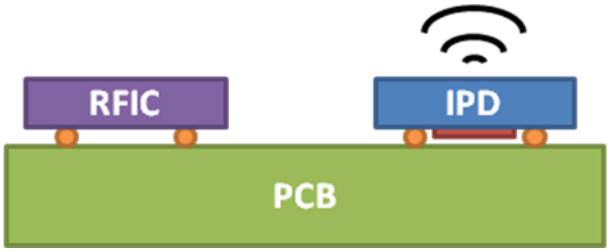

Fig. 46 Direct integration of the antenna and the RFIC into the PCB using the IPD process.

1. Balun on IPD technology

As a proof-of-example, a miniature balun has been designed to transform a 50 ohm single port to a 30 ohm differential port. The transformer integrated on the IPD technology use the M2 and M3 copper levels. The layout of the structure is presented in Fig. 47.a and a very small size of 420*420um^2 is obtained.

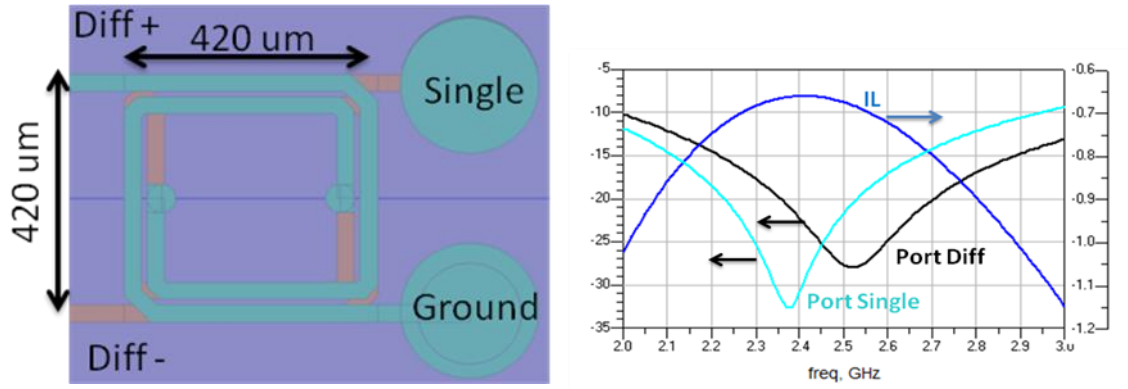

Fig. 47 (a) Balun transformer on IPD^{TM}, (b) Simulated scattering parameters of the balun with Port single impedance of 50 ohm and Port Diff impedance of 30 ohm

S-parameter simulation using ADS simulator and ST design kit are presented in Fig. 47.b. An 0.7 dB insertion loss is obtained on the 2.4 GHz band and the reflection coefficient is lower than -20dB on this entire band.

2. Single ended 2.4 GHz antenna on IPD technology

A monopole antenna using a thin meander line of 50 um width is presented in Fig. 48.a. The antenna is realized with the M2 and M3 copper layer to decrease the resistivity of the line.

The antenna is integrated on a 40*60mm² printed circuit board (PCB) and a picture is presented in Fig. 48.b.

Fig. 48 3D view of the monopole integrated on IPD, (b) picture of the protype (c) Measured and Simulated Reflection coefficient

The electromagnetic solver HFSS is used for the simulation of the structure. A prototype was realized and measured on a 40x60mm² FR4 substrate. The reflection coefficient of the radiating structure is presented in Fig. 48.c.

The antenna is matched with a -8 dB criteria from 2.4 to 2.5 GHz. A total efficiency of 45% is obtained on a Satimo Starlab station. This antenna is suitable for WIFI, Zigbee or Bluetooth communications with a miniaturized size.

The previous balun and the small meandered monopole are then co-integrated on the IPD^{TM} technology. To improve the matching of the system, a shunt capacitor is added on the differential port of the balun, as shown in Figure 8.

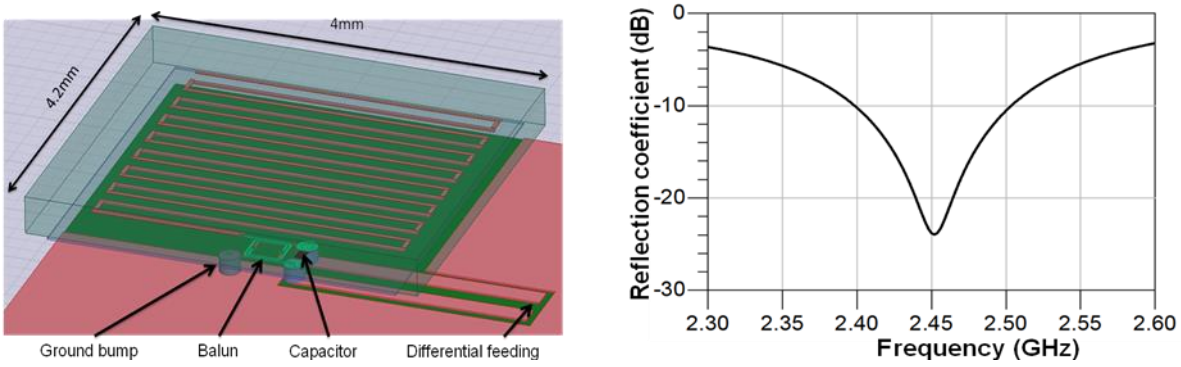

Fig. 49 (a) 3D view of the co-integration of the balun and the monopole , (b) Simulated Reflection coefficient of the structure

The whole structure is simulated using HFSS and ADS software. Reflection coefficient of the system is presented in Fig. 49.a. The structure is matched with a -10dB criteria from 2.4 to 2.5 GHz as shown in Fig. 49.b. Two different effects are improving the matching bandwidth of the antenna: first the losses added by the balun which induce a resistive matching and secondly a reactive matching from the capacitor and the balun. Thus, the simulated structure shows promising performance for the 2.4GHz ISM band.

3. Dipole 2.4 GHz antenna on IPD technology

Implantable antennas for biological application have to be strongly miniaturized. Single ended antenna as monopole needs a large ground plane to radiate. Thus, we design differential antenna for this application. However, miniaturized dipole is very hard to measure because of the current on the feeding cable. Then, we leverage the previous balun to co-integrate the

differential antenna with it, and make it easier to measure. A protype was fabricated, the size of the antenna is 7x3.3mm² and a UFL connector is placed on the opposite face of the PCB as shown in Fig. 50.

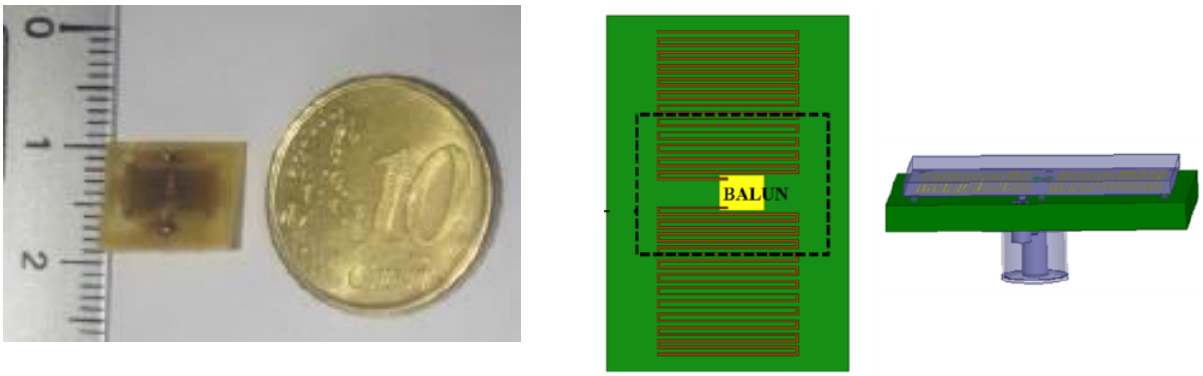

Fig. 50 (a) Antenne dipôle miniature en technologie IPD, (b) Simulation du rayonnement de la structure

Simulated model include the connector and the cable. The protoype was measured and compare with the simulation in Fig. 51.a and a fair agreement is observed. Three different resonnance are observed. In order to understant which part of the structure is radiating, a near-field test bench from CIMPACA was used to measure the antenna with its UFL cable. Results for H field presented on Fig. 51.b show that resonnances at 1.9 and 2.15 GHz are generated by the antenna. However, the resonnance at 2.65 GHz is mainly due to the cable and should not be considered. At 2.4 GHz, a total efficiency of 4.8% was simulated and 5.6% was measured on the Satimo station.

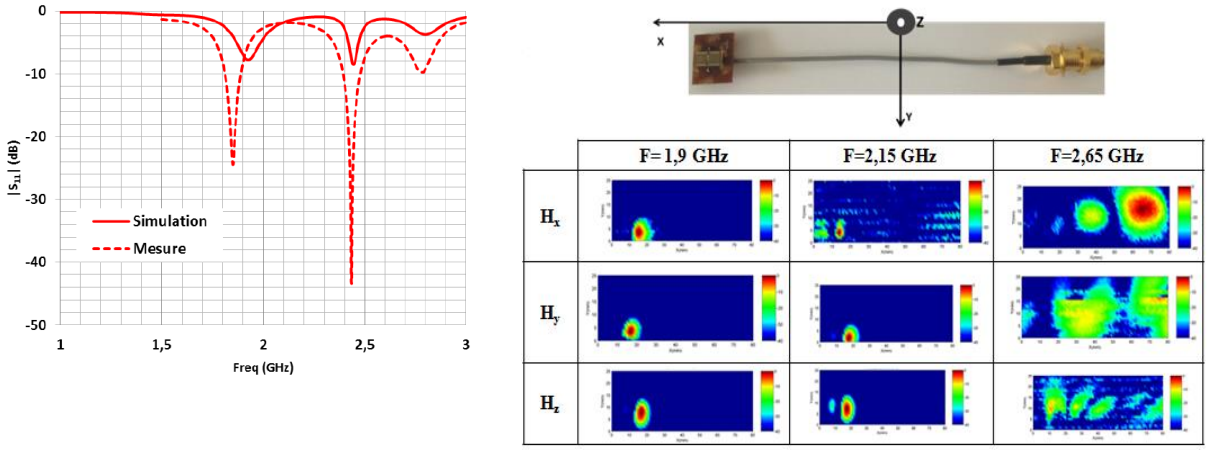

Fig. 51 (a) Simulated and measured S11, (b) Near-field measurement of the antenna with the cable

C. Wearable antennas

This work was done in the frame of the MetaVest project (ANR) by Marcio Pimenta, also supervised by Robert Staraj and Jean-Marc Ribero. The main objective was the design of wearable antenna using metamaterial concept. This work was focused on the design of Global Navigation Satellite Systems (GNSS) antenna for Firemen and military soldiers application. In order to add communication feature, Irridium standard was also studied and Specific absorption rate (SAR) was measured for this application.

1. Dual band circular polarization for GNSS

Several satellite navigation systems have been and are being developed around the world. Global Navigation Satellite Systems (GNSS), provides reliable positioning in real time. The GNSS includes GPS (USA), Compass (P.R.China), GLONASS (Russia), and currently Galileo, with the arrival of the own Europe GNSS. Multiband GNSS antennas having compact size, lightweight, and low cost are needed for GNSS receivers on small satellites, air planes, ships, and mobile terminals on the ground.

We have proposed in this work a new concept able to cover the entire different GNSS standard. The antenna is a slotted square patch with a dual-feed for circular polarization. The dual-band operation is achieved with slots etched and well placed in the patch, the circular polarization is obtained with a dual-feed in quadrature of phase. The two modes TM_{100} and TM_{300} of the patch are exited in order to have similar radiation pattern properties with no nulls on the broadside direction. The antenna is printed over a 0.127 mm thick duroid TACONIC TLY 5 sheet, which has a relative permittivity constant ε_r of 2.2 and a loss tan δ equal to 0.001. This element is stick over a foam plate of 6 mm thick, the relative permittivity ε_r is 1.05 and the loss tan δ are 0.001, supported by a ground plane made up of a copper plate of 170 * 170 mm². The square patch is 100 mm^2 large. The slots are 2 mm large and 92 mm long and etched at 0.7 mm of the edge. The double feeding is realized with a via, soldered to the patch at 24 mm of the edge, and connected to a hybrid coupler as shown on Fig. 52.a.

The S-parameters of the antenna alone are presented in Fig. 52.b. A good agreement is obtained between simulation and measurement. Reflection coefficients S_{11} and S_{22} show the dual-band behavior of the structure but also an additive non-radiating resonance centered on 1.4 GHz which corresponds to the coupling between the two ports. The first resonance is the TM_{100} mode and the third one is the TM_{300} mode, with respectively the central frequencies of 1.197GHz and 1.577 GHz. We achieve a S_{11min} of -24dB at these central frequencies. The S_{11} bandwidth, taken with -10dB criteria, is 2.5% for the two central frequencies 1.197GHz and 1.577 GHz. We can observe that the antenna is matched only on the L1 and L2 GPS bands.

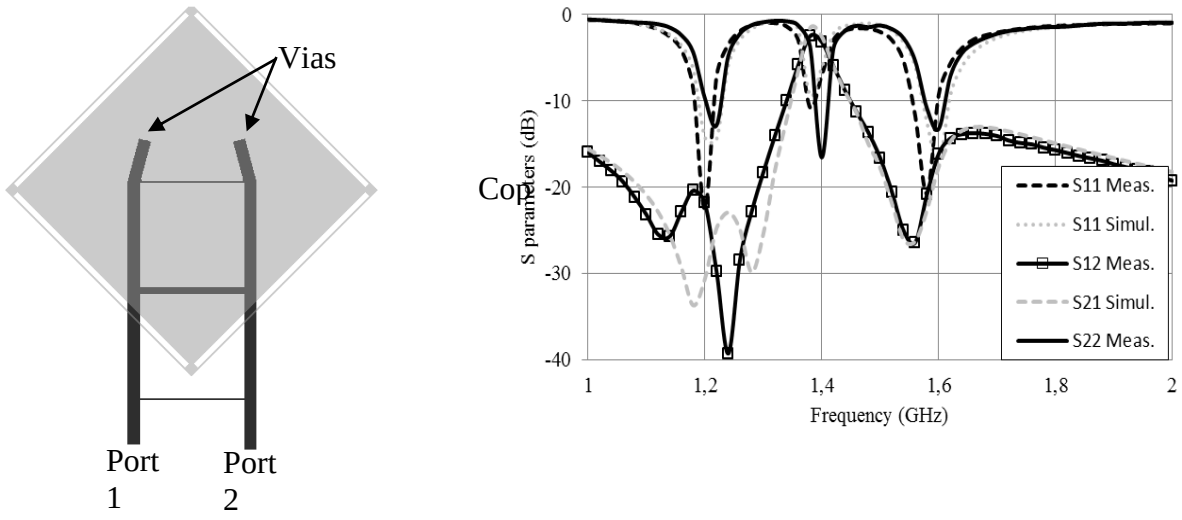

Fig. 52 (a) Dual-band antenna, (b) Simulated and measured S parameters of the proposed antenna.

The radiation pattern is measured in anechoic chamber, and the total gain and the axial ratio in the broadside direction of the antenna is presented Fig. 53. We achieved a maximum total gain of 6 dBi and 8.4 dBi at the central frequencies of 1.23GHz and 1.6GHz respectively. However, the Axial Ratio AR is less than 3dB in all the GNSS standard bands. This AR

bandwidth is 20% and 11.3% at 1.2GHz and 1.58GHz respectively (Fig. 53). Thus, this structure is compatible with GPS, GLONASS and Galileo standard.

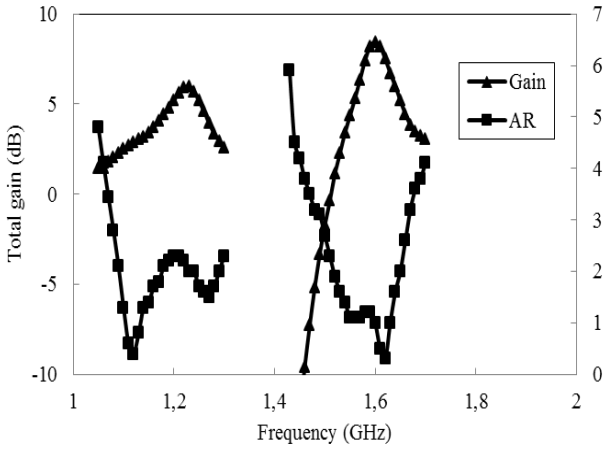

Fig. 53 Total gain and axial ratio measurements in broadside direction to the antenna.

2. Textile GPS dual-band antenna for GPS application

An Artificial Magnetic conductor (AMC) cell was designed for dual-band operation. This cell is a double stack patch with dimension presented in Figure X. The reflection phase properties of the AMC cell will be used to isolate the antenna from the body and will reflect half power of the monopole antenna. A prototype of the AMC was realized with material suitable for wearable applications.

The metallization is realized by the use of an electro-textile, a Nickel and copper plated conductive flexible fabric, with a non-conductive hot melt adhesive, the thickness is 0.17 mm with a conductivity of 0.5 Ohm/sq.A 3*3 cells prototype is realized to measure the reflection phase with two horns. The simulation and the measurement of the reflection phase of the cell are shown on Figure 2, the bandwidth, taken from -90° to 90° of phase, is about 5.1% and 4 % at 1.165 GHz and 1.593 GHz respectively. There is a good agreement between simulation and measurement results. However the magnitude of the cell reflexion shows that the cell absorbs the 50% of the incident power (Fig. 54.a), this is due to the loss in the used material in comparison with the simulation of a non_lossy material which reflects all the energy. The simulation of the magnitude of the reflexion of the cell show that for low loss (tan δ = 0.001) is reflecting almost all the power (Fig. 54.b).

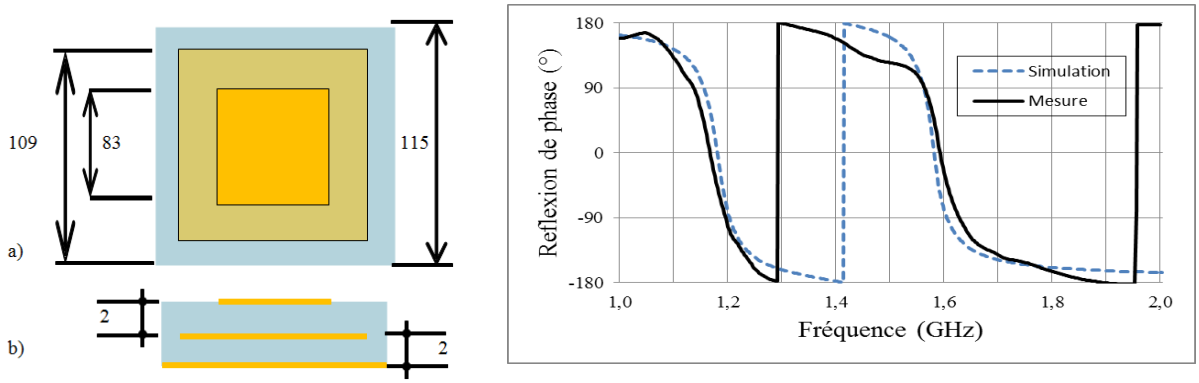

Fig. 54 (a) Dual band amc cell, a) Front view, b) Side view dimension in mm, (b) Reflexion phase of the dual band cell

The monopole and the AMC surface are designed separately. The monopole type is matched (S_{11} < -10 dB) over 1.2 GHz to 1.6 GHz. It is a simple patch fed by a CPW 50 Ohms feed line (Fig. 55.a). The antenna is printed over a thin sheet of Duroid with 0.127 mm thick and a permittivity ε_r 2.2; we choose this substrate in order to have a flexible antenna. The dimensions of the antenna are presented in Fig. 55.a.

The AMC surface is composed of 3*3 units cell, the prototype is 345 mm * 345 mm (1.38 λ_0). The cells are glued with a non-conductive hot melt adhesive. The thickness of the AMC surface is 4 mm.

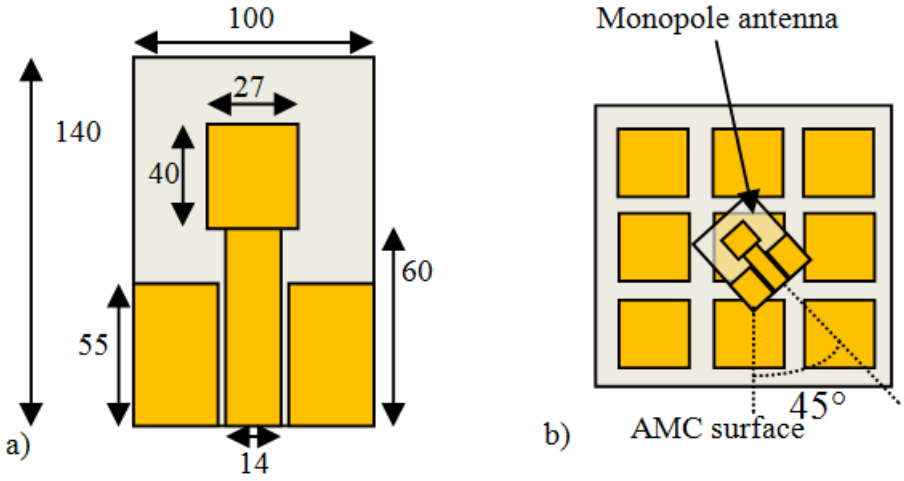

Fig. 55 a) Monopole antenna, b) Monopole + AMC surface dimension in mm

The antenna is place over the AMC surface, separated by 2mm thick foam. The orientation of monopole antenna is along the diagonal of the AMC surface (Fig. 55.b). The reflection coefficient and radiation pattern of the monopole are measured in free space and over the AMC surface.

We measure the return loss (S_{11}) of the monopole (Fig. 56.a) over the AMC surface, aver a simple mass plan and in free space. The monopole antenna is oriented at 45° with regard to the AMC surface. The efficiency and the radiation pattern for this configuration are measured in a Starlab radiation measurement system from SATIMO.

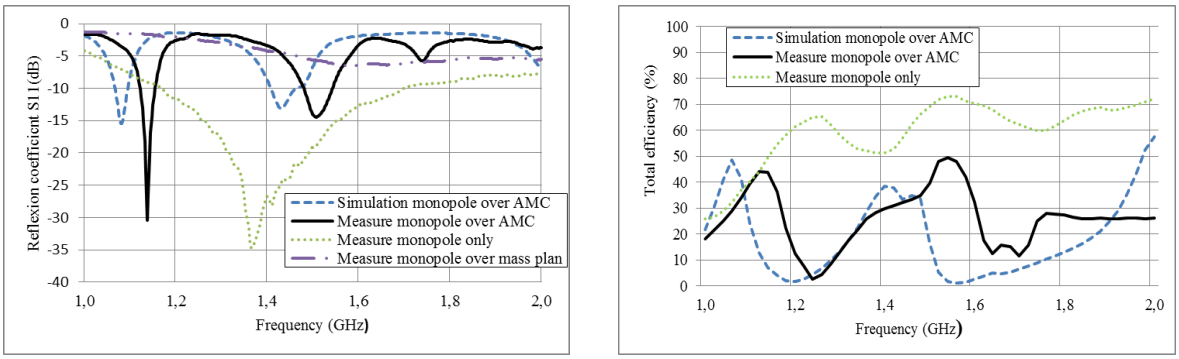

Fig. 56 (a) Reflexion coefficient measurement, (b) Efficiency measurment

The measurement of the monopole over a ground plane shows that the monopole is totally unmatched (Fig. 56.a). The antenna over the AMC surface shows a dual band operation, the dual band operation is obtained with dual band AMC cells. The monopole is matched in the

frequency band of the AMC surface. The bandwidth is about 3.5% and 3.9% at f = 1.14 GHz and f = 1.52 GHz respectively. Here, there is a frequency shift of the antenna over the AMC surface because we have taken the bandwidth criteria of the cell in the range 0° ± 90° of phase instead of the 90° ± 45° predicted in [SAM03]. There are also a frequency shift of 7% between the simulation and measurement of the S parameters. Comparing the efficiency of the monopole with and without the AMC, we observe a decrease of 20% of the efficiency due to the loss of the substrate (Fig. 56.b). These decreases of the efficiency are from the AMC which absorb the half power of the monopole, we can solve this problem by using a lossless textile material. The maximum efficiency is about 50% where the antenna is well matched, i.e. at 1.14 GHz and 1.51 GHz.

The radiation pattern is measured for the minimum S_{11} at the two frequencies of 1.12 GHz and 1.52 GHz. The maximum gain of the antenna only is about 2.65 dBi in free space. The total gain measurement show an increase of the maximum gain in the normal direction of the antenna with the AMC surface at the two frequencies. The maximum gain is about 5 dB and 6 dB at 1.12 GHz and 1.52 GHz respectively. The AMC surface reflects the half power of the monopole antenna in the perpendicular direction.

D. Mimo antenna using hollow coupling element

This work was realized in the frame of Aykut Cihanghir PhD, supervised by Cyril Luxey. Coupling elements (CE) are widely used for mobile terminal antennas, to obtain a wide-band response using the space available for the antenna, which is typically electrically-small. In this scenario, the CE is used just as an exciter to induce the proper currents on the terminal ground plane, whose dimensions are generally close to a quarter wavelengths in the frequency band of 700-960MHz. A new coupling element was proposed to obtain a more space-efficient structure with negligible performance trade-off.

The newly proposed hollow CE was evaluated in a MIMO antenna scenario. As widely known, it is a challenging problem to obtain a MIMO antenna with reasonable ECC (envelope correlation coefficient) and isolation for a typical mobile terminal in the LB, where the antenna is electrically small and most of the radiation comes from the excitation of the ground plane. Due to this fact, it is hard to obtain a good level of isolation between the two antenna feeds. Although a good isolation in terms of s-parameters is obtained, it is not sufficient to get an acceptable Envelope Correlation Coefficient (ECC) since the radiation patterns will be approximately the same (doughnut shape) for both antennas as the ground plane is the main radiator. For this purpose, two identical hollow CEs were placed on the two corners of the short edge of the PCB, to excite the diagonal mode of the ground plane currents as in [CHI13]. By this way, a good ECC from the 3D pattern point of view can be expected. To increase the port to port isolation between the two CEs, the neutralization technique, which is explained in [ZHA13] was used.

The simulation model of the antenna can be observed in Fig. 57. An FR4 substrate of 0.8mm thickness was used as the PCB. The height of the antenna is 4.2mm above the substrate. The CEs on each corner are identical; each with a MN of 4 SMD components at the antenna feeds (Fig. 58). To increase the inductive effect of the neutralization line, an inductor of 100nH was used.

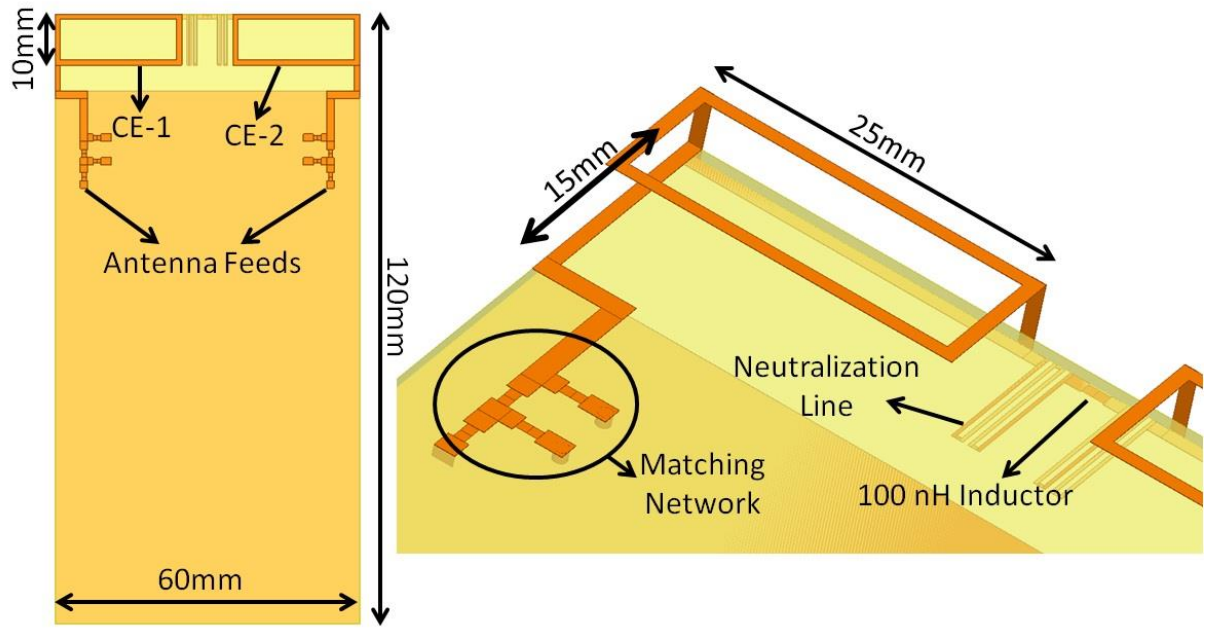

Fig. 57 Figure 3 The LTE MIMO Antenna Simulation Model

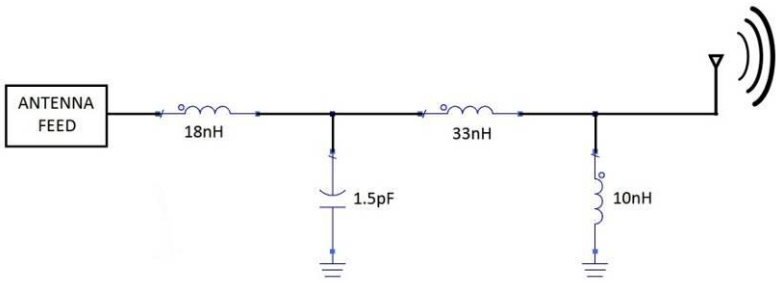

Fig. 58 Figure 4 The MN for LTE MIMO CEs

To illustrate the effect of the MN on the input impedance, simulation results have been plotted in Figure 29, plotted between 700-960MHz. As shown with the red curve, the single CE is far from being matched without the MN. The MN (optimized using Optenni Lab software), creates an optimally overcoupled response to obtain the highest bandwidth possible.

As previously mentioned, the main aim for placing the CE on the corner of the PCB is to excite the diagonal mode of the ground plane, in order to be able to get a reasonable ECC in terms of 3D pattern between two CEs.

Another very important point for this antenna is the neutralization line added between the two CEs, connecting them inductively to increase the isolation between their feeds. The main idea behind this technique is to create an additional inductive path (to the existing capacitive coupling path) and by this way force the currents between the two antennas to flow somewhere else than their feeds. Detailed description of the methodology is not given here for the sake of brevity. The antenna (consisting of both CEs on each corner with MNs) was simulated both with and without the neutralization line and the results are presented in Fig. 59.a. The isolation is poor in the absence of the neutralization, falling down to 4.5dB around 720MHz. After the neutralization line is introduced, a significant improvement is seen in the

isolation, being better than 10.2dB through the target band. The simulated reflection coefficient for the CEs (with MNs) is below -6dB between 740-940MHz.

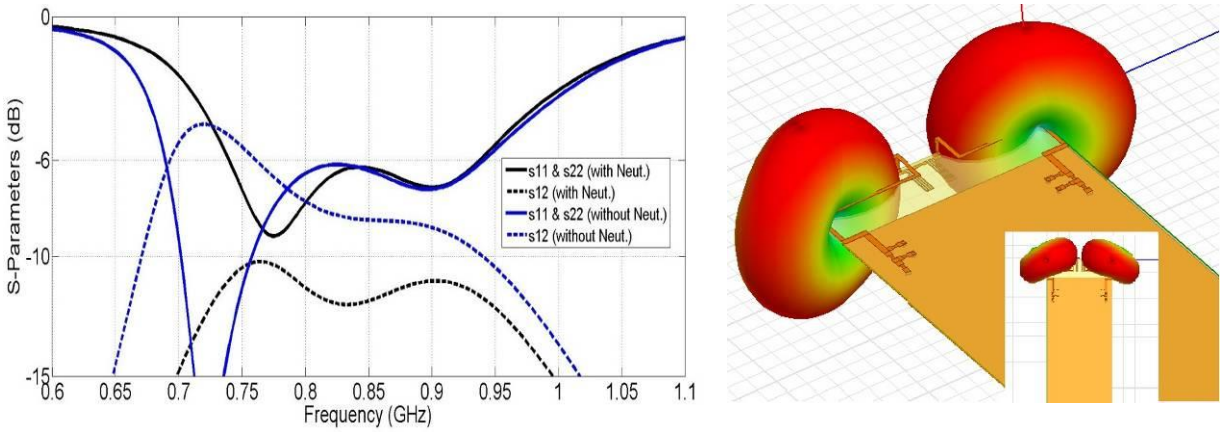

Fig. 59 (a) Effect of the Neutralization Line on Simulated S-Parameters, (b) Figure 5 3D Radiation Pattern of Dual CE Antenna

The simulated 3D radiation patterns for the whole antenna system can be observed in Fig. 59.b, where the pattern for CE-1 is plotted when the other port is matched and vice versa. The rotated dipole type patterns in opposite directions for the two CEs verify the excitation of the two diagonal modes of the ground plane.

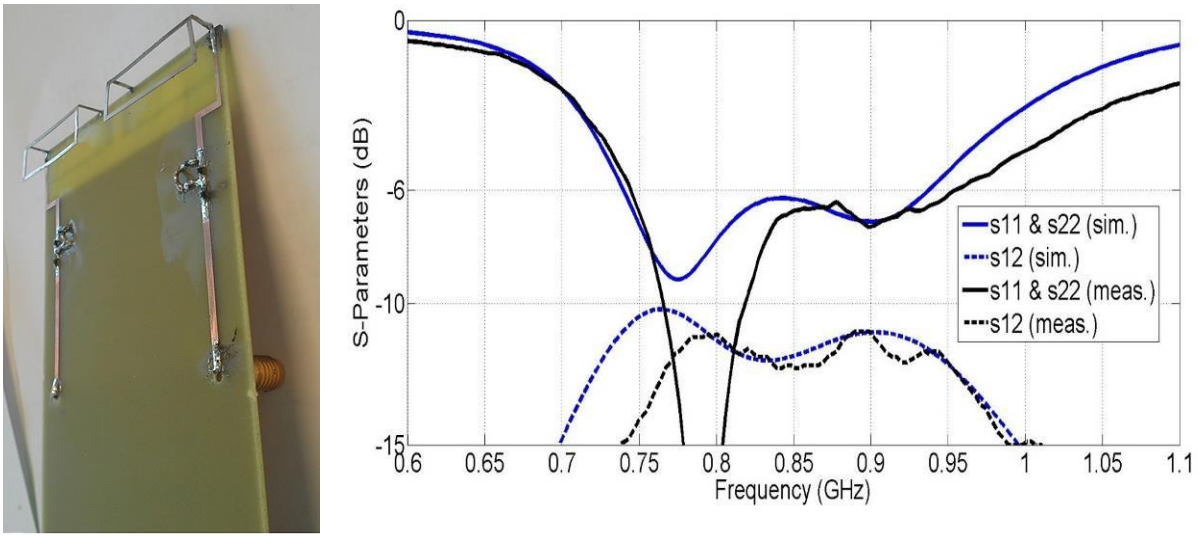

Fig. 60 (a) Manufactured MIMO Antenna Prototype, (b) Simulated and Measured S-Parameters of the MIMO Antenna

The proposed antenna has been manufactured on FR4 substrate (Fig. 60.a). The S-parameter measurements have been performed, whose results are presented in Fig. 60.b. A fair agreement can be observed between simulation and measurements. The frequency region between 740-950MHz can be covered with a reflection coefficient below -6dB and the isolation between the two ports are always better than 11dB in the measurements.

The total efficiency of the MIMO antenna system was measured in a Satimo Starlab station, where the unmeasured port is terminated with a match load. The antenna has a measured total efficiency between -6dB and -4dB in the coverage band. Envelope correletation coefficient (ECC) was calculated using Equ. 7.

$$\rho_e = \frac{\left|\iint_{4\pi} F_1(\theta,\phi)^*.F_2(\theta,\phi)d\Omega\right|^2}{\left(\iint_{4\pi}|F_1(\theta,\phi)|^2 d\Omega\right).\left(\iint_{4\pi}|F_2(\theta,\phi)|^2 d\Omega\right)} \qquad \text{(Equ.7)}$$

The comparison of the simulated and measured ECC using the radiation patterns is given in Fig. 61. The agreement between simulation and measurement seems fair. The measured ECC turns out to be below 0.5 (a generally accepted value for mobile terminals) between 765MHz and 950MHz which contains most of the coverage band.

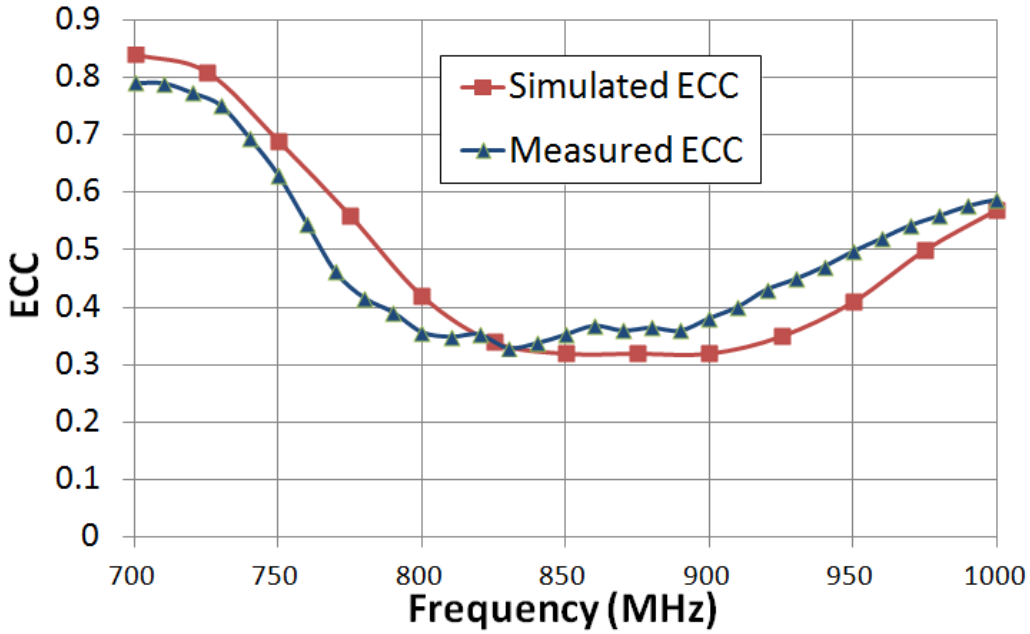

Fig. 61 Simulated and Measured ECC of the MIMO Antenna

A new CE was used to evaluate MIMO performance in the LB, using two CEs situated on the two corners of the PCB. With this layout, the diagonal modes of the ground plane was were excited for both CEs, enabling a level of default isolation. To improve the isolation further, the neutralization line technique was applied to the CEs. The S-parameter and ECC measurements were performed and presented for the MIMO antenna.

E. References

[YAG05] Yaghjian, A.D.; Best, S.R., "Impedance, bandwidth, and Q of antennas", Antennas and Propagation, IEEE Transactions on , vol.53, no.4, pp.1298,1324, April 2005

[HOL11] J. Holopainen, "Compact UHF-band antennas for mobile terminals:focus on modelling, implementation, and user interaction," Ph.D. dissertation, Department of Radio Science and Engineering, AALTO University, Helsinki, 2011.

[PUE89] H.F. Pues, A.R. van de Capelle, "An impedance-matching technique for increasing the bandwidth of microstrip antennas," IEEE Transactions on Antennas and Propagation, Vol. 37, No. 11, November 1989, pp 1345-1354.

[STM12]http://www.st.com/internet/analog/class/1806.jsp

[CHI11] Chih-Yin Hsiao; Hsu, S.S.H.; Da-Chiang Chang; , "A Compact V-Band Bandpass Filter in IPD Technology," Microwave and Wireless Components Letters, IEEE , vol.21, no.10, pp.531-533, Oct. 2011

[ART11]T. Arthur, "RF Integrated Passive Devices: The Next Big, Small Thing", Microwave Journal, Nov.2011.

[SHI11] S. Shim and S. Hong, "A CMOS Power Amplifier With Integrated-Passive-Device Spiral-Shaped Directional Coupler for Mobile UHF RFID Reader", IEEE Transactions in Microwave Theory and Techniques, Vol. 59, No. 11, pp. 2888-2897, November 2011.

[SAM13] F. Yang, R. Samii, “Microstrip antennas integrated with electromagnetic band-gap (EBG) structures: a low mutual coupling design for array application”, Transactions on Antennas and Propagation, Vol. 51 Issue 10, October 2003.

[CHI13] C.-Y. Chiu, X. Liu, F. Gao and Z. Ying, “Reduction of Envelope Correlation on Non-metallic and Metallic Chassis Phones,” International Workshop on Antenna Technology 2013 (iWAT 2013), Karlsruhe, Germany, March 2013.

[ZHA13] S. Zhang, A.A. Glazunov, Z. Ying, S. He, “Reduction of the Envelope Correlation Coefficient With Improved Total Efficiency for Mobile LTE MIMO Antenna Arrays: Mutual Scattering Mode,” IEEE Trans. on Antennas and Propagation, vol. 61, no. 6, pp.3280-3291, June 2013.

VIII. Millimeterwave modules and measurement technique

A last important part of my research was focused on millimeter wave system. This work was mainly done in the frame of Diane Titz PhD, and different master studies (Syazatul Maryam AZHAR, Aimeric Bisognin, Nguyen Hong Duc). Cyril Luxey was the main supervisor of Diane Titz, and several academic and industrial scientists have contributed to this work. This study was also realized in the frame of the CREMANT, Orange Company was involved in this project through the contribution of Patrice Brachat and Frederic Devillers. ST Microelectronics company is also closely associated to this work : Fréderic Gianesello et Romain Pilard from STM Crolles, and Claire Laporte and Hilal Ezzeddine de STM Tours were involved in many part of this study. Finally, several collaborations have been realized on this topic.

A. Motivation

Because of emerging data consuming application as video, the demand for high data rate communications is growing exponentially worldwide. The future introduction of 5G communications will require several hundreds Mb/s data rate wireless communications. For Wireless Local Area Networks (WLANs), IEEE 802.11.AC standards can offer peak rates of 867 Mb/s for handheld device. However, this is realized with 160MHz of bandwidth, and by taking all existing channels. The existing norms and coding can be improved but the data rate will still be limited by its carrier frequency, as actual wireless communications only exploit the 300 MHz-6 GHz band for its long range communications.

Moving to higher frequencies where large bandwidth can be obtained and towards non-licensed band is very promising. Millimeter-wave (Mmw) frequencies from 30 GHz to 300 GHz have been used for many years for military applications. With the recent advances in circuit technologies and low-cost integration solutions, Mmw spectrum can now be targeted for high volume market applications.

One specific band has occupied the worldwide research and industrial community for more than 10 years now; it is the Industrial, Scientific and Medical (ISM) 60 GHz band. Following the Shannon theorem, the channel capacity is directly proportional to the bandwidth. So, one way to increase the data rate of a communication is to increase its bandwidth. This is possible around 60 GHz where lies one of the largest worldwide unlicensed band allocated in history. The bandwidth reaches 7 GHz from 57 to 64 GHz in the US, Canada, and Korea; from 59 to 66 GHz in Japan; and up to 9 GHz from 57 to 66 GHz in Europe, as shown in Fig. 62. Another interesting feature of working at Mmw frequencies is the short wavelength. Many topologies, impossible to implement at lower frequencies, become feasible. Among them, traditional microwave board elements that use Transmission Lines (TL), as 90° couplers, hybrids, Bulter matrix, etc… The compact size of the 60 GHz radio also permits multiple antenna solutions at the user terminal that are more complicated at lower frequency.

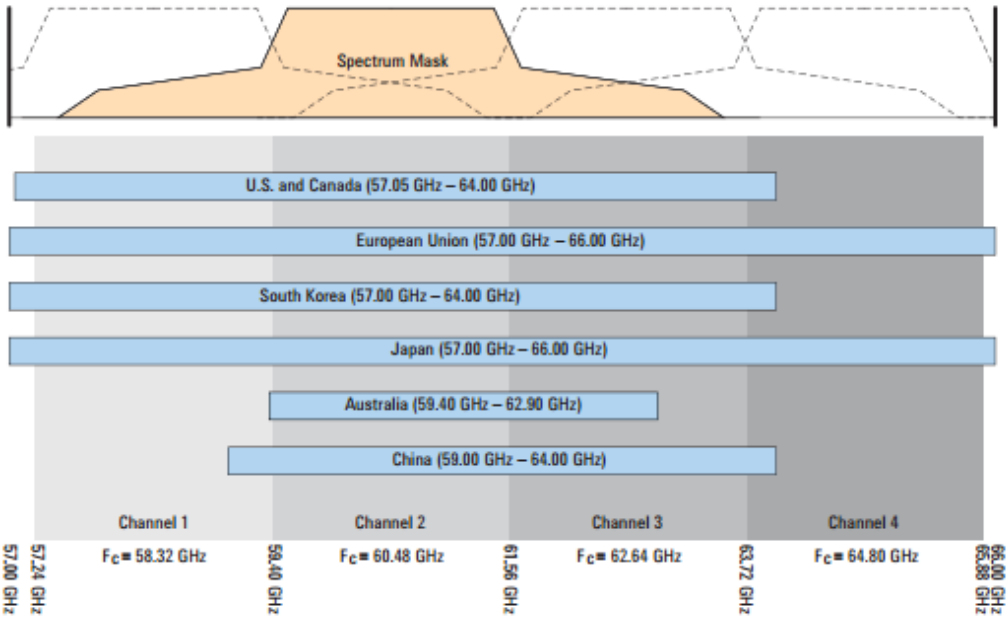

Fig. 62 Figure I.6. Worldwide spectrum avaibility in the 60 GHz band, from the WiGig consortium.

B. Design of passive millimeter wave circuits

A first important part of this study was focused on the design of mmW passive hybrid coupler. We focus our effort on the integration of broadband and miniature couplers at millimeter-wave frequencies. Due to the decrease of the wavelength (λ = 5 mm), couplers using quarter-wave length lines become feasible. These passives circuits are used in mixers, amplifiers, vector modulators .Their implementation on Silicon substrates is then necessary. They are also very useful in beamforming networks where electronically-steered antenna arrays are used to overcome the inherent oxygen absorption at 60 GHz, in medium-range communications. Among the best available solutions, reflection-type phase shifters [3] and Butler matrices [4] are often employed. The necessary couplers must be reasonably small and enough wideband to maintain good results.

We designed a new wideband miniature branchline coupler integrated at 60 GHz in a BiCMOS9MW technology and IPD technology, both from ST Microelectronics. First, theory and equations of the novel coupler are presented. As a proof-of-concept, a 2.2 GHz coupler is designed on a duroid substrate and measured. Then, designs at 60 GHz in Silicon and IPD technologies are described and compared to state-of-the art recently published couplers. Finally, the integration of the IPD coupler in a low-cost Butler matrix is fully described.

1. Coupler design

a) Coupler Theory and Design

Branchline couplers are usually avoided when compacity is needed because of their large size. However, compared to coupled-line and Lange couplers, their implementation is less dependent on process variation and easier either on multi-level or single metallization processes. To cover the 57-66 GHz band, wideband performance is necessary. The use of an all-lumped component version is then usually excluded because of their narrowband characteristics. Our coupler takes advantage of both microstrip lines and lumped capacitors as an efficient mix to achieve a small footprint and a wide bandwidth.

As shown in Fig. 63, the proposed coupler is based on two cascaded Quasi-Lumped Quadrature Couplers (QLQC). In addition, a short-circuited stub is used in the central connection between the two couplers for matching purpose.

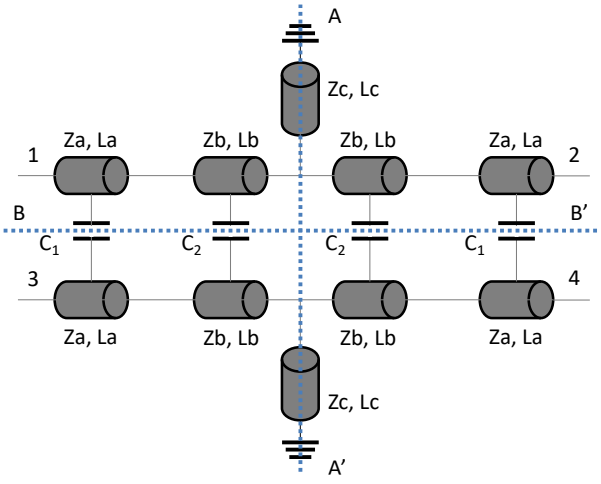

Fig. 63 Proposed Coupler Topology.

b) Duroid Implementation at 2.2 GHz

As a proof of concept, two couplers were realized on a 0.762-mm thick Duroid substrate (ε_r = 2.2, tan δ = 0.001) using Interdigitated (Int) capacitance and discrete capacitors. To comply with our realization capability, the central frequency was set to 2.2 GHz. The quarter-wavelength is equal to 2.3 cm which lead to an estimated overall footprint of 7.8 cm² for a conventional branchline coupler. The realized couplers occupy an area of 6.0 cm² with the Int capacitance, which gives a 23% size reduction and an area of 5.6 cm² with the discrete capacitors (Fig. 64.a).

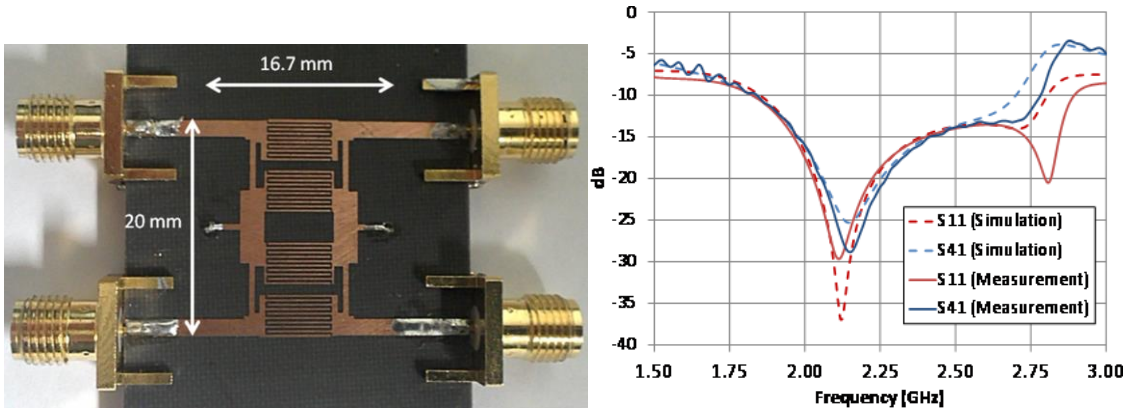

Fig. 64 Fabricated couplers at 2 GHz on PCB substrate. with interdigitated capacitance, (b) Simulated and measured reflection coefficient $|S_{11}|$ and isolation $|S_{41}|$ of the coupler.

The Interdigitated coupler was simulated using Momentum. The comparison between simulation and measurement is presented in Fig. 64.b and Fig. 65. A quite good match is obtained except a slight frequency shift of 4 %, mainly due to realization accuracy. We obtain a measured -10 dB matching bandwidth of 36 % as expected from 1.89 GHz to 2.66 GHz (Fig. 64.b), a ±1 dB amplitude imbalance, and a ±2° phase imbalance around 90° (Fig. 65.b) of 28 % from 1.97 GHz to 2.57 GHz. These results show great promise for implementation at higher frequencies.

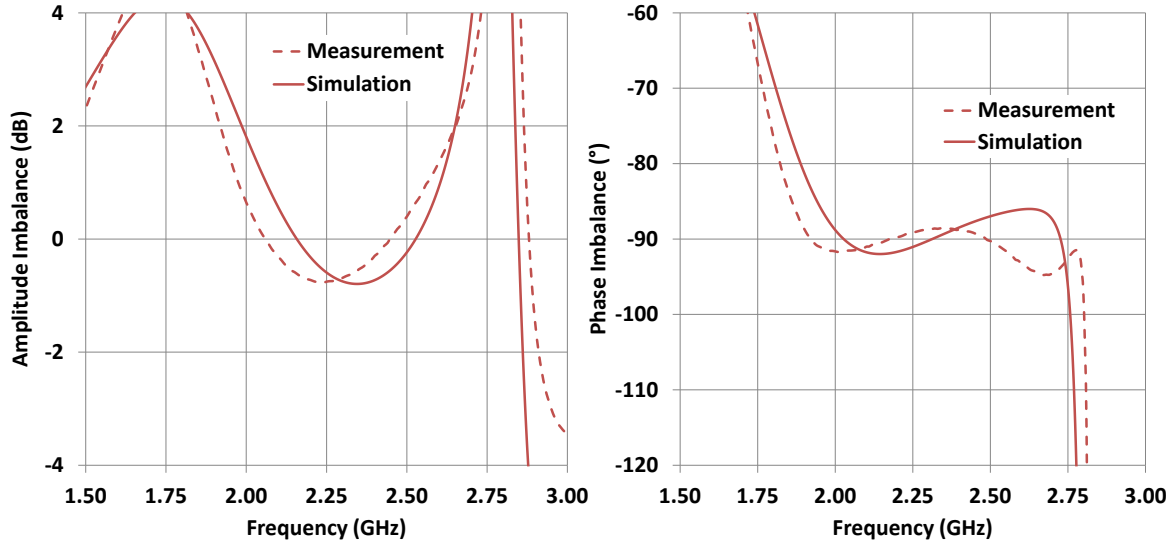

Fig. 65 Simulated and measured amplitude and phase imbalance of the coupler.

c) Silicon Integration and Design

The coupler was designed and fabricated in BiCMOS9MW technology (Fig. 66) because its back-end of line (BEOL) has been optimized for millimeter-wave frequencies. In order to minimize transmission losses, the microstrip lines are etched on the 3.88 µm-thick M6-Alucap layers and its ground plane on the 1 µm-thick M1-M2 layers. It was simulated using HFSS for full-wave simulations. MIM capacitors from the ST Microelectronics Design Kit were used. The full 60 GHz band (57-66 GHz) is covered with a 0.5 dB amplitude imbalance and a 1° phase imbalance at worst, for a 82% size reduction compared to classical branchline couplers in the same technology (0.08 mm² instead of 0.44 mm²).

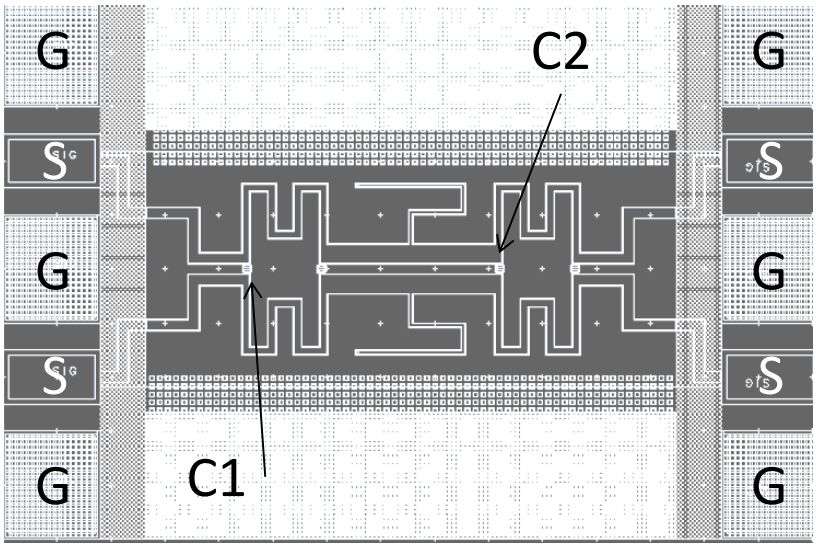

Fig. 66 Layout of the realized couplers in BiCMOS9MW.

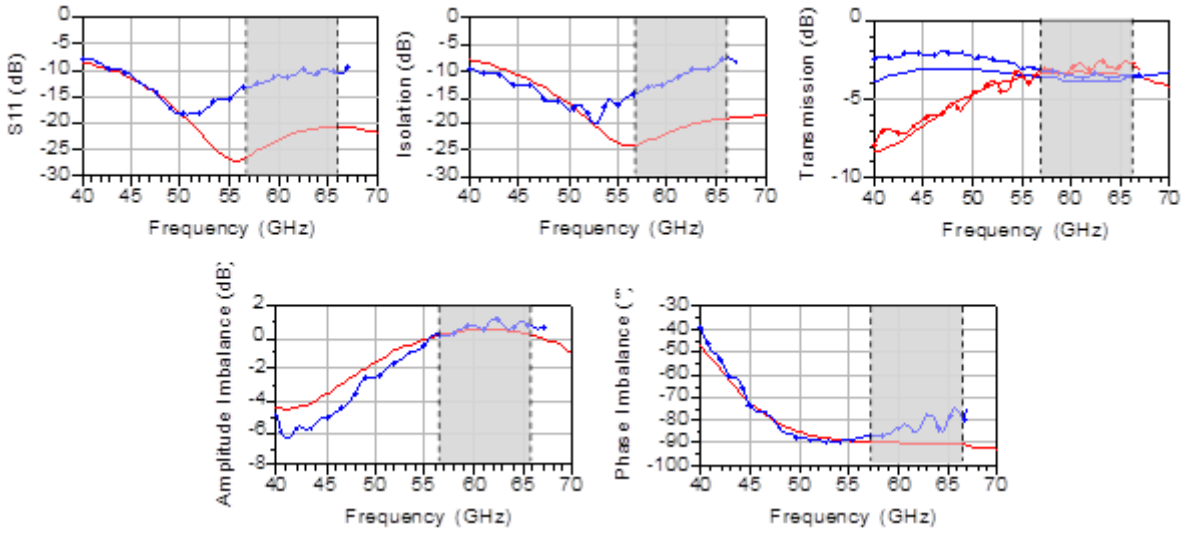

Fig. 67 . De-embedded performance of the two realized couplers (thick lines) compared to HFSS simulation (crossed lines).

d) IPD Integration and Design

A promising way to think about the integration of the IC's and the radiating element is the antenna-in-package solution. In this integration scheme, the antenna is realized on a low-loss substrate and can be directly implemented into the packaging. Lately, the tendency has been going to PCB package because they are low-cost. The IC is flip-chipped on the PCB board

and the antenna and beamforming network are implemented at the RF level. The proposed solution is to use the IPD technology from ST Microelectronics for the couplers and associated low-loss passive circuits. Indeed, the IPD technology is low-loss when compared to Silicon technology and allows scaling down passive components.

The signal lines of the realized coupler (Fig. 68) are etched on the 3-µm thick M3 layer and its ground plane on the 6-µm thick M2 layer. They were simulated using HFSS. MIM capacitors between layers M2 and M3 are used. Simulated results are summarized in Tab. 4. We obtained the same performance than for the Silicon couplers with a 73% size reduction (0.2 mm² instead of 0.73 mm²).

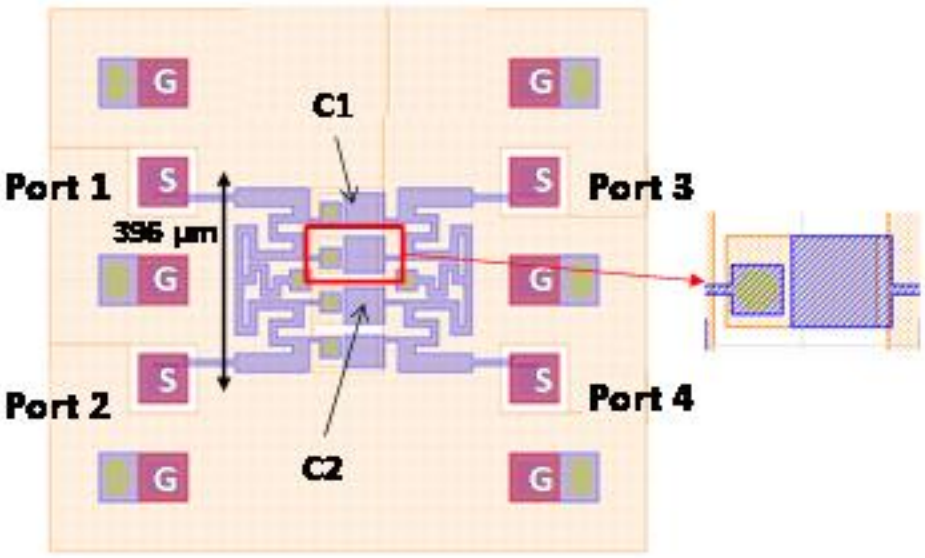

Fig. 68 Layout of the fabricated coupler in IPD

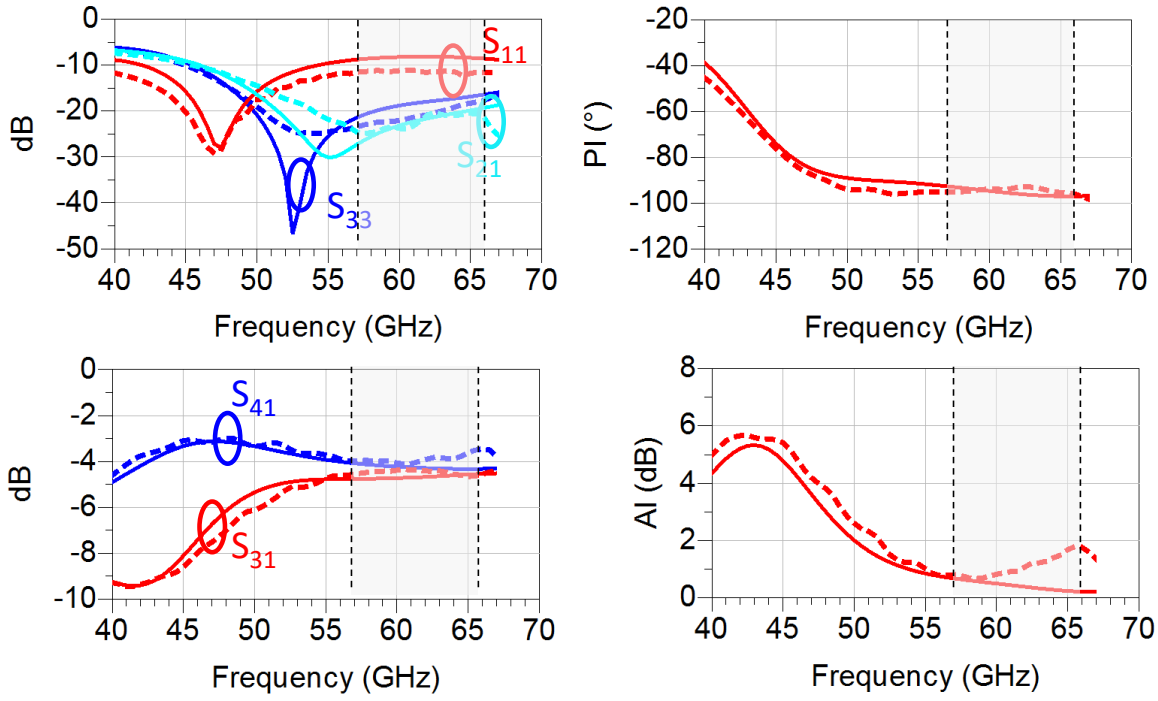

Fig. 69 Simulated (solid lines) and measured (dashed lines) S-parameters, Amplitude Imbalance and Phase Imbalance of the DT coupler.

e) Comparison with state-of-the-art published couplers

Several couplers have already been presented at 60 GHz in the literature [HET10-HAR10-KUO11]. A comparison is given in Fig. 70 regarding several parameters. In the x axis, we represent the ±1 dB amplitude bandwidth and in y, the ±5° phase bandwidth. The circle size is proportional to the coupler area. Expected performance for our couplers should be state-of-the-art.

Technology	Return loss at 60 GHz	Isolation at 60 GHz	Insertion loss at 60 GHz	Phase shift at 60 GHz	-10 dB Bandwidth (GHz)	± 0.5 dB Amplitude Imbalance	± 1° Phase Imbalance	Size (mm²)
BiCMOS9 MW	23.3 dB	22 dB	0.8 dB	90.2°	43-80 (> 61 %)	53-68.5 (26 %)	54.5-66 (19 %)	0.080 (82 %)
IPD	18.4 dB	15.1 dB	1.1 dB	90.4°	44.5-80 (59 %)	56-71.5 (26 %)	56-76 (33 %)	0.200 (73 %)

Tab. 4 Summary of Simulated Performance of Proposed Couplers

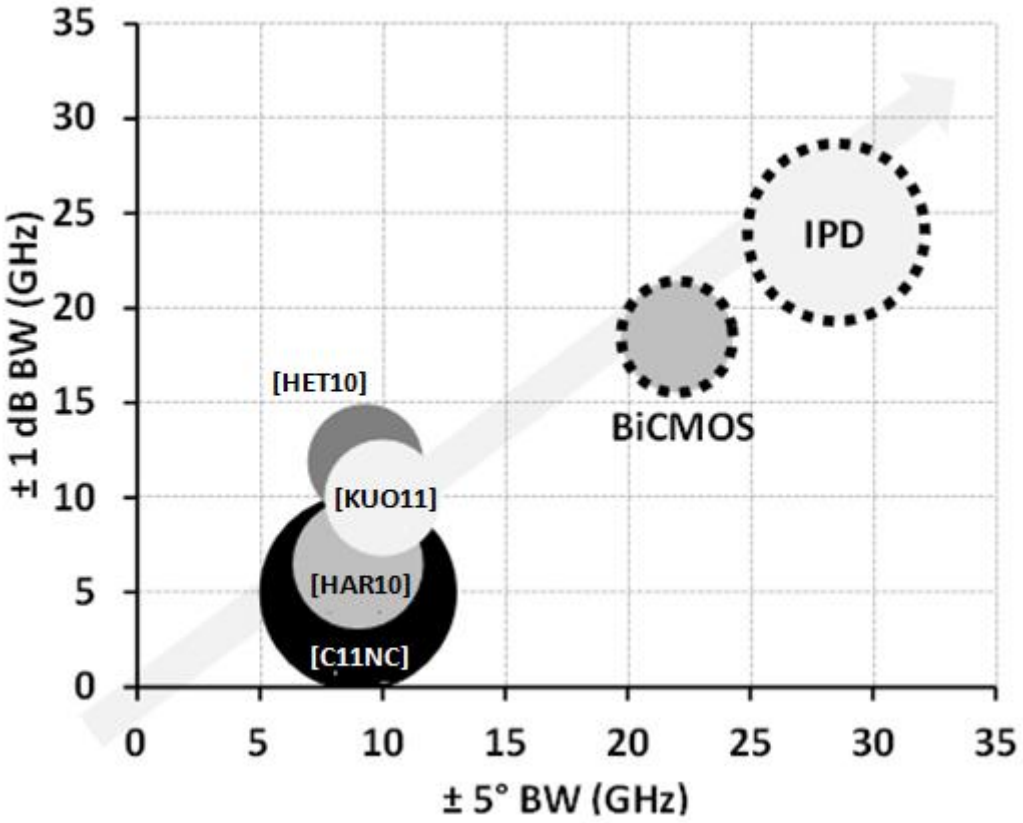

Fig. 70 Comparison of the proposed coupler to the literature. Proposed couplers are listed following their technology

2. Butler Matrices

The use of phased-array antennas is commonly proposed to improve the budget of a Mm-wave Tx link. Compared to continuous phased-arrays, discrete phased-arrays can be used if only beam-steering in fixed directions is targeted. One of the solutions is the Bulter matrix. It is a passive network. Hence, there is no power consumption and the complexity of the

transceiver architecture is relaxed. Compared to other solutions, namely the Rotman lens and the Blass Matrix, the Butler matrix is chosen for its easier implementation.

As shown in Fig. 71, a 4x4 Butler matrix is made of four 90° couplers, two 45° phase shifters and two crossovers [BUT61]. By selecting one of the inputs while the remaining are matched to 50 Ω, four different sets of phase differences are produced between the output ports of the matrix. Usually, the selection of the input port is made by an SP4T switch. When the matrix is followed by an antenna array, it then generates four different radiated beam angles pointing in the ± 15° and ± 45° directions depending on the input port with the configuration presented in Fig. 71. 8x8 matrices can also be designed. They generate eight different beams, but their layout becomes more complicated and larger with an increase into the insertion loss.

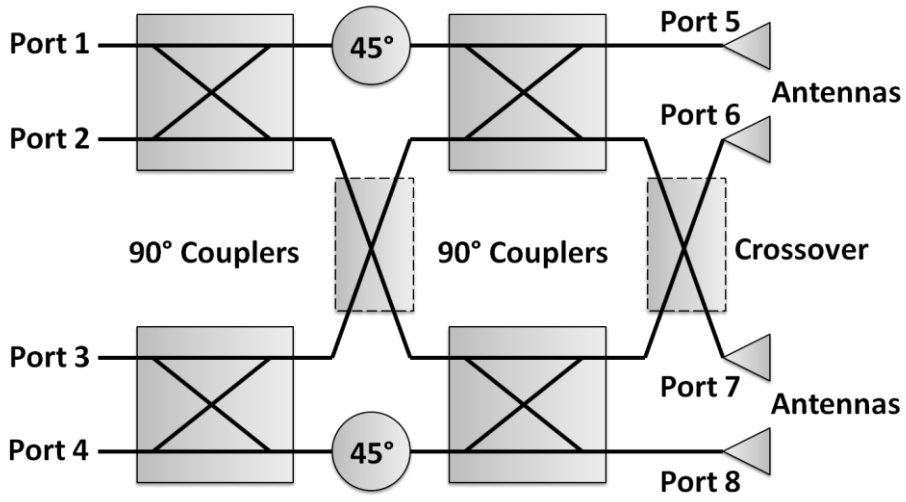

Fig. 71 Schematic of a Butler matrix.

a) Design in IPD Process

The layout of the Butler matrix realized in IPD process is shown in Fig. 72. The IPD process was chosen compared to an implementation on Silicon because its cost is lower and it enable to fabricate the beamforming network and antennas on the same substrate. The simulations were performed using the FEM solver, HFSS. These results were presented in [J14CP].

It uses the optimized 90° couplers presented in B.1.d to miniaturize its size while maintaining good performance over the all bandwidth. Due to the good isolation of the coupler, the Bulter matrix can operate without loading the unused ports, thus, without inserting any bulky and lossy switch for port selection, not easy to design at this frequency.

When using microstrip lines and single layer technologies, crossovers are most of the time made by cascading two 90° couplers [MOU10] which is a quite large solution, as presented in previous section. Here, the proposed crossovers are achieved by crossing the lines on different layers of the IPD Process using the multilayer feature [CHI10]. One of the line remains on M3, while the other one is laid on M2 linked by two vias. For matching purpose, the line on M2 is made wider. In our case, as the ground plane is set on M2, we etched away on purpose around the crossover. Simulated results show amplitude and phase imbalances between the two lines being respectively below 0.017 dB and 2.8° in the 60 GHz band.

An efficient 45° phase shifter can be designed with different techniques. In our design, we choose to insert a simple delay line. Simulation results show amplitude and phase imbalances between the microstrip lines being respectively below 0.14 dB and 10° in the whole 60 GHz band. The overall footprint of the Butler matrix, pads not included, is 1.6 x 1 mm².

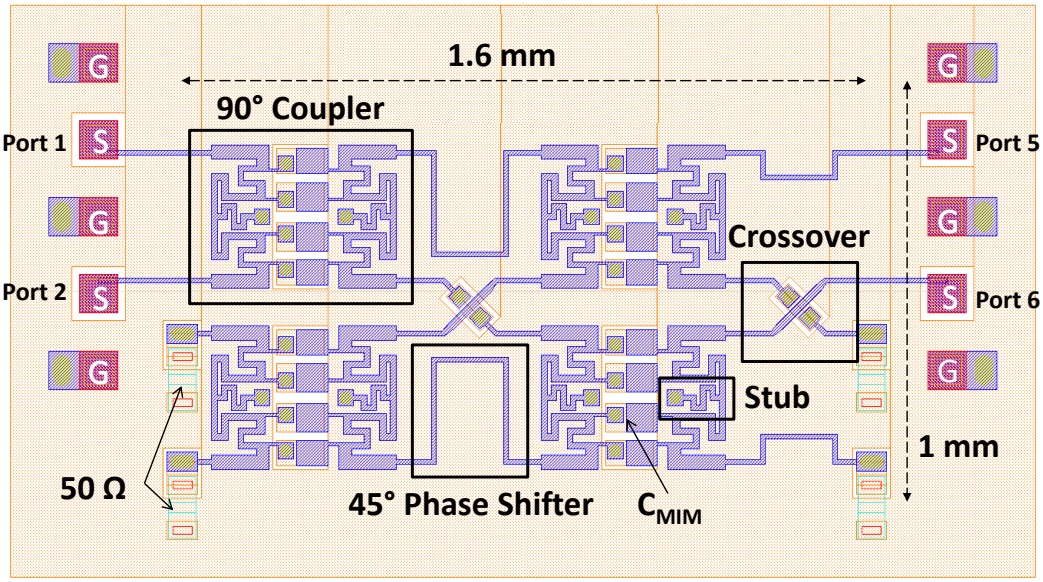

Fig. 72 Layout of the fabricated Butler matrix. Ports 3, 4, 7 and 8 are matched to 50 Ω.

b) Realization and Results

The measurement of the matrix was performed in STMicroelectronics, Crolles using on-wafer probing and a setup composed of two GSGSG Infinity probes and a 67 GHz VNA. Since this passive network is symmetrical, only two input ports (Port 1 and 2) and two output ports will be fed using GSGSG probes. In the first configuration, the output GSGSG pads are connected to ports 5 and 6 (Fig. 72) and in the second one, to ports 7 and 8. The others input ports (Port 3 and 4) are always matched to 50 Ω. For the 50 Ω load, we used resistors from the low frequency STMicroelectronics DK.

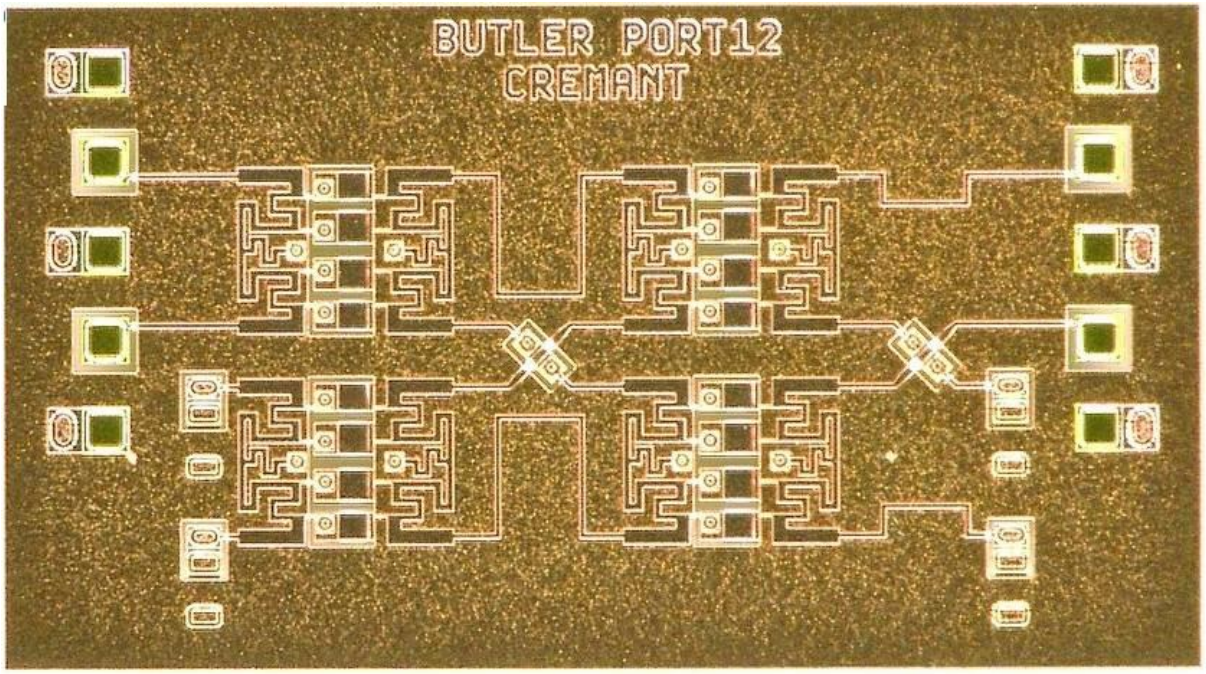

Fig. 73 Picture of realized Butler matrix

The measured and simulated results for the two configurations are presented in Fig. 74. First, the insertion loss (IL) and phase difference (Phase Diff) from Port 1 to Port 5, 6, 7, and 8 are presented, and then for Port 2. The IL is lower than 11 dB at 60 GHz and on the whole 57-66

GHz BW. If we take into account the inherent loss of hybrid couplers (6 dB since two couplers are used per path), then we achieve IL lower than 5 dB. As the couplers, presented in previous section, achieve approximately 1.5 dB IL on the BW, we can deduce than 2 dB IL come from the crossovers and 45° phase shifters. Another reason to explain the value of these losses can be found into the implementation of the 50 Ω resistors. We used elements from the low frequency STMicroelectronics DK. We suspect these resistances to be different from 50 Ω value. Fig. 75 shows another representation of the measured and simulated results using the Smith chart. For a better visibility, the frequency is only plot between 58 to 62 GHz on the Smith chart. The closer we are from the center of the chart, the higher the losses. A good amplitude imbalance is obtained if all the plotted S-parameters are on the same circle. This is almost true when port 2 is fed. It can be seen on Fig. 75 that when fed through Port 1, the signal has a delay around 45° between the adjacent ports, while when fed through Port 2, the delay is close to 135°. A maximum phase error of 13.6° at 60 GHz is measured. The reflection coefficient is lower than -10 dB over the 57-66 GHz band for all ports and the isolation higher than 15 dB.

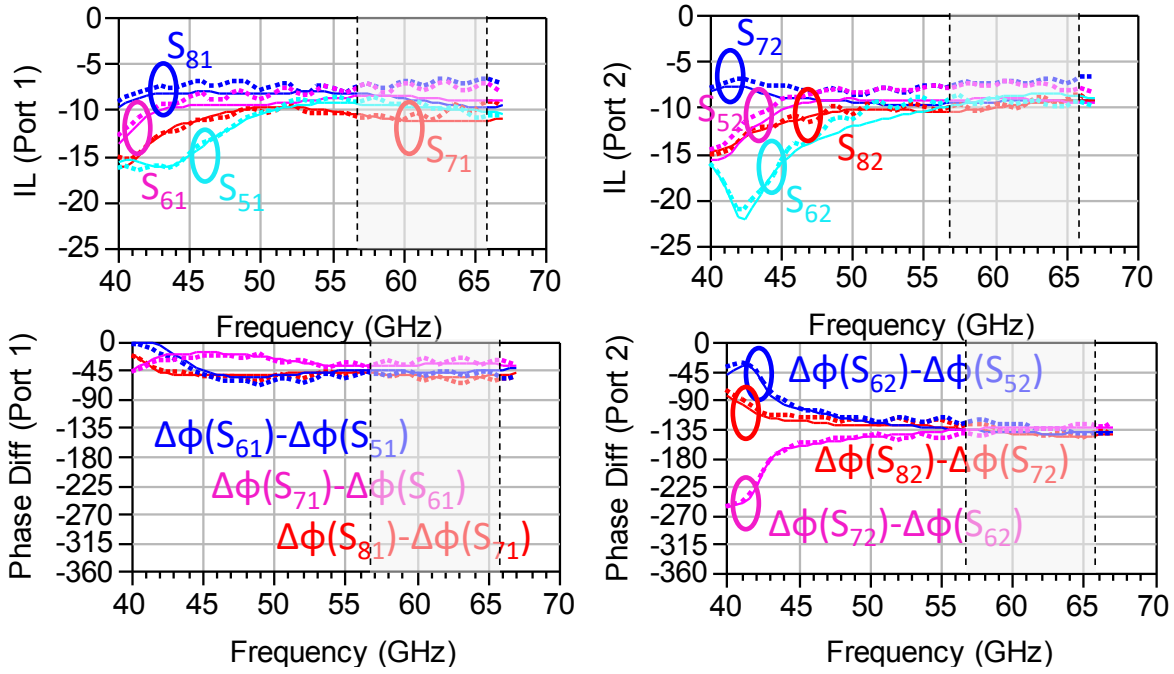

Fig. 74 Simulated (solid lines) and measured (dotted lines) insertion loss and phase difference for Port 1 and 2.

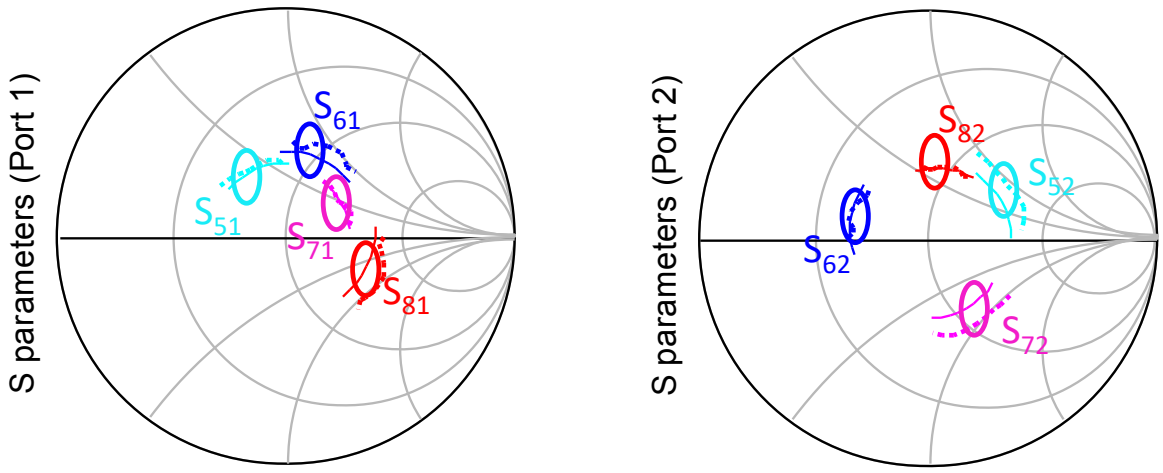

Fig. 75 Simulated (solid lines) and measured (dotted lines) S-parameters for Port 1 and 2. Frequency from 58 to 62 GHz.

c) Integration with a Vivaldi antenna array

The proposed Butler matrix was integrated with end-fire Vivaldi antennas for beam-forming application, the Vivaldi antenna structure was presented in [J14AW]. Vivaldi antenna-types have been used for decades as wideband and directive radiators. However, in order to obtain those characteristics, a long transversal size compared to the operating wavelength is required. To keep a compact structure, we intentionally degraded the potential performance of our Vivaldi design by reducing its dimensions. Realized gain and relative bandwidth goals were respectively set to 4dBi and 15% for 60 GHz WPAN applications. The thicker metal layer was used for the Vivaldi slot. The slot was optimized to be 1.6 mm long, with a minimal width of 50µm and a maximal opening of 0.7 mm (Fig. 76.a). The 50Ω microstrip feeding line of the Vivaldi slot was placed on the top metal layer (total length of 1.2 mm). A simple balun was used to convert the single-ended microstrip mode into a differential slot-mode (Fig. 76.b).

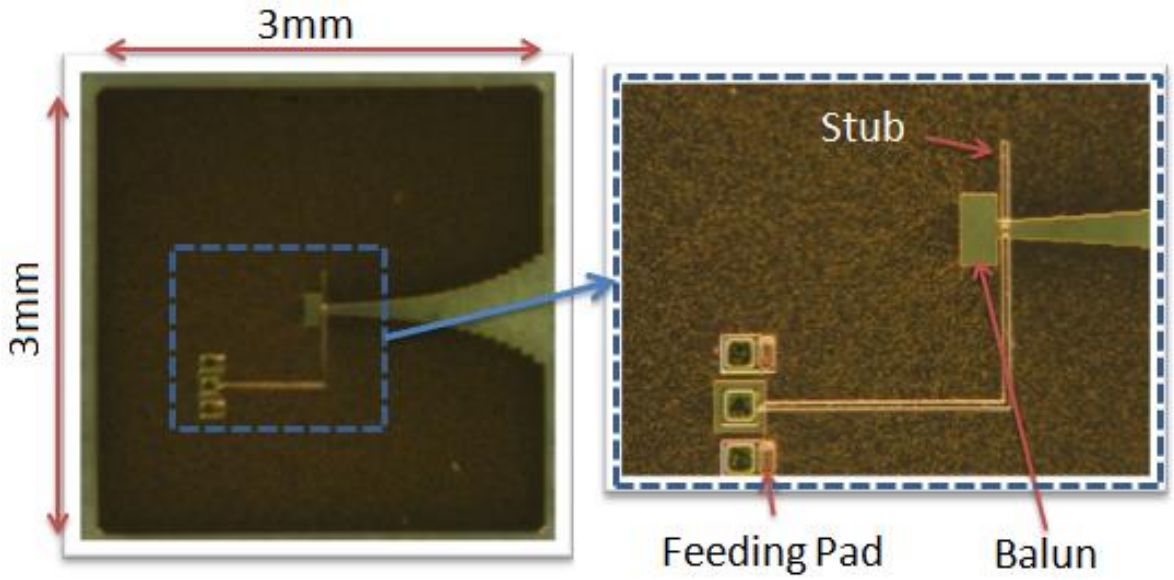

Fig. 76 Top full-view (left) and zoomed-view (right) of the fabricated IPD Vivaldi

Based on this Vivaldi type radiating element, a 4 element linear antenna array was designed as shown in Fig. 77. The distance between the 4 antennas is equal to a halfwavelength (2.5mm). The antenna array was connected to the 4x4 bulter matrix presented previously.

The antenna array was measured on the mmW set-up for two different configurations: when the port 1 is fed (Fig. 78.a) and when the port 2 is fed (Fig. 78.b). A maximum gain of 7.32 dB is obtained with a beam tilt of 22.5° as expected.

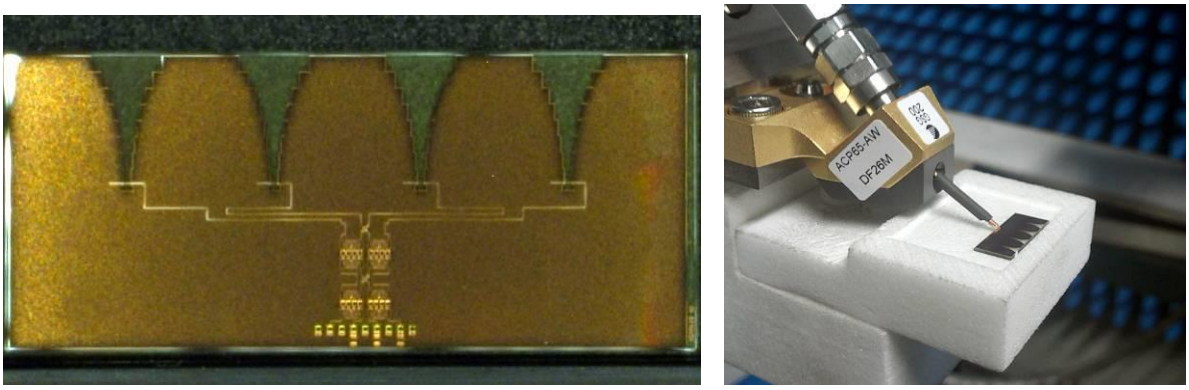

Fig. 77 Pitcure of the antenna array prototype and probe-fed measurement of the structure

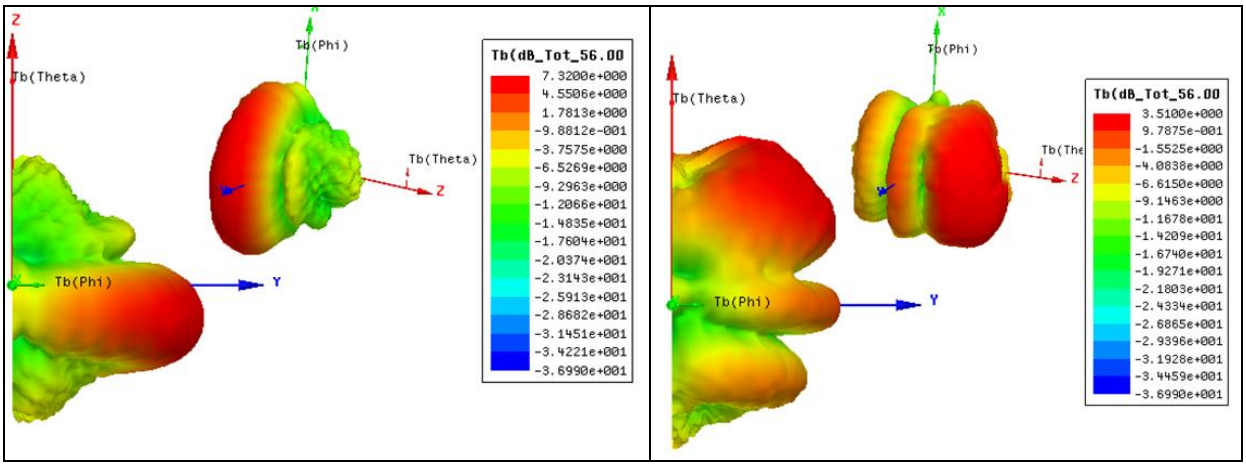

Fig. 78 3D radiation pattern measurement for Port 1(a) and Port 2 (b) fed

C. Antenna in Package design for millimeter waves

Concurrently to the design of mmW circuit, we have also studied to best solution for the antenna system. Two antenna main solutions have emerged at 60 GHz. The first one is the Antenna-on-chip (AoC) technology where the antenna is directly integrated with the front-end circuit on the same substrate. This solution has become affordable at millimeter wave frequencies thanks to the short wavelength (λ_0 = 5mm) and high permittivity of the RF front-end substrates, usually in silicon technology (ε_r = 11.9). The entire realization of the antenna and circuits on the same die helps in reducing the manufacturing costs and simplifying the front-end/antenna interconnection. The second technique is the Antenna-in-Package (AiP) solution. The antenna is fabricated on a separate substrate and/or package which will enclose the RF chip. At millimeter wave frequencies, the RF die has to be placed as close as possible to the antenna solution to avoid huge losses. This is the most employed low-frequency solution as the antennas can be realized on a cheaper and low-loss substrate. High gain and high total efficiency are easy to achieve for the antenna element at the expense of higher complexity and losses in the interconnections with the front-end module compared with the AoC solution.

The AiP solution seems to be the most promising antenna solution to highly integrate Mmw radios for high-speed short-range wireless communications because of high gain and broad bandwidth. Low-loss and low-cost substrates can be used at the expense of more complicated antenna to RF chip interconnections.

Materials and process technologies capable of realizing AiP solutions in high volume while respecting the above criteria are limited. Among them, we can cite HR silicon, Teflon, ceramics, and polymers. In recent years, an increase interest has been focused on low and high temperature cofired ceramic (LTCC and HTCC) and organic materials.

1. Designs with IPD Process

The IPD™ process developed by ST Microelectronics Tours has been especially created for lossless and miniature passive devices like resistors, capacitors or inductors at low frequencies. It has already been used previously to implement couplers and a Butler matrix. A simplified side view of the most significant layers of this process is presented in Fig. 79 (a). On top of the glass substrate (εr=4.6), we choose to use the third level of metallization (Meta3, h=3 µm) which is covered by a BCB material (εr=2.7) to etch the patch antenna. In an AiP perspective, an organic package could benefit from the IPD technology to widen the antenna bandwidth but it will be more expensive. The IPD superstrate is flip-chipped on the organic package. Two bump sizes are available, 140 µm and 240 µm, respectively called micro and macro bumps. The general SiP strategies developed in Fig. 79.a would then become the one presented in Fig. 79.b and c. In both configurations, thanks to the use of the IPD no cavity could be needed in the organic package.

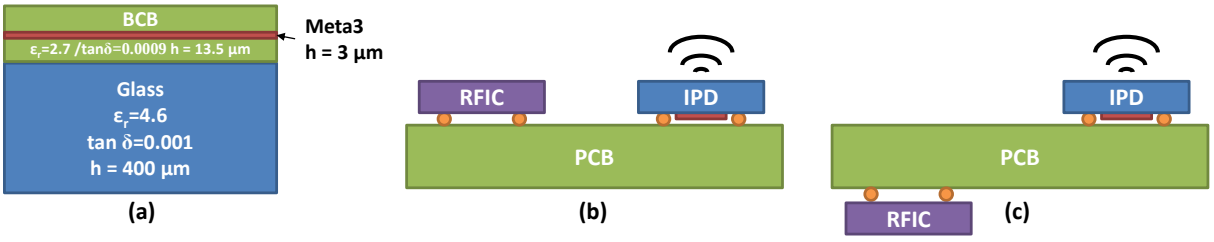

Fig. 79 (a) IPD process build-up. (b) Top die attach and (c) bottom die attach strategies using IPD.

a) Antenna design

Several size of bumps have been used during this study, I will here present the last antenna version using macro-bumps. These results have been presented in [C12EU]. A direct coupling from a microstrip line etched on the Taclamplus substrate is used to feed the patch fabricated on the IPD™ substrate. As before, the microstrip is fed using GSG pads and incorporates a double-tuning stub. This part is still etched on the Taclamplus material. Then, above the line, we electromagnetically couple the IPD™ patch. The IPD™ substrate is flip-chipped and soldered onto the Taclamplus using micro-bumps. After assembly, the air height between the IPD™ and the Taclamplus is given to be around 90µm with a ±10 um tolerance. The HFSS model and its coordinate system, as well as the realized antenna are presented in Fig. 80.a.

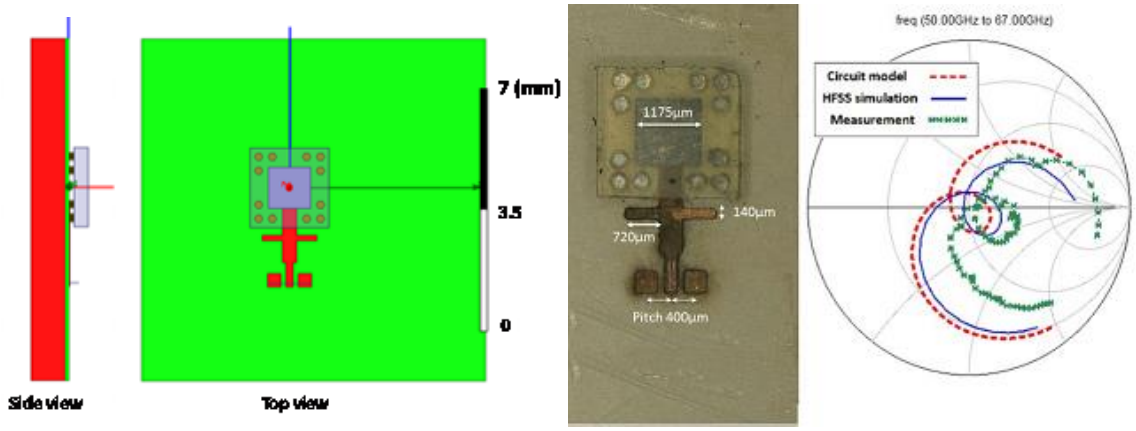

Fig. 80 (a) HFSS model of the coupled IPD patch antenna with macro-bumps. (b) Picture of the realized coupled IPD patch antenna.

After assembly, the air height between the IPD™ and the Taclamplus is given to be around 160 µm with a ±10 um tolerance. These results have been presented in [C12LA].

Simulated and measured reflection coefficients are presented in Fig. 81. The agreement is very good with a measured S_{11} below -10 dB from 55 to 64.2 GHz. However, we obtain a frequency shift of 1 %. We can see in Fig. 81.b that a variation of ±10 um can cause this kind of frequency shift. Using macro-bumps, we have gained more the 4 GHz of bandwidth.

Fig. 82.a presents the realized gains in the broadside direction $(\phi,\theta) = (0°,90°)$ which is the direction of maximum radiation. Co-polarization and total realized gains are superposed as the antenna is LP. The total realized gain is higher than 6 dBi from 53 to 66 GHz with a cross-polarization level lower than -10 dBi. The simulated and measured radiation patterns are plotted in the two main planes (E and H) at 60 GHz (Fig. 82). We obtain a maximum measured realized gain of 9.31 dBi at Phi=28° and Theta=90° in the E-plane and a measured realized gain of 7.87 dBi in the broadside direction $(\phi,\theta) = (0°,90°)$ very close to the simulated result (7.88 dBi). Simulated radiation efficiency is equal to 96 % at 60 GHz.Fig. 83.b presents the measured and simulated 3D patterns. We obtain a very good agreement. If we use the proposed method in Chapter III to compute the efficiency, we find that 83.3% of the radiation efficiency is due to the 74% measured pattern and 12% due to the 26 % simulated pattern. This gives us a radiation efficiency equal to 95.3%, very close to the 96% expected.

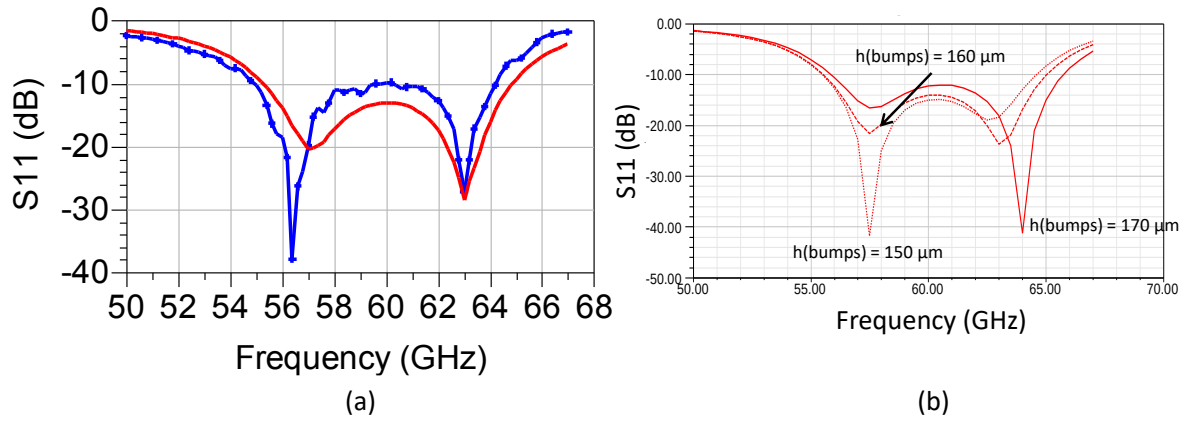

Fig. 81 (a) Measured and simulated reflection coefficient. (b) Variation of the reflection coefficient wit the height of the bumps.

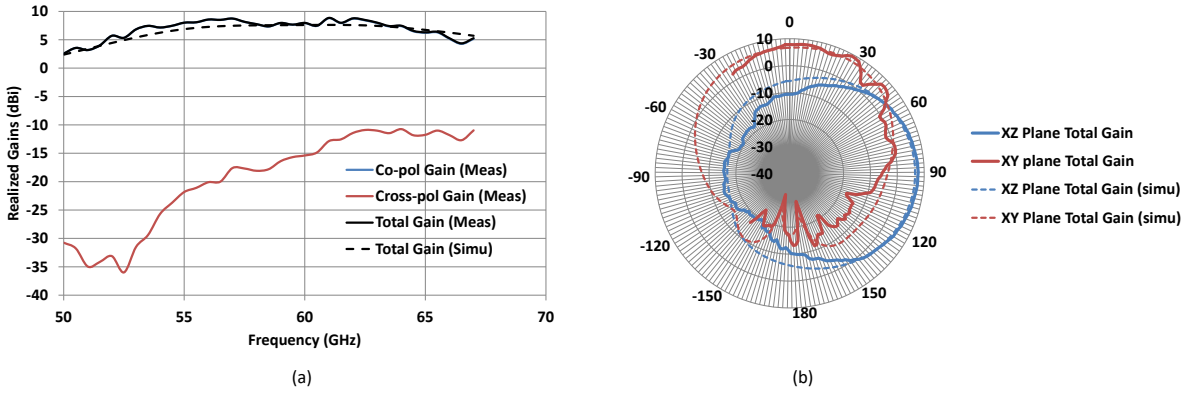

Fig. 82 (a) Measured and simulated realized gains with frequency in the broadside direction. (b) Measured and simulated realized gain radiation patterns at 60 GHz.

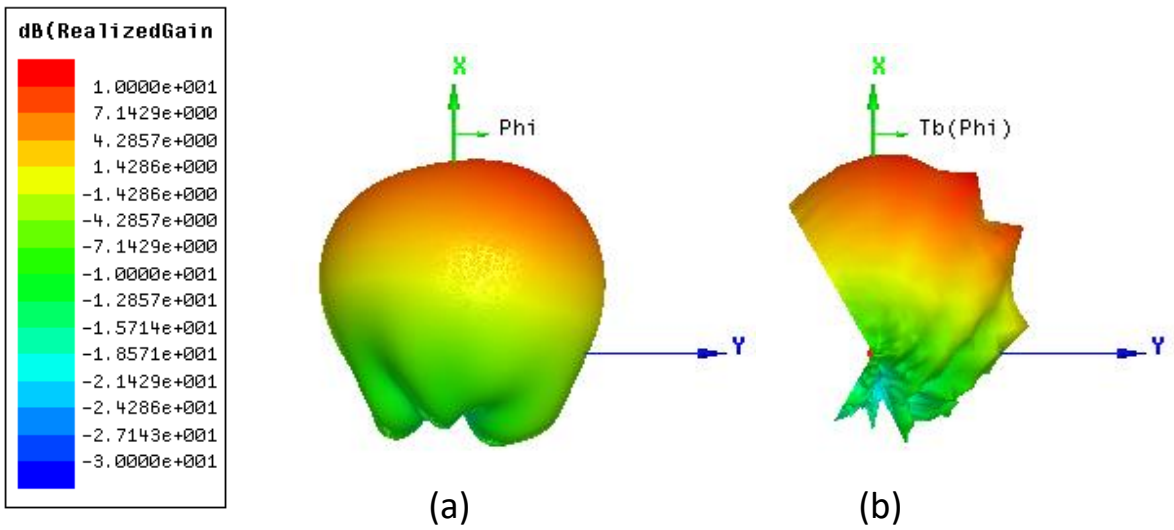

Fig. 83 (a) Simulated and (b) measured 3D total realized gain radiation patterns of the coupled IPD patch antenna with macro-bumps.

2. Designs on Organic Package

Within our collaboration with STMicroelectronics, we have been able to start the design of several antennas on their organic stack-up. This led us to work together with the Berkeley Wireless Research Center (BWRC). The aim of this project is to achieve I/Q spatial combining, the I and Q signals at the output of a transmitter are not combined on chip anymore, but spatially thanks to two different antenna arrays.

The objectives of this part are to design two linear antenna arrays on the organic package in a limited size while achieving same characteristics and especially for each element of each array. The return loss of each antenna has to be below 10 dB from 57 to 66 GHz, the gain of each element above 5 dBi on the same band, with a ±30° aperture at least. The chosen topology is an aperture coupled antenna. The antenna is fed on the top part of the package and radiates through the bottom part. Hence, the IC on the top of the package won't be disturbed by the antenna radiation.

Fig. 84 presents the top, bottom and side view of the package. On the top, the IC will be flip-chipped to the package using bumps and a 250-µm pitch. On Fig. 84, only the feed lines to the antennas are represented but this metallization will also be used for other RF, DC feeds and SMD components if necessary. We can see the slots on the second metallization on the top view of the aperture coupled antennas and the patches on the bottom view. All around each I and Q arrays there is a metalized ring, from the ground plane to the bottom metal layer. This ring is here to avoid substrate and surface modes. It is represented as a metal wall in simulation, but will be made of vias in the practical realization. Both simulations showed that we can model these vias by a wall with good approximation of the behavior of the vias, leading to faster simulations. The package dimensions are 12 x12 mm. Because the IC has its I and Q outputs on two opposite sides of the chip, the arrays have been put symmetrically on two opposites sides of the package. The two arrays could not be put closer because of the IC and the necessary space for the feed lines. The elements of each array are put at $\lambda_0/2$ (2.5 mm) from each other and the two arrays at 1.5 λ_0 from each other.

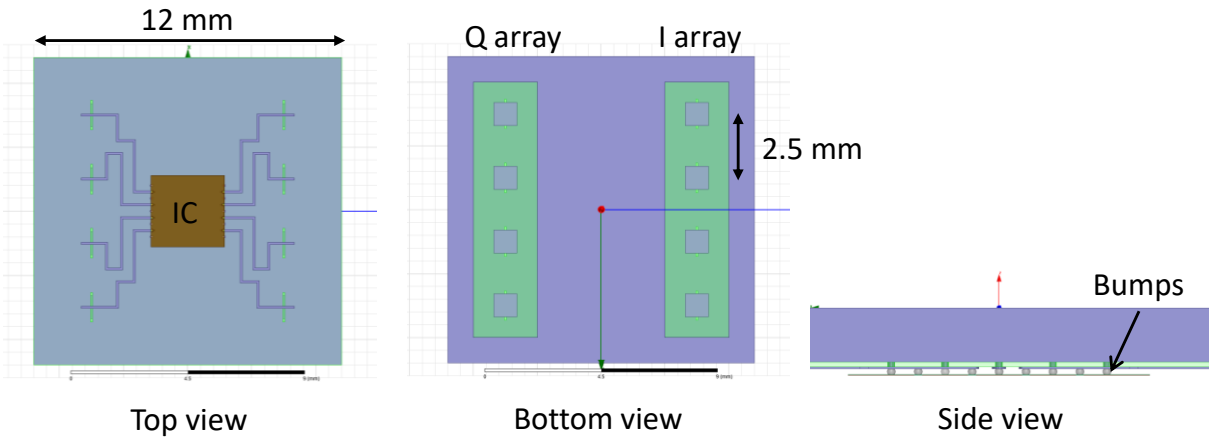

Fig. 84 Organic package design.

A prototype was realized and a picture is presented on Fig. 85. Antenna elements are measured one by one as the global array can only be fed from the chip. $|S_{11}|$ measurements, achieved with a microelectronic probe from our measurement set-up are presented in Fig. 86.

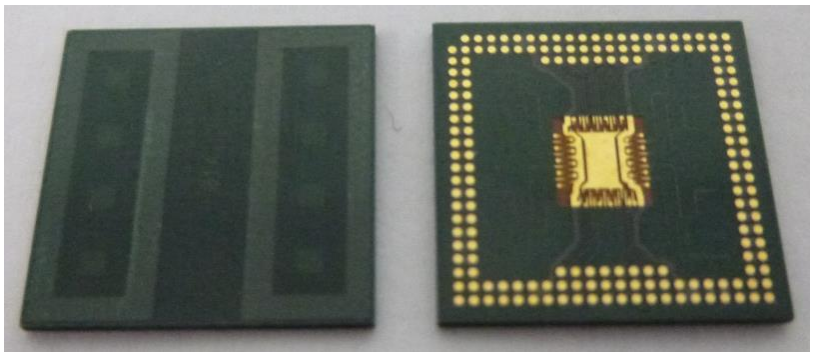

Fig. 85 Fabricated HDI module. Top (left) and bottom (right) views.

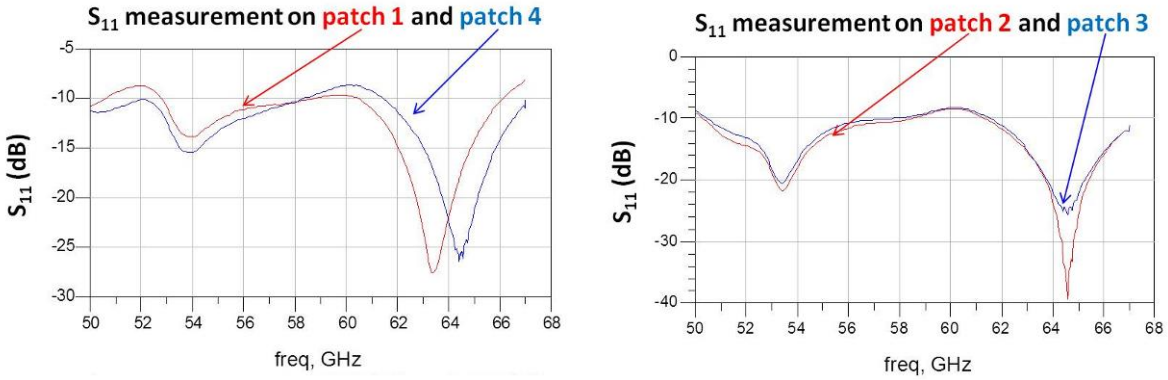

Fig. 86 $|S_{11}|$ measurement of various patches of the fabricated array.

Co-polarized realized gain measurements are compared to simulations in Fig. 87.a. Simulated and measured 3D radiation pattern is presented in Fig. 87.b. Co-polarized realized gain measurement in the H plane for patch 1 is presented in Fig. 88. Overall behavior is quite similar. However, lower measured gain is obtained. This can be due to the fact that as we measure one antenna only, the other ones are left open (and not matched to 50Ω as this is done in simulation). The measurements were done on several samples showing a good reproducibility.

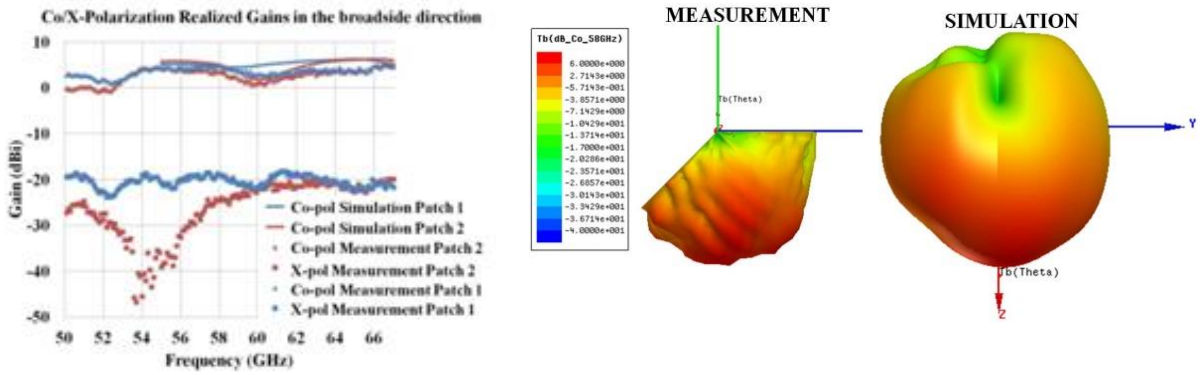

Fig. 87 (a) Realized gain measurement versus frequency, (b) 3D co-polarized realized gain measurement for patch 1.

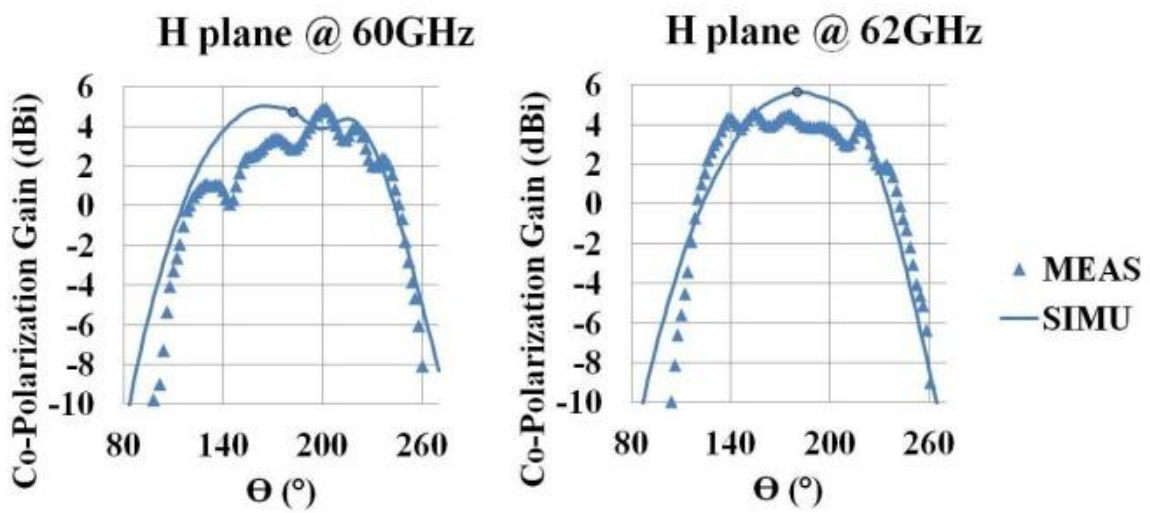

Fig. 88 Co-polarized realized gain measurement in the H plane for patch 1.

To conclude this part, based on the collaboration with Berkeley Wireless Research Center, a complete system was assembled and tested. A measurement with the BWRC chip was realized and presented in [C13JS]. The organic prototype was not available to meet the ISSCC deadline, and a specific design made on Rogers material was done for this purpose and is presented in Fig. 89.a. Main results for the Other the Air measurements (realized by BWRC) are presented in Fig. 89.b. A maximum data rate of 6Gb/s is obtained for a 16-QAM modulation with a power amplifier average efficiency of 16.5%.

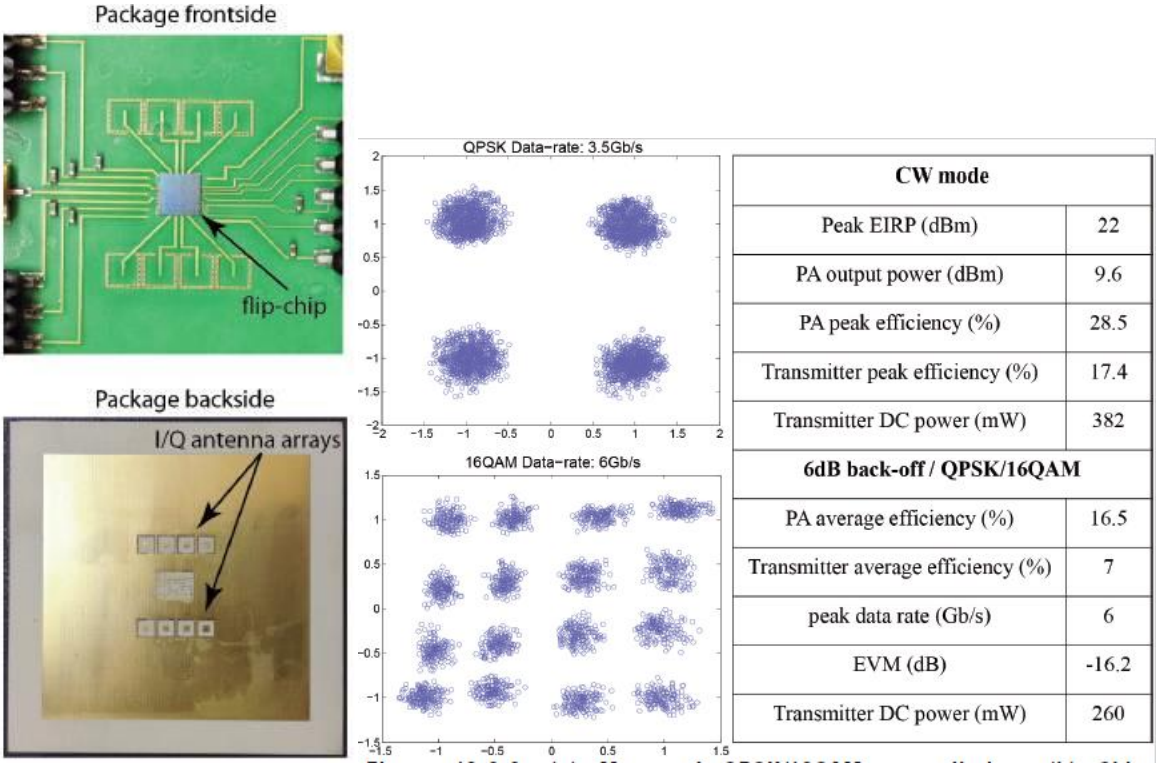

CW mode	
Peak EIRP (dBm)	22
PA output power (dBm)	9.6
PA peak efficiency (%)	28.5
Transmitter peak efficiency (%)	17.4
Transmitter DC power (mW)	382
6dB back-off / QPSK/16QAM	
PA average efficiency (%)	16.5
Transmitter average efficiency (%)	7
peak data rate (Gb/s)	6
EVM (dB)	-16.2
Transmitter DC power (mW)	260

Fig. 89 (a) Picture of the protype (b) Measured QPSK and 16PSK constellation (c) Demo parameters

D. MillimeterWave system caracterization

The main catalist of the different innovation in the millimeterwave domain was the development of an innovative set-up for mmW antenna characterisation. This system was first designed by Sylvain Ranvier during his PhD, and improved during the Diane Titz PhD.

At 60 GHz, the antenna can be on-chip but more recently, the millimeter community is moving to integration into a different substrate. Based on these two integration schemes, two different ways to characterize their radiation performance have arisen.

The integration of the antenna into a low loss substrate which is different from the Integrated Circuit substrate is the best solution at low frequency and those antennas are connector-fed to be measured in large anechoic chambers. A logical approach could have been to reproduce this characterization scheme at 60GHz. However, it was shown in [RAN09] that the connector, being as big as (or even bigger than) the antenna itself, is strongly disturbing the accuracy of the recorded radiation pattern. As a small improvement, it was demonstrated possible in [LAM10] to obtain acceptable results if placing some absorber sheets over the connector. However, another issue is the de-embedding of the connector from the measurement as it won't physically exist in the final design. Indeed the soldering stage can modify or deteriorate the small antenna before the measurement. Another important point is the big size of an anechoic chamber at lower frequency which is not compatible with a mmW frequency transmission characterization of medium gain antenna (<10 dBi) as the free-space attenuation of the electromagnetic waves is quite large and it would require high level power sources which is expensive and difficult to achieve. Finally, the connector-fed approach is not compatible with the Antenna-on-Chip (AoC) technology where the antenna is closely integrated within the RF front-end module.

We believe the other way to handle an accurate characterization setup is to think how to measure an Antenna-on-Chip. As the microelectronic Radio-Frequency (RF) circuits are closely integrated within the antenna, a logical approach is to derive a probe measurement procedure. However, several drawbacks exist. The close environment of a probe tester is usually all metallic, composed of a chuck base, a microscope, the probes and the positioners. The first measurements made in this way proved that the radiation pattern was completely disturbed [LAN10]. A first step is to get rid of the metallic chuck as was done in [PIL09], [ZWI04]. Also, the AUT has to be horizontally maintained very accurately to ensure a stable and solid contact between the microelectronic probe and the antenna pads which is important for characterization accuracy and also to avoid damaging the expensive probe. In [PIL09], the metallic chuck was replaced by a rexolite chuck as a first interesting enhancement. In [ZWI04], no chuck is anymore used and the antenna is maintained by two substrate pieces of FR4 (Flame Resistant 4). A better solution would be to use a material with a lower permittivity and possibly close to one. Hence, the radiation pattern of the antenna would not be disturbed at all by the holding pieces: metal-free for the chuck or holder. Then we decide to develop a solution based on a special holder made of foam. Thus, the radiation pattern below the antenna (if the antenna is fed by the probe on its top face) can be recorded and the foam won't disturb the measure at all. Then, another issue is the probe itself. A study has to be made concerning its influence on the radiation pattern and especially how to extract the exact losses introduced by the probe itself only. Considering the two aforementioned options, we tried to keep the best from both, and we concurrently developed a setup quite similar to the one described [BEE10].

1. Description of the Setup

This principle of the setup was first described in [RAN09]. A picture of the latest configuration of the measurement setup is shown in Fig. 90.

Fig. 90 Pictures of the measurement setup (Global view and closer view).

a) RF Parts

Several configurations have been used on this set-up and I will present the configuration based on a 60GHz VNA.

A schematic view of the setup is presented in Fig. 91. A signal is generated by the Agilent Vector Network Analyzer (VNA) E8361A. To control the power level of this signal and for calibration purpose, an Agilent E4418B power meter connected through a 10dB coupler is used after this amplification. The output power is about a 0-dBm at 60 GHz. An Agilent V281A Mmw-to-coax adapter allows conveying this signal to the microelectronic probe through a specific 60 GHz semi-rigid cable. A Ground Signal Ground (GSG) microelectronic probe feeds the Antenna Under Test (AUT).

At the receiver side, an HP 11970V harmonic mixer is directly connected to a Flann 25240-20 horn antenna to down-convert the received 60 GHz signal. This direct attachment is indeed really important because the Local Oscillator (LO) and Intermediate Frequency (IF) low frequency signals, at respectively 4.3 GHz and 310 MHz, can be conveyed with low-cost flexible coaxial cables allowing the mechanical parts of the setup freely moving during the measurement slot. This option especially helps to record the received signal with a better accuracy. The power level of the LO signal is then monitored with an HP 8563E spectrum analyzer or directly with the Agilent Vector Network Analyzer (VNA) E8361A. The VNA and spectrum analyzer are controlled from a computer via a General Purpose Interface Bus (GPIB) bus and a custom-made Labview code.

The Agilent Vector Network Analyzer (VNA) E8361A enables the S11 measurement of the AUT.

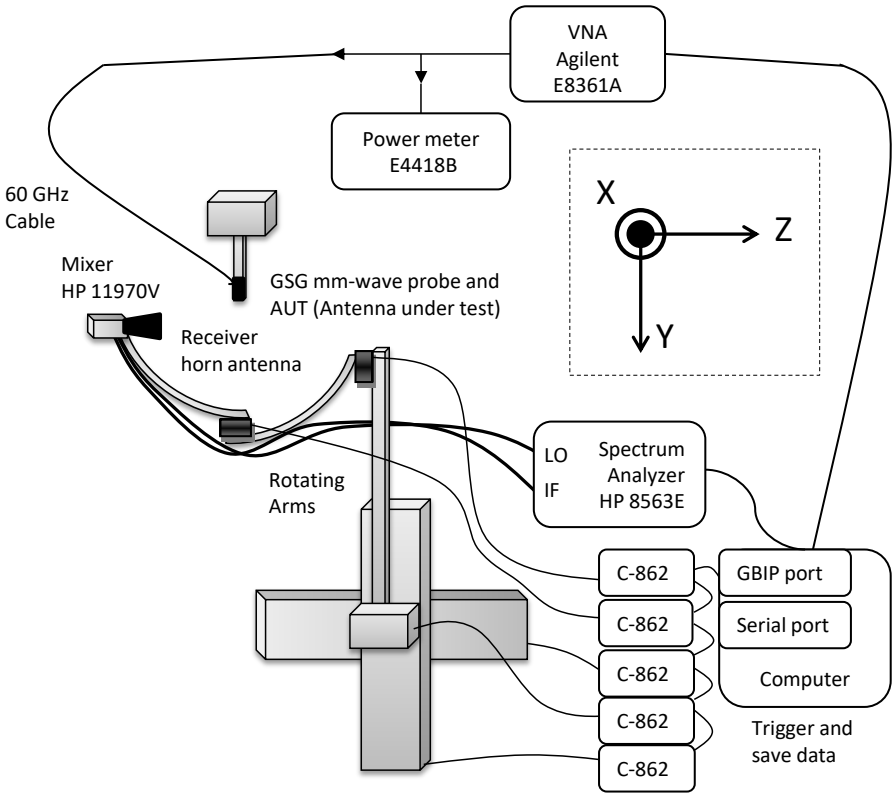

Fig. 91 Schematic view with a VNA.

b) Mechanical Parts

Two rotating arms are used to scan the quasi-3D sphere over the AUT, one of them holding both the receive horn antenna and the attached down-converter (mixer), the other holding this latest arm. The two rotations and the three translation axis of these arms are controlled by a computer and allow the measurement of 74 % of the total sphere with Phi from -30° to 220° in the XY Plane and Theta from -30° to 210° in the YZ Plane (Fig. 92). The distance between the receive horn and the AUT is chosen to be 20 cm. As the transmission distance is small, we are able to measure low-gain antennas. The far-field distance d_{far} can be computed from (Equ. 8) where λ_0 is the free-space wavelength and D the largest dimension of the AUT.

$$d_{far} = \frac{2D^2}{\lambda_0} \qquad \text{(Equ.8)}$$

Setting 20 cm and 60 GHz values in (Equ. 8) allows claiming we are able to measure antennas with a largest dimension D equals to 2.2 cm. The largest dimensions of the aperture of the horn antenna is equal to 2 cm. Compared with existing systems and more precisely to on-wafer setups, we do not use any metallic chuck to maintain the AUT. Therefore, no metallic parts are closely positioned to the AUT and strongly modify its radiation pattern. For each antenna, we always fabricate a specific foam holder which is screwed to a special carrier fabricated in rigid polyurethane material (Fig. 93). The foam holder is chosen because its permittivity is close to one and does not introduce additional losses. The mechanical parts fit in less than 1 m^3.

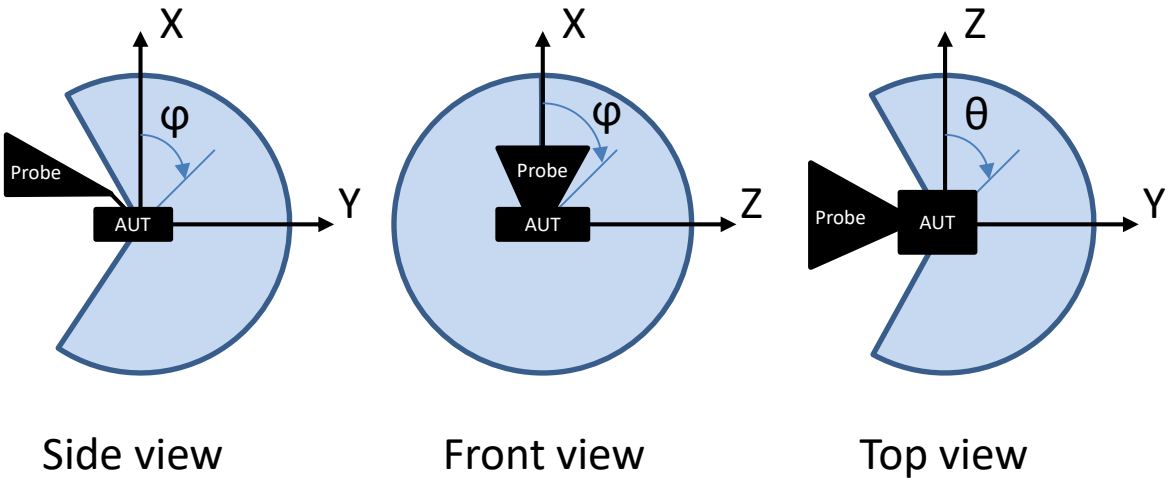

Fig. 92 Measurable part of the sphere in the XY, XZ, and YZ planes.

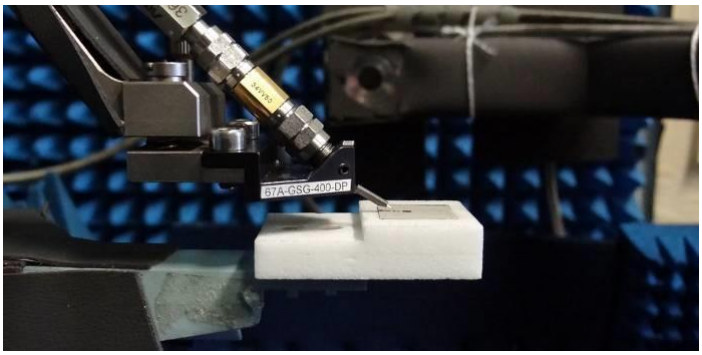

Fig. 93 RF probe and foam holder

2. Calibration

a) Mechanical Calibration

Several mechanical steps must be performed before starting the RF calibration. First, the AUT has to be positioned on its holder and the holder has to be screwed on the carrier. To maintain the AUT a cavity is made into the foam holder whose dimensions are those of the antenna (Fig. 94.a). Then, two laser pointers, which can fit into the center of the rotating arms, are used to accurately position the AUT at the center of the measurement sphere using the x, y, and z translation motors (Fig. 94.b). Because the overall assembly of the two arms with the mixer and the horn antenna is a bit heavy (1 kg), a slight inflexion of the two arms is observed (<2°). However, we truly checked that no vibrations were happening during the measurements mainly because the two arms were designed in reinforced but lightweight aluminum. To avoid any electromagnetic reflections and diffractions, these two aluminum arms are covered by thin-sheet absorbers. Then, a movable microscope is necessary to place the probe in-situ.

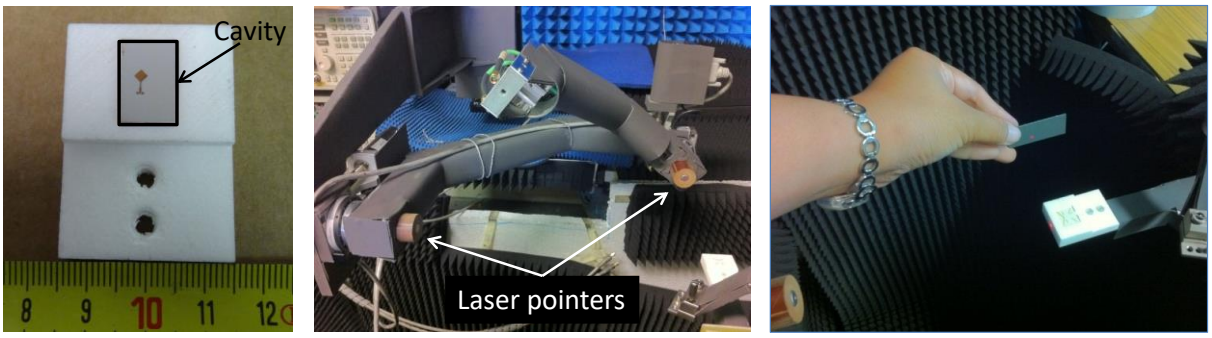

Fig. 94 AUT in its foam holder maintain into a cavity. (b) Laser pointer for accurate positionning of the AUT.

b) RF Calibration Methodology

The calibration and the associated accuracy of such a setup are not trivial. In classic anechoic chambers, the RF calibration is usually achieved with two reference antennas, having a known realized gain. Designing a reference integrated antenna at these frequencies is quite challenging. Reference antennas as horn antennas are often fed by a waveguide. By doing so, the probe is not taken into account in the calibration procedure and the transmitted horn antenna should be at the exact place of the AUT which would be quite complicated and a long procedure in our case. So, we decided to implement a different sort of calibration.

We directly connect the 60-GHz cable to the receiving mixer using a waveguide-to-coax adapter instead of connecting this cable to the AUT via a probe (Fig. 95). The 20-dB coupler is useful to monitor the output power of the VNA. With 12.5 dB lost in the cable and 0.5 dB lost in the adapters, the mixer experiences an input power close to -13 dBm, which is 10dB lower than its 1-dB compression point (-3 dBm). The schematic with VNA is given in Fig. 95.

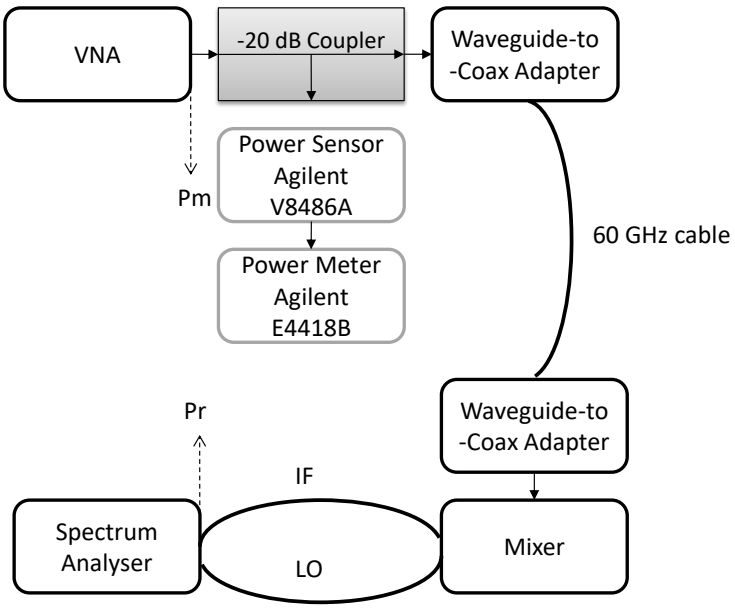

Fig. 95 Schematic of the calibration procedure with the VNA.

This calibration is done for each polarization direction because we are forced to slightly twist the two cables and add two short cables when we turn the receiving horn in order to measure the cross-polarization level. Both calibrations are generally really close to each other. The

overall losses of the setup given in dB are then deduced from (Equ. 9) using a simple transmission measurement knowing the output power of the amplifier (Pa) and the LO power (Pr) measured on the spectrum analyzer. They can also be calculated between the output power of the mm-wave source module (Pm) and the LO power (Pr).

$$\begin{aligned} Losses &= Pr - Pa \\ &= Losses\ (LO, IF\ cables) + Losses\ (Mixer) \\ &+2 \times Losses\ (Adapter) + Losses\ (60\,GHz\ cable) \\ &+Losses\ (-20\,dB\ coupler / coupled\ port) \\ &+Losses(Mmwave\ source\ module) \\ &+Losses\ (-10\,dB\ coupler / direct\ port) \end{aligned} \quad \text{(Equ.9)}$$

c) Computation of the Gain of an AUT

Knowing the overall losses computed during the calibration of the setup before every measurement, a very simple budget link is used to compute the gain of any AUT to be measured, for each polarization. This is done with the help of the simple Friis Equation given in dB in (Equ. 11) where Gr and G are respectively the gains of the receive horn and the AUT (PL being the free space loss defined by Equ. 11). The gain of the horn (Gr) and the losses of the probe ($Losses\ (Probe)$) are given by the manufacturers of the corresponding devices and can be verified by dedicated measurements. The losses in the 20 dB coupler and the adapters are extracted:

$(Losses\ (-20\,dB\ coupler / coupled\ port), Losses\ (-20\,dB\ coupler / direct\ port), Losses\ (Adapter))$

from their calibration and presented in Tab. 5. We can compute the path loss in dB from the distance between the AUT and the receive horn antenna, following (Equ. 10). Then, the gain of the AUT can be extracted from (Equ. 11) as the value of all the others quantity is known.

$$\begin{aligned} G = Pr - (Pa + Gr + PL + Losses) - Losses\ (Probe) + Losses(Adapter) \\ -Losses\ (-20\,dB\ coupler / direct\ port) + Losses\ (-20\,dB\ coupler / coupled\ port) \end{aligned} \quad \text{(Equ.10)}$$

$$PL = -20 \times log10(\frac{4\pi d}{\lambda_0}) \quad \text{(Equ.11)}$$

TERM	Value (in dB) @ 60 GHz	Uncertainty (in dB) @ 60 GHz
$Losses\ (Adapter)$	-0.5	0.1
$Losses\ (-20\,dB\ coupler / coupled\ port)$	-19.5	0.1
$Losses\ (-20\,dB\ coupler / direct\ port)$	-0.33	0.1
PL	-53.81	0.2
$Losses\ (Probe)$	-0.5	0.1
Gr	19.6	0.2
TOTAL	16.04	0.8

Tab. 5 Losses and accuracy of each term for the computation of the gain.

d) Measurement Accuracy

To double-check the accuracy of our calibration, two calibrations are performed for a single measurement: one before the measurement and one afterwards. Those two measurements give us the repeatability of the computed losses (Losses in (Equ. 10). However, for every term

from the link budget (Equ. 11), we need to know its uncertainty (Tab. 5). The uncertainty of the adapter and the -20 dB coupler has been measured with a 60-GHz VNA. The uncertainty of the computation of the path loss comes from the measurement of the distance between the transmitting and the receiving antennas. We estimated this distance to be 19.5 ± 0.5 cm, which leads to a path loss uncertainty of ±0.2 dB. The losses of the probe and the gain of the horn antenna are from the datasheet of the manufacturers or from dedicated measurements. The combination of all these numbers gives an overall gain uncertainty of ±0.8 dB for both vertical and horizontal polarizations. At those frequencies, it is very tricky to improve this accuracy due to the difficulty to measure the exact losses of each part of the setup.

3. Three-Gamma Method

In the previous calibration procedure, the losses of the probe simply taken from the datasheet of the manufacturer were subtracted in the computation of the realized gain (see equ. 10). With the three gamma method, we present a way to measure the true loss of the probe within our measurement setup. This is done with only S_{11} measurements. Moreover, a further step is developed to handle the situation for the probe to be loaded by a non 50 Ω load (antenna non-matched or outside resonance). We demonstrate it is essential to possess these losses to alleviate the link budget by an uncertainty.

a) Measurement Procedure

The method has been completely presented in [J14AW]. The probe can be modeled as a quadripole characterized by its S-parameters. It has an input and output reflection coefficient (Γ_{in} and Γ_{out}) when loaded by an impedance (Z_{load}). The input reflection coefficient depends on the output reflection coefficient which is connected to the load. Then, if the quadripole (i.e. the probe) is loaded by three different reference impedances (open, short and load), we obtain three equations with three unknowns, S_{11_probe}, S_{22_probe}, and Δ_s, described in Equ. 13. For a passive quadripole, as the probe, S_{12_probe} is equal to S_{21_probe}, we can then extract the S-parameters of the probe from Equ. 14 and therefore compute the losses of the loaded probe Equ. 15.

$$\begin{bmatrix} \Gamma_{in\_open} \\ \Gamma_{in\_short} \\ \Gamma_{in\_load} \end{bmatrix} = \begin{bmatrix} 1 & \Gamma_{in\_open}\Gamma_{out\_open} & \Gamma_{out\_open} \\ 1 & \Gamma_{in\_short}\Gamma_{out\_short} & \Gamma_{out\_short} \\ 1 & \Gamma_{in\_load}\Gamma_{out\_load} & \Gamma_{out\_load} \end{bmatrix} \begin{bmatrix} S_{11\_probe} \\ S_{22\_probe} \\ -\Delta_s \end{bmatrix} \quad or \quad \left[\Gamma_{in}\right] = \left[\Gamma_{3\times3}\right]\left[S_{probe}\right] \qquad \text{(Equ.12)}$$

$$\Delta_s = S_{11\_probe}S_{22\_probe} - S_{12\_probe}S_{21\_probe} \quad \text{(Equ.13)}$$

$$\left[S_{probe}\right] = \left[\Gamma_{3\times3}\right]^{-1}\left[\Gamma_{in}\right] \qquad \text{(Equ.14)}$$

From the developed equations, we need to measure two sets of data, Γ_{in} and Γ_{out}. To do that, two different S_{11} calibrations must be done. The first one is a calibration in the plane before the probe, hence at the end of the coaxial cable or the waveguide. With this calibration, we will be able to measure Γ_{in} when we will load the probe by the three reference standards. The second one is a calibration in the plane after the probe. Hence, we use a calibration substrate, which will give us Γ_{out}. After these two calibrations, we load the probe by the reference impedances (open, short and load) and measure S_{11} with the two different calibrations. This procedure is called the three-gamma method.

4. Circular Polarization

Circularly Polarized (CP) antennas are very interesting when placed at one side of a radio link, when the orientation of the two communicating devices is not known in advance. We have presented the first measurement of probe-fed CP antennas including the axial ratio (AR) in one direction, in 2D planes and in 3D.

a) Typical Ways to Measure a CP Antenna

To completely characterize the polarization of an antenna, it is necessary to determine the polarization ellipse (Axial Ratio and Tilt Angle) and the sense of rotation of the electric field vector. From the IEEE Standard Test Procedures for Antennas [IEE79], we can count four different methods that may be employed to measure polarization: polarization-pattern method, rotating-source method, multiple-amplitude-component method and phase-amplitude method.

In the polarization-pattern method, the linear receive antenna is rotated until the received gain is at its maximum, the tilt angle of the horn antenna is then measured, then the AR and tilt angle can be measured but not the sense of rotation. A disadvantage is that the probe antenna shall be rotated 360° which is not convenient when the AR has to be measure for several positions.

In the rotating-source method, the Linearly Polarized (LP) source antenna is still rotated, but the direction of observation is changed at the same time. But, the rotation of the source antenna should be much greater than its movement. The pattern is plotted at the same time as the AR, but nor the tilt angle neither the sense of rotation can be measured.

In the multiple-amplitude-component method, all the polarization characteristics can be determined. Four different antennas having different polarizations (vertical or horizontal LP, 45° or 135° LP, right-hand or left-hand CP) with known gains are used to measure the response of the AUT. Using all six antennas is even more accurate. A modified version involving only LP antennas can be employed to determine the AR and tilt angle provided that the sense in not required. This method is the one that will be implemented. It will be more detailed in b).

In the phase-amplitude method, all the data required for complete polarization determination can be measured simultaneously. But, it needs a measurement set-up with phase capability which is quite expensive and difficult to implement with satisfactory accuracy at 60 GHz.

b) Measurement of CP Antennas

In our measurement setup, the method I developed uses the modified version of the multiple-amplitude-component method. We are then able to measure the AR and tilt angle by rotating the LP receive horn antenna at 0° (horizontal), 45°, 90° (vertical), and 135° (-45°), for a fast four point measurement. For that purpose, a motor could be used to rotate the horn and record many points but because of weight issues in our setup, we decided to design a special horn holder with four possible angle positions. The four positions of the horn antenna are shown in Tab. 6. Measuring LP antennas, only 0° and 90° positions are required, but at least a third position (45° or -45°) is mandatory to be able to compute the polarization ellipse as shown in Fig. 96. This method was published in [J12AM].

Position	0°	90°	45°	-45°
Aperture view of the horn antenna				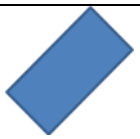

Tab. 6 Positions of the horn antenna for the measurement of CP antennas.

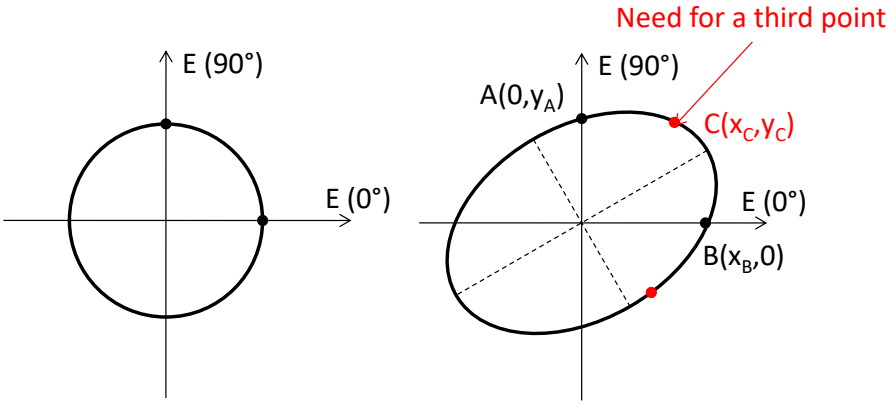

Fig. 96 Polarization ellipse of a CP antenna.

We can determine the polarization pattern from Equ.15 with G_i being the gain of the AUT in the direction θ_i alternatively equal to 0, 45, 90 or -45° (Tab. 6). Eq. 16 corresponds to the ellipse equation in polar coordinates. In Eq. 15, b is the semi-minor axis, e the eccentricity and τ the tilt angle of the ellipse. Then, b, e and τ can be computed from only three out of four measurements (G_0, G_{45}, G_{90} for example) from Equ. 17, Equ. 18 and Equ. 19. G_{-45} can be used as a verification check in this example. Hence, from the four gain measurement points, four different ellipses can be computed, giving four different values for the AR and the tilt angle. When the AR is low (below 3 dB), the four ellipses are the same or quite the same. When it increases and the polarization of the antenna becomes linear, the four ellipses can be quite different. The accuracy of this method is then the best when we have low AR. To determine which value of the AR and tilt angle is the right one, we use the fourth point (not use in the ellipse equation). The ellipse which is the closest to the fourth point is chosen. We will call this method the Ellipse method. Another method which was also implemented plots the closer ellipse to the four points using a Mean-Square (MS) optimization. We will call this method the MS method. Then, the AR, as stated into its definition (in [IEE93]), will be determined using Equ. 19 and the polarization ellipse plotted by taking the root-square of Equ. 15.

$$G_i = r_i^2 = \frac{b^2}{1 - e^2 \cos^2(\theta_i + \tau)} \quad where\ i = 0, 45, 90, -45 \qquad \text{(Equ.15)}$$

$$\left[\frac{1}{G_\varphi^2} + \frac{1}{G_\theta^2} + \frac{4}{G_{45}^2} - \frac{2}{G_\varphi G_\theta} - \frac{4}{G_\varphi G_{45}} - \frac{4}{G_\theta G_{45}}\right] b^4 + \left[\frac{4}{G_\varphi} + \frac{4}{G_\theta}\right] b^2 - 4 = 0 \qquad \text{(Equ.16)}$$

$$e^2 = 2 - b^2\left(\frac{1}{G_\varphi} + \frac{1}{G_\theta}\right) \qquad \text{(Equ.17)}$$

$$\begin{cases} \sin(2\tau) = 1 - \frac{2}{e^2}\left(1 - \frac{b^2}{G_{45}}\right) \\ \cos(2\tau) = \frac{b^2}{e^2}\left(\frac{1}{G_\theta} - \frac{1}{G_\varphi}\right) \end{cases} \qquad \text{(Equ.18)}$$

$$AR = \frac{a}{b} \text{ with } a = \frac{b}{\sqrt{1-e^2}} \qquad \text{(Equ.19)}$$

As explained earlier, the polarization sense cannot be extracted with the proposed method, but the maximum and minimum values of the LHCP and RHCP realized gains (G_{RHCP}, G_{LHCP}) can be computed from Equ. 20 and 21.

$$\begin{cases} G_{tot} = G_{RHCP} + G_{LHCP} \\ \sqrt{G_{RHCP} G_{LHCP}} = \frac{G_{tot}}{2} \frac{AR^2 - 1}{AR^2 + 1} \end{cases} \qquad \text{(Equ.20)}$$

$$\begin{aligned} \max(G_{RHCP}, G_{LHCP}) &= \frac{G_{tot}}{2} \frac{(AR+1)^2}{(AR^2+1)} \\ \min(G_{RHCP}, G_{LHCP}) &= \frac{G_{tot}}{2} \frac{(AR-1)^2}{(AR^2+1)} \end{aligned} \qquad \text{(Equ.21)}$$

c) Practical Example

The same antenna, used for the 3ϒ method, is here presented as an example for CP antenna measurement. We designed a CP patch antenna using the Taclamplus substrate from Taconic. A 400-µm GSG pad is used to probe the antenna through a microstrip line. The HFSS model of the optimized patch is presented in Fig. 97.a along with its feeding structure and the chosen coordinate system. A quarter-wave transformer is necessary to match the antenna to 50 Ω as the patch is galvanically fed to its corner.

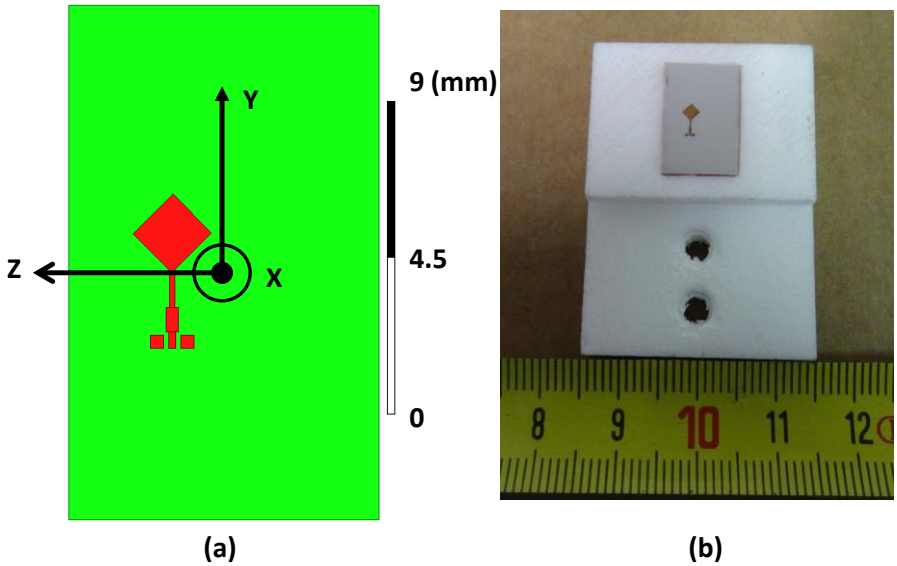

Fig. 97 (a) Top-view of the HFSS model of the patch antenna. (b) Fabricated patch antenna in its foam holder.

The realized gain of the fabricated antenna (Fig. 98) has been measured in the broadside direction (φ=0° and θ=90°, Fig. 2). Four different realized gains are measured G_0, G_{45}, G_{90}, and G_{-45}. As G_0 and G_{90} are orthogonal, as well as G_{45} and G_{-45}, the total gain can be computed from their sum, respectively called Realized Total Gain (0°+90°) and Realized Total Gain (-45°+45°). As can be seen, there is a perfect match between these two total gains on the whole band which is a proof of a repeatable measurement, meaning also that the AUT is at the center of the measurement sphere for the four positions of the horn. A good match is obtained between these measurements and simulations (Fig. 98) even though a very small frequency shift exists (1%). Due to fabrication tolerances, the prototype antenna can have shifted dimensions. To ensure a proper comparison with simulation, the device values are measured after the fabrication using Keyence microscope. Then, exact dimensions are used to fairly compare simulation and measurement. From these measurements, the AR can be computed using the three (AR (Ellipse)) or four (AR (MS)) measured gains. A quite good match is obtained between measurement and simulation (Fig. 100) with almost the same AR value at 59.5 GHz (only a 0.2 dB difference).

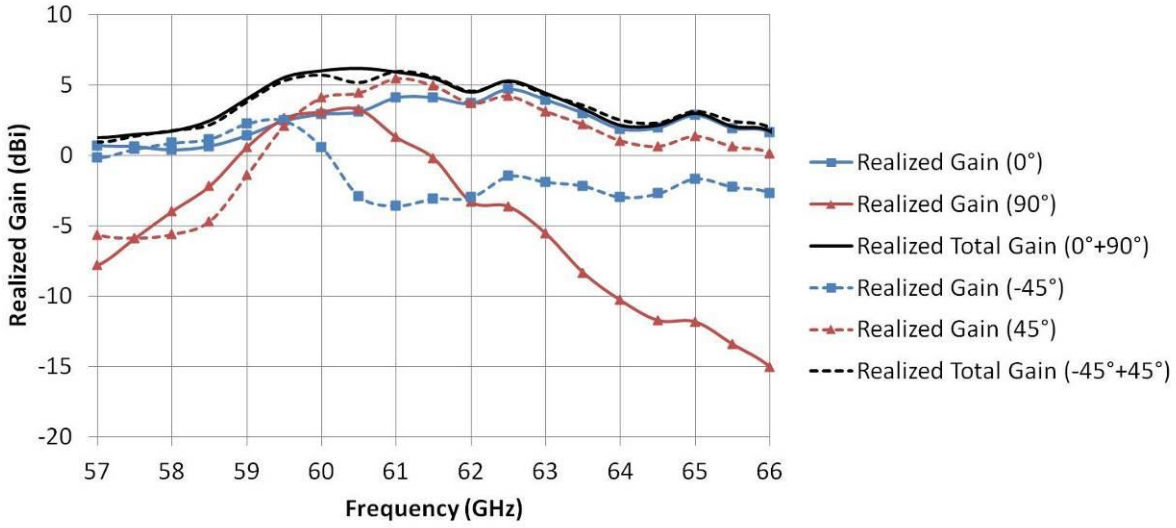

Fig. 98 Measured realized gains versus frequency.

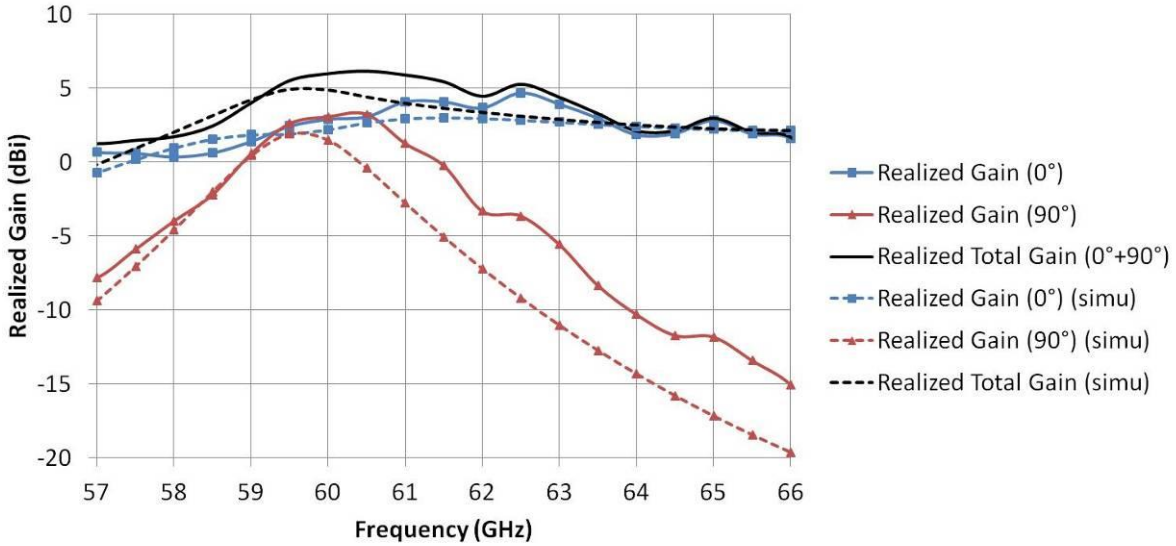

Fig. 99 . Measured and simulated realized gains versus frequency.

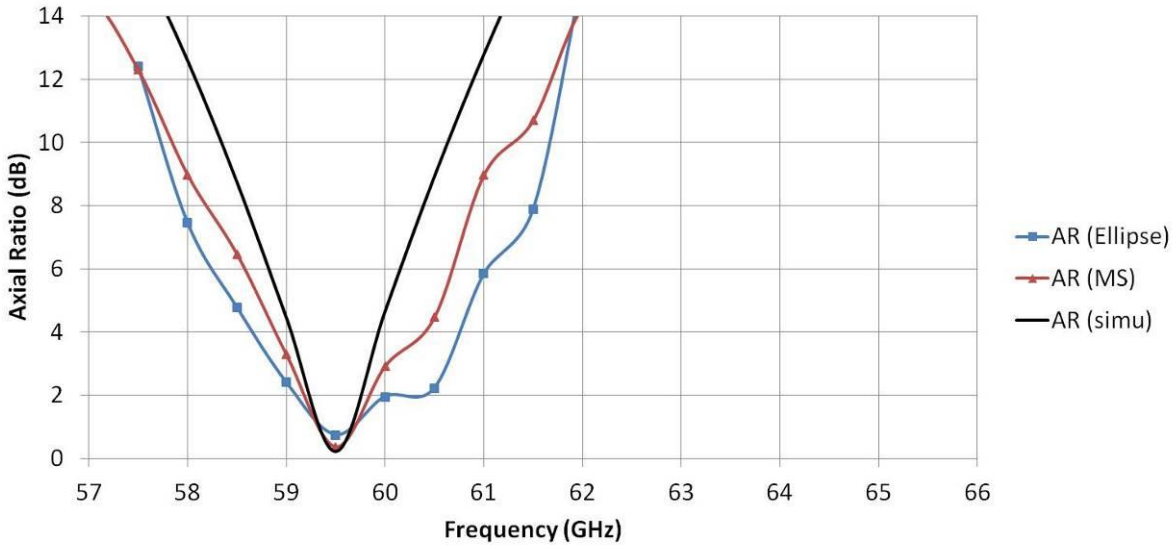

Fig. 100 Measured and simulated AR versus frequency.

As the setup enables the measurement of the quasi-3D sphere, the measurement of the CP antenna can also be realized in the two E- and H-planes in 5 minutes for each rotation of the horn antenna and along the 3D pattern in a half-day. From the value of the AR (from the two methods) and total realized gain in the planes, we can compute the LHCP and RHCP patterns. As we cannot know the sense of polarization from our measurement, we have to rely on the simulation. The RHCP and LHCP measurement in the E- and H- planes compared to simulation are presented in Fig. 101 and Fig. 102. From it, we can deduce that the antenna is left-handed circularly polarized. We obtain a very good match proving the validity of the measurements.

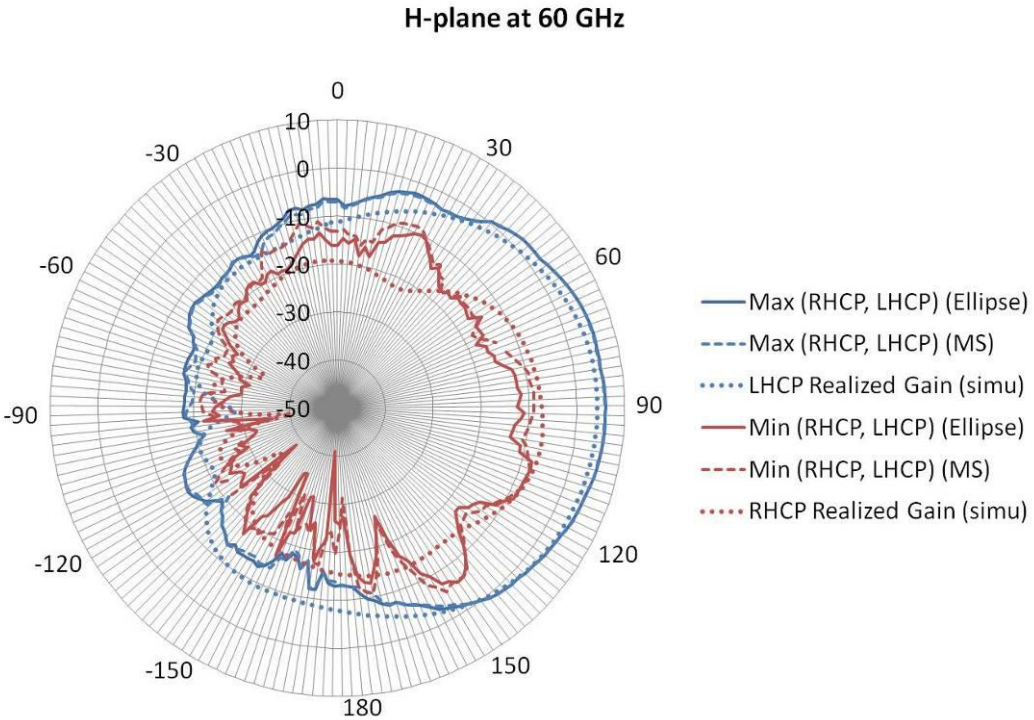

Fig. 101 Measured and simulated LHCP and RHCP realized gains in the H-plane at 60 GHz.

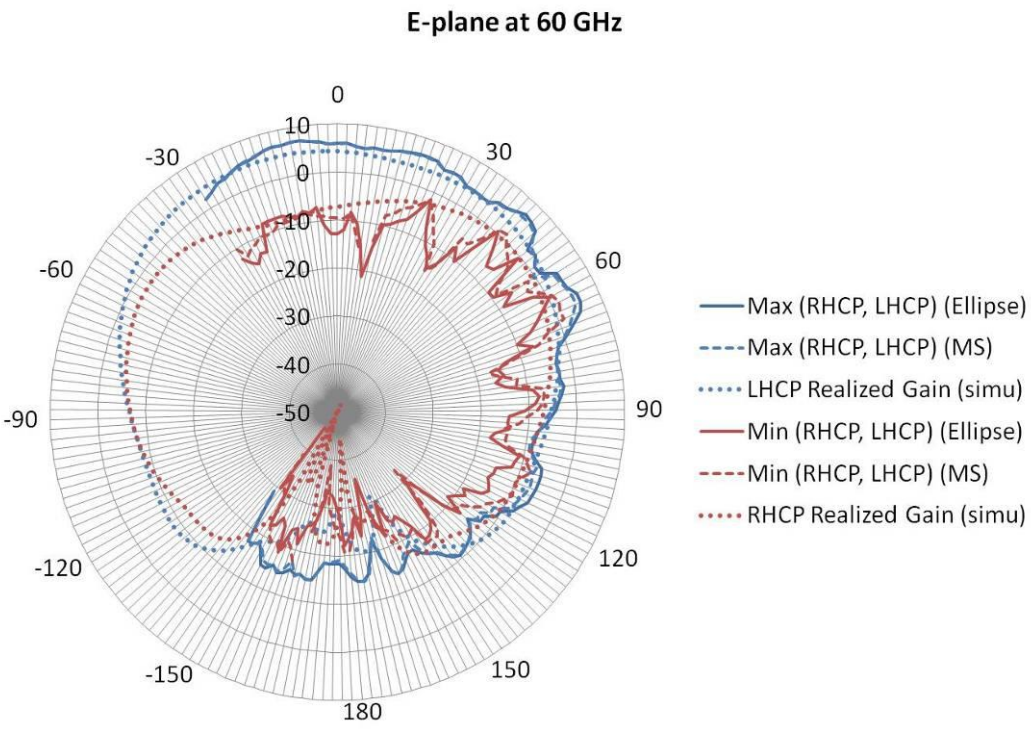

Fig. 102 Measured and simulated LHCP and RHCP realized gains in the E-plane at 60 GHz.

Fig. 103 presents the 3D measurement of the total realized gain with still a very good match between the realized total gain (0°+90°) and realized total gain (-45°+45°). The maximum achieved total realized gain for (0°+90°) and (-45°+45°) are 7.1 dB and 6.9 dBi respectively in the direction (ϕ, θ) = (-10°, 88°). The 3D measurement of the AR is presented in Fig. 103 with the Ellipse and MS methods respectively. A rectangular plot was chosen for more clarity. The blank parts are just out of range values. The AR is minimum around the broadside direction (ϕ, θ)=(0°,90°). Ellipses computed from the method are super-imposed with the 3D diagram. A good match is again obtained between simulation and measurement proving the accuracy and usefulness of the method.

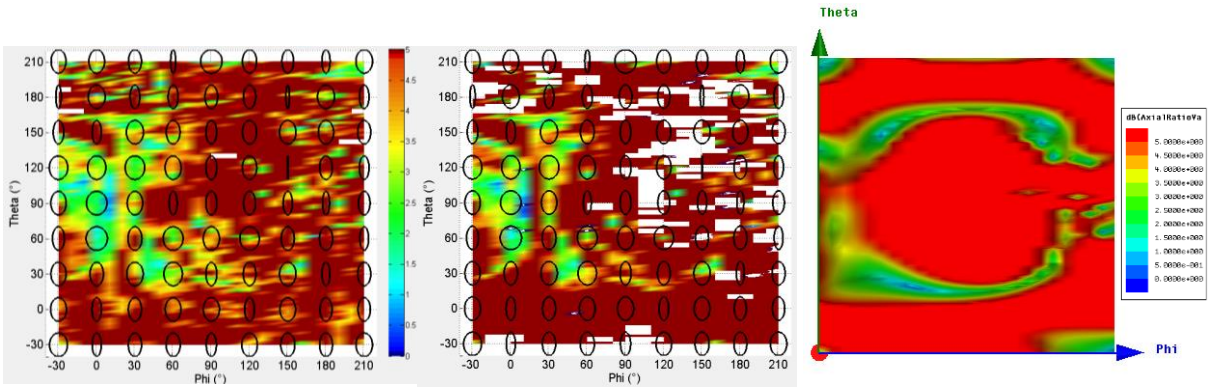

(a) (b) (c)

Fig. 103 Measured AR by (a) the Ellipse method and (b) the MS method compared to simulation (c).

The comparison between the two methods has still to be implemented and their accuracy be computed, but both method give quite satisfactory results.

5. Radiation Efficiency

Another important issue when dealing with antenna measurement is the measurement of antenna efficiency which is maybe one of the most important parameter of an antenna. Several methods have been developed at lower frequencies for connector-fed antennas.

a) Typical Ways to Measure Radiation Efficiency

From [IEE93], the radiation efficiency is the ratio of the total power radiated by an antenna to the net power accepted by the antenna from the connected transmitter (Equ. 23). The gain and directivity are then related by the radiation efficiency.

The first thing that comes to mind to measure the efficiency is to deduce it from gain and directivity measurements, where the radiation efficiency (η_R) is defined as the ratio of the peak gain to the peak directivity (Equ. 22). But, this method does not give accurate results, especially for directive antennas, because of the difficulty in calculating directivity from the measured patterns with sufficient accuracy.

$$\eta_R = \frac{peak\ gain}{peak\ directivity} \qquad \text{(Equ.22)}$$

Other solutions include the Wheeler Cap method [WHE59] or the use of a reverberation chamber [KIL04]. But, they are quite difficult to implement at Mmw frequencies, especially because of the presence of the probe. They would also need new measurements or a different measurement setup.

b) Measurement of efficiency using the proposed measurement setup

The value extracted for the measurement setup, is the realized gain, defined by Equ. 23. We can then deduce the incident power entering the antenna (P_{inc}), and compute the total efficiency (e_{tot}) from Eq. 37 where P_{rad} can also be developed as in Equ. 24.

$$e_{meas} = e_{tot} = \frac{P_{rad}}{P_{inc}} = \eta.(1-|S_{11}|^2) \qquad \text{(Equ.23)}$$

$$P_{rad} = \int_0^{2\pi}\int_0^{\pi} U(\varphi,\theta)\sin(\theta)d\theta d\varphi \qquad \text{(Equ.24)}$$

Then, e_{tot} can be expressed from Equ. 25, which simplifies into Equ. 26. As we are measuring the realized gain by steps in ϕ and θ, Equ. 26 can be re-arranged in Equ. 27 using discrete points. A value of the gain is associated to an area of the sphere, the smaller the steps in ϕ and θ, the smaller the numerical error.

$$e_{tot} = \frac{P_{rad}}{P_{inc}} = \frac{\int_0^{2\pi}\int_0^{\pi} U(\varphi,\theta)\sin(\theta)d\theta d\varphi}{P_{inc}} \qquad \text{(Equ.25)}$$

$$e_{tot} = \frac{P_{rad}}{P_{inc}} = \frac{1}{4\pi}\int_0^{2\pi}\int_0^{\pi} G_{real}(\varphi,\theta)\sin(\theta)d\theta d\varphi \qquad \text{(Equ.26)}$$

$$e_{tot} = \frac{P_{rad}}{P_{inc}} = \frac{1}{4\pi}\Delta\theta.\Delta\varphi.\sum_{j=1}^{M}\sum_{i=1}^{N} G_{real}(\varphi_j,\theta_i)\sin(\theta_i) \qquad \text{(Equ.27)}$$

But, in Equ. 26, ϕ and θ vary from 0 to 2π and 0 to π respectively, which corresponds to the measurement of the total 3D sphere. However, in our measurement setup, this is not possible due to the positioner. During the 3D measurement, 73.5% of the total sphere is measured with

ϕ and θ varying from -30° to 220° by 10° and -30° to 210° by 2° respectively. Hence, we can only deduce the total efficiency on a part of the sphere. But, as Equ. 27 is a sum, if we simulate the missing part and the simulated and measured realized gains are in agreement, we can trust the simulation and compute the efficiency on the missing 26.5% from the simulation and add the two efficiencies to obtain a good idea of the total efficiency of the antenna. Fig. 104 presents a radiation pattern summarizing the proposed method to compute the total efficiency of the antenna. One part of the radiation pattern is measured, the other one simulated and using both of them we can compute the total efficiency.

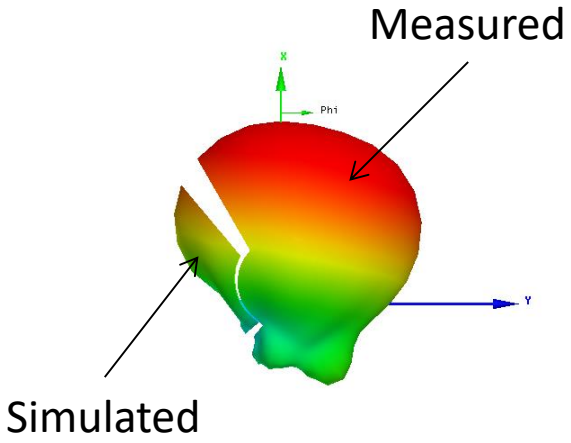

Fig. 104 Method to compute the total efficiency from the 3D radiation pattern.

To compute the radiation efficiency, by knowing the reflection coefficient of the antenna, we can deduce η from Equ. 23. But, as was demonstrated in [J14AW], to determine the gain from the realized gain, not only the mismatch loss has to be deduced, then to determine the radiation efficiency with accuracy, the gain has first to be deduced for the realized gain and Equ. 26 used with gain instead of realized gain.

E. References

[BUT61] J.L. Butler, and R. Lowe, "Beam forming matrix simplifies design of electronically scanned antennas," Electronic Design, vol. 9, pp. 170-173, Apr. 1961.

[HET10] K. Hettak, et al., "A Novel Compact three-Dimensional CMOS Branch-Line Coupler using the Meandering ECPW, TFMS, and Buried Micro Coaxial Technologies at 60 GHz", IEEE MTT-S International, pp. 1576-1579, May 2010.

[HAR10] I. Haroun et al., "Experimental analysis of a 60 GHz compact EC-CPW branch-line coupler for mm-wave CMOS radios", IEEE Microw. Wireless Compon. Lett., pp. 211-213, Apr 2010.

[KUO11] C.-Y. Kuo, at al., "Miniature 60 GHz slow-wave CPW branch(ine coupler using 90 nm digital CMOS process", Electron. Lett., Aug 2011.

[RAN09] S. Ranvier, M. Kyrö, C. Luxey, C. Icheln, R. Staraj, and P. Vainikainen, "Compact 3-D on-wafer radiation pattern measurement system for 60 GHz antennas", Microwave and Optical Technology Letters, vol. 51, pp. 319-324, February 2009.

[LAM10] A. Lamminen, and J. Saily, "Wideband millimetre wave end-fire antenna and array for wireless short-range applications", European Conference on Antennas and Propagation (EuCAP), Barcelona, Spain, April 2010.

[MOU10] W.F. Moulder, et al, "60-GHz Two-Dimensionally Scanning Array Employing Wideband Planar Switched Beam Network", IEEE Ant. Wireless Propag. Lett. , vol. 9, pp. 818-821, 2010.

[BAR10] M.H. Barakat, C. Delaveaud, and F. Ndagijimana, “60 GHz high resistivity silicon on insulator interdigitated dipole antenna”, Microwave and Optical Technology Letters, vol. 52, no. 5, pp. 1197-1201, May 2010.

[LAN10] J. Lantéri, L. Dussopt, R. Pilard, D. Gloria, S.D. Yamamoto, A. Cathelin, and H. Hezzeddine, “60 GHz antennas in HTCC and glass technology”, European Conference on Antennas and Propagation (EuCAP), Barcelona, Spain, April 2010.

[MUR11] J. Murdock, E. Ben-Dor, F. Gutierrez, and T.S. Rappaport, “Challenges and approaches to on-chip millimeter wave antenna pattern measurements”, IEEE International Microwave Symposium (MTT-S), Baltimore, MA, June 2011.

[PIL09] R. Pilard, S. Montusclat, D. Gloria, F. Le Pennec, and C. Person, “Dedicated measurement setup for millimetre-wave silicon integrated antennas: BiCMOS and CMOS high resistivity SOI process characterization”, European Conference on Antennas and Propagation (EuCAP), Berlin, Germany, pp. 2447-2451, March 2009.

[ZWI04] T. Zwick, C. Baks, U.R. Pfeiffer, D. Liu, and B.P. Gaucher, “Probe based MMW antenna measurement setup”, IEEE International Symposium on Antennas and Propagation (APS), Monterey, CA , pp. 747-750, June 2004.

[BEE10] S. Beer, and T. Zwick, “Probe based radiation pattern measurements for highly integrated millimeter-wave antennas”, European Conference on Antennas and Propagation (EuCAP), Barcelona, Spain, April 2010.

[IEE79] “IEEE Standard Test Procedures for Antennas”, ANSI/IEEE 149-1979.

[WHE59] H. A. Wheeler, “The radiansphere around a small antenna,” Proceedings of the IRE, vol.47, pp. 1325-1331, August 1959.

[KIL04] P-S. Kildal, and K. Rosengren, “Correlation and Capacity of MIMO Systems and Mutual Coupling , Radiation Efficiency, and Diversity Gain of their Antennas: Simulations and Measurements in a Reverberation Chamber”, IEEE Communications Magazine, pp. 104-112, 2004.

[CHI10] T-Y. Chin, et al., “A V-band 8x8 CMOS Butler matrix MMIC”, IEEE Transactions on Microwave Theory and Techniques, vol. 58, no. 12, pp. 3538-3546, December 2010.

[IEE93] “IEEE Standard Definitions of Terms for Antennas”, IEEE Std 145-1993, 1993.

IX. Research Perspectives

These years of research gave me the opportunity to work on ambitious projects within talented senior researchers. Thanks to this great experience, it is time for me to develop my own research subjects.

I believe that the Internet of Things is going to promote a new telecommunication domain with the need of a completely different wireless infrastructure, maximizing sensitivity and minimizing power consumption. The development of this research area will be assisted with different project proposals.

My objective is to leverage my experience gained in millimeter wave systems and antenna miniaturization to develop miniature and autonomous end point devices as well as to design efficient and high capacity edge node gateways.

A. Motivation

The Internet of Things (IoT) refers to everything that is connected to the internet and that goes beyond classical computers or mobile phones. According to a recent report by Cisco [CIS11], it can be expected that over 50 billion objects will be connected to the internet by 2020. This growth is creating unprecedented opportunities for industries, businesses and people.

Most of IoT systems are characterized by the transmission of small amounts of data at low transmission rate, which drastically reduces the bandwidth requirements and leads to the development of ultra-sensitive modulation schemes based on Ultra Narrow Band (UNB) (e.g., SigFox [SIG15]) or frequency spreading (e.g., LoRa [SEM15]) techniques. Usually, less than 1 MHz bandwidth is enough for most of the applications. Sub-GHz bands, such as the 868 MHz band in Europe and the 915 MHz band in the USA, are often preferred because of their more reliable propagation characteristics.

IoT market is preparing to take off. Bouygues Telecom and Orange have announced the deployment of a national network for 2016 based on LoRa technology. However, we have to consider that LoRa, in its actual form, is just going to be the appetizer of IoT market. LoRa technology has been chosen because it is the unique solution that combines extreme sensitivity (-137dBm), ultra-low power consumption, bidirectional capability and high security level (network and application 128-bit AES encryption keys). Moreover, the next LoRa update will include localization using triangulation technique. On the other hand, LoRa uses a derivative of Chirp Spread Spectrum modulation [LOR15] and to achieve the maximal sensitivity, a time on air larger than 2 s is needed to transmit just a few Bytes. Considering that thousands of connected objects will cohabit in the same cell, signal collisions will quickly increase, especially if collided data are just re-transmitted. Nevertheless, the LoRa

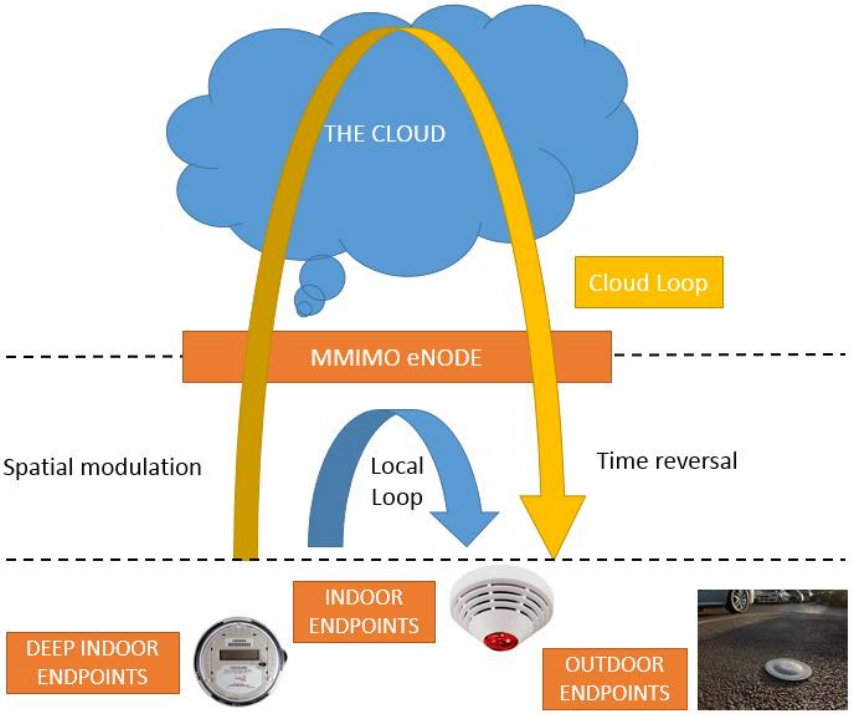

radiofrequency performance will become a market reference enabler. Finally, at the moment, LoRa technology is using just a single antenna on the gateway side and many improvements could be done also on this part (multiple antennas, sectorization, etc …).

3GPP standardization has started to develop specific features for IoT (LTE enhancements for Machine-Type Communication) with LTE MTC Cat 0 in release 12 and LTE MTC Cat M/-1 in release 13. A novel work item dedicated to narrow band is actually discussed (NB-IoT) and is really promising for ultra-low power applications [3GP15].

Several papers have proposed to integrate innovative techniques, as Time Reversal (TR) [CHE14] for efficiency improvements and spatial modulation (S-MIMO) [YOU14] in low-power multiple input multiple output (MIMO) systems. TR has been implemented for SISO [LER04] and MIMO [THA13]. Recently, a theoretical study of TR techniques with Massive MIMO [PIT15] has shown promising results. S-MIMO has been proposed for very high data rate application [ZJI15], but has not been considered for low-cost and low-power end point applications.

In order to get the requested properties, electronic complexity, power consumption and processing have to be moved away from the IoT device.

A large number of objects could benefit from the IoT connectivity, leading to a massive number of endpoints per surface unit. The gateway, also called edge node, will be the central hub for connecting the IoT devices to the cloud. Thus, the edge node will become a key element of the IoT chain. More than a simple gateway, it should be able to filter multiple received signals, give instantaneous acknowledge and local information, or transmit the received data to the cloud. Using the received data, the edge node should be also able to provide localization of the incoming signals. In order to widespread consumer adoption of new IoT products and services, there is a consensus on the fact that security must be the critical enabler. No clear approach is defined on how to optimally implement security in IoT at the device, network, and system levels.

B. Research proposal

In order to solve the different scientific challenges for IoT applications, I would like to propose a new methodology to fulfill the IoT network requirements. It consists in moving all the complexity and intelligence to the edge node side, and using ultra-low power technique on the end point. MMIMO will be used on the edge node in order to increase sensitivity, to enable signal processing to limit data collisions, and using channel information for end point localization. Sub-GHz bands are targeted because of their better propagation and penetration properties, leading to several challenges in the MMIMO antenna design. For the downlink, the TR technique will be leveraged to focus the signal wave on the end point.

On the IoT device (end point), low-cost and low-power electronics will be associated with a miniature and environment independent antenna. In order to maximize the uplink budget link, S-MIMO at the endpoint level using reconfigurable super-directive antennas will be optimized. A model of the entire network will be used to develop the suitable Medium Access Control (MAC) layer and to develop innovative cryptographic techniques based on physical layer information.

The goal of the project is to leverage this multi-factor approach to enable the connection of 100000 IoT devices on a 3km radius cell, with 5 to 10 payload transmissions per day. Compared to actual M2M technology (LTE release 12), we are expecting a sensitivity improvement of 20 to 30 dB, and an overall power consumption divided by 1000.

The different research activities of my project are divided in 3 different parts, addressing the different levels of the system: Edge node, End Point and Network level.

1. Network level

A model of the entire network is essential to study complicated scenarios with a massive number of devices. A network simulator (such as Omnet++) will be extended to take into account the different techniques developed in the frame of the project. The model will be used to quantify the impact of the different approaches on the network energy efficiency and capacity. A dedicated MAC layer will be developed and optimized for a massive number of end points. This work will be realized in close collaboration with LEAT MCSOC team. MCSOC team will provide skills in modeling and design of autonomous systems. This thematic will be integrated in CREMANT axis N°3.

A second part of this topic will consider the security aspect of the network, which is a critical functionality for consumer adoption. We propose to leverage the disruptive approach based on channel analysis to propose a Cryptographic Random Number generator based on channel physical layer information, which has the potential to reduce the power consumption and the cost at the secure end point side [FRA07]. A second security technique will use the unique location-specific channel impulse response (CIS) signature to provide additional physical-layer leveraging the TR technique. This topic will be lean on a collaboration with the System and Software Security group in Eurecom.

2. Edge node level

The main motivation of this vision is the design of an asymmetrical network with all the complexity moved at the edge node level. The use of a massive number of antennas will increase the uplink sensitivity, and the downlink signal will be focused in time and space domain using TR approach leveraging the reciprocity and multi-path characteristics of the

channel. Specific processing in order to decrease data collisions when a large number of IoT devices are connected to a cell will be studied. Accurate channel models are a pre-requisite for the MMIMO system design and performance evaluation. We plan to conduct channel measurements with the Open Air Interface MMIMO testbed [JIA15]. It will provide a true full MIMO channel including mutual coupling and the RF chain as it will be experienced by the devices. Specific scenarios suitable for IoT applications such as deep indoor communication will be targeted.

A second important part of this topic will be the MMIMO antenna design. The deployment of reasonably sized sub-GHz edge Node with a very large number of antennas implies that these antennas have to be densely packed, which raises obvious concerns about spatial correlation (SC) and mutual coupling (MC) between radiating elements. Future UHF MMIMO antennas must be strongly miniaturized by minimizing the single element size and decreasing the coupling among the different elements. Different isolation techniques (Electromagnetic Band Gap structure, neutralization technique) and size reduction methods (Artificial magnetic conductor, parasitic elements) will be focused for array miniaturization. The optimal element spacing distance in terms of efficiency, compactness and MIMO capabilities will be studied.

3. End point level

The end point RF has to be low power, low cost, and efficient in most of the situations. The operating bandwidth required by IoT systems is usually very narrow, with one or few MHz that are usually enough. In this framework, high Q antennas will be preferred and consequently a new design approach based on the simoultaneous miniaturization of the antenna and maximization of its radiation efficiency will be considered during the project. A specific study will be dedicated to antenna fundamental limits on efficiency [GUS07]. First results have shown that, in practical applications, the conductivity of the metal used to realize the antenna must be carefully taken into account [LIZ15]. The modification of the environment surrounding the antenna can cause a variation of its resonant frequency. This can become a serious problem in dealing with narrow band antennas. In order to obtain radiating structures that are independent on environment changes, the possibility of enclosing the UNB antennas into isolating radomes will be investigated. A second approach consists in providing the antenna with frequency reconfigurability. Towards this end, active components able to reconfigure some antenna characteristics will be integrated into the antenna and used to restore the antenna resonance to the desired frequency.

MIMO techniques have been largely used to improve link spectral efficiency. However, spatial multiplexing using multiple antennas require one transmitter for each Tx antenna, and complex processing, making it unusable for IoT devices due to the complexity and consumption of the required hardware. However, because of the clear advantages of MIMO techniques for channel capacity, new approaches for energy efficient multiple antenna transmissions are needed. S-MIMO has the potential to provide MIMO key advantages with a reduced hardware and power consumption cost. The basic principle is based on a reconfigurable antenna with multiple radiation patterns, with the different radiation patterns corresponding to the symbol of a spatial constellation diagram. This approach is adding a new dimension to digital modulation schemes thanks to this spatial domain. From a hardware point of view, a single RF chain is required with a fast RF switching unit, which is power efficient. This solution could be leveraged to improve the budget link for up-link communication.

Considering that IoT technologies will preferably use sub-GHz band, some challenges arises for the design of miniature reconfigurable antennas. In order to implement such MIMO technique, several key research areas will be gathered as digital modulation, signal processing

at the transmitter and the receiver, link and channel modelling and super-directive antennas [HAR58]. A reconfigurable super-directive antenna with beam steering capabilities will be used at the end-point level and interfaced with the network testbed. Several approaches from the simple spatial diversity, to more advanced spatial spreading codes will be studied.

C. Research Project Impact

The proposed project aspires to provide efficient IoT network solutions based on the innovative TR and S-MIMO paradigm enabling the realization of highly efficient and secure networks to support the increment of the number of connected objects expected for the next years. The techniques proposed to obtain environment independent and energy efficient antennas enable green, programmable and agile infrastructures capable of adapting to the dynamic demands of different existing and future IoT applications as well as to reach energy consumption levels that are economically and environmentally sustainable. This project, in fact, represents the opportunity for me, within the SophiaTech campus, to promote collaborations and shared activities between the different research centers (Eurecom, INRIA, University Nice Sophia Antipolis). Moreover, this action fall into the Université of Côte d'Azur initiative, that has been created in Feb. 2015 and gathers 13 different members (UNS, INRIA, OCA, Skema, CHU, etc …). Finally, the University Côte d'Azur has won the highly coveted "IDEX" award of the French Investments for the Future Program. The invested capital of about 580 million euros that will be attributed to the UCA will generate 14.5 million euros of interest income per year, meaning that a total of 58 million euros will be injected into research, training, and innovation in the Côte d'Azur region over the next four years.

From the scientific point of view, the proposed research project is expected to have a strong impact in the research community. Starting from the very limited requirements and capabilities of IoT endpoint devices, the proposed approach of an asymmetric network leveraging TR and S-MIMO techniques is completely new. This implies the need to face new research challenges as the identification of upper bound limits on the antenna directivity, the development of a more efficient and secure signal processing, and the study of an optimized MAC layer to increase the overall network performance.

In order to broadcast the project results to a broader audience, F. Ferrero and L. Lizzi have started the SOFIA (SOphia For Internet of Anything) Hub, a joint initiative of LEAT and the Polytech Nice-Sophia engineering school of UNS aimed at promoting and supporting research and teaching activities in the field of wireless communications for the Internet of Anything (IoA) (www.sofiahub.unice.fr).

The IoT is an application domain that results are particularly suitable for technological transfer. The telecommunication solutions developed during the project will be easily exploited to strengthen already existing industrial and academic collaborations of LEAT and will serve as building block to promote the creation of collaborative projects.

The proposed research project falls within the involved researchers' idea of making the SophiaTech campus the national reference for the research and teaching on IoT thanks to the different subjects located on the campus, as the UCN@Sophia LABEX partners. This will allow the study of all the IoT aspects, from the physical level of the single device (LEAT) to network management and security issues (EURECOM) and the signal processing and theoretical aspects (INRIA, I3S).

D. References

[3GP15] NarrowBand IOT, http://www.3gpp.org/news-events/3gpp-news/1733-niot, accessed Jan. 2016

[CAS14] Andrea Castagnetti, Alain Pegatoquet, Trong-Nhan Le and Michel Auguin, “A Joint Duty-Cycle and Transmission Power Management for Energy Harvesting WSN”, IEEE Transactions on Industrial Informatics Journal, Special section on “Industrial Wireless Sensor Networks”, Volume 10, Issue 2, pp. 928-936, May 2014.

[CIS11] D. Evans, “The internet of things. How the next evolution of the internet is changing everything”, Cisco White Paper, 2011.

[CHE14] Yan Chen; Feng Han; Yu-Han Yang; Hang Ma; Yi Han; Chunxiao Jiang; Hung-Quoc Lai; Claffey, D.; Safar, Z.; Liu, K.J.R., "Time-Reversal Wireless Paradigm for Green Internet of Things: An Overview," in Internet of Things Journal, IEEE , vol.1, no.1, pp.81-98, Feb. 2014

[CHE14] Yan Chen; Feng Han; Yu-Han Yang; Hang Ma; Yi Han; Chunxiao Jiang; Hung-Quoc Lai; Claffey, D.; Safar, Z.; Liu, K.J.R., "Time-Reversal Wireless Paradigm for Green Internet of Things: An Overview," in Internet of Things Journal, IEEE , vol.1, no.1, pp.81-98, Feb. 2014

[CIS15] The Network: ‘Toronto Selected as Site for $100 Million Cisco Global Innovation Centre’, http://newsroom.cisco.com/press-releasecontent? type=webcontent&articleId=1362116, accessed August 2015

[FRA07] Francillon, A.; Castelluccia, C., "TinyRNG: A Cryptographic Random Number Generator for Wireless Sensors Network Nodes," in Modeling and Optimization in Mobile, Ad Hoc and Wireless Networks and Workshops, 2007. WiOpt 2007. 5th International Symposium on , vol., no., pp.1-7, 16-20 April 2007

[GUS07] Mats Gustafsson, Christian Sohl, Gerhard Kristensson, "Physical limitations on antennas of arbitrary shape", Proc. R. Soc. A 2007 463 2589-2607; DOI: 10.1098/rspa.2007.1893. Published 8 October 2007

[JIA15] Jiang, X.; Cirkic, M.; Kaltenberger, F.; Larsson, E. G.; Deneire, L. & Knopp, R., “MIMO-TDD Reciprocity and Hardware Imbalances: Experimental Results”, CC 2015, IEEE International Conference on Communications, 8-12 June 2015, London, United Kingdom

[JON15] M. Gustafsson, B. L. G. Jonsson, Antenna Q and stored energy expressed in the fields, currents, and input impedance, IEEE Transactions on Antennas and Propagation, vol. 63(1) pages 240-249, 2015.

[HAR58] R. F. Harrington, “On the gain and beamwidth of directional antennas,” IEEE Trans. Antennas Propag., vol. 6, no.3, pp. 219-225, Jul. 1958.

[LER04] G Lerosey, J De Rosny, A Tourin, A Derode, “Time reversal of electromagnetic waves”, Physical review letters, 2004

[LOR15] AN1200.22LoRa™ Modulation Basics, Application note, Revision 2, May 2015, www.semtech.com.

[LIZ11] L. Lizzi and A. Massa, “Dual-band printed fractal monopole antenna for LTE applications,” *IEEE Antennas and Wireless Propagation Letters*, vol. 10, pp. 760-763, 2011

[LIZ15]L. Lizzi and F. Ferrero, “On the use of UNB Miniature Antennas for IoT Applications”, *Electr. Lett.*, 2015.

[PIT15] Pitarokoilis, A.; Mohammed, S.K.; Larsson, E.G., "Uplink Performance of Time-Reversal MRC in Massive MIMO Systems Subject to Phase Noise," in Wireless Communications, IEEE Transactions on , vol.14, no.2, pp.711-723, Feb. 2015

[SEM15] Semtech Investor News: ‘Bouygues Telecom Announces June Launch of France’s First "Internet-of-Things" Network Based on LoRa Technology’, http://investors.semtech.com/releasedetail.cfm?ReleaseID=904103, accessed August 2015

[SIG15] Gigacom Research: ‘Sigfox brings its internet of things network to San Francisco’, https://gigaom.com/2014/05/20/sigfox-brings-its-internet-ofthings-network-to-san-francisco/, accessed August 2015

[THA13] Vu, Tran Ha; Hieu, Nguyen Thanh; Tam Linh, Ho Duc; Dung, Nguyen Thuy; Van Tuan, Le, "Channel capacity of multi user TR-MIMO-UWB communications system," in Computing, Management and Telecommunications (ComManTel), 2013 International Conference on , vol., no., pp.22-26, 21-24 Jan. 2013

[TLE14] T-N. Le, A. Pegatoquet, O. Berder, O. Sentieys and A. Carer, “Energy Neutral Design Framework for Supercapacitor-based Autonomous Wireless Sensor Networks”, to appear in ACM Journal on Emerging Technologies in Computing Systems (JETC), 2014.

[YOU14] Yousefbeiki, M.; Alrabadi, O.N.; Perruisseau-Carrier, J., "Efficient MIMO Transmission of PSK Signals With a Single-Radio Reconfigurable Antenna," in Communications, IEEE Transactions on , vol.62, no.2, pp.567-577, February 2014

[ZJI15] Zhiyuan Jiang; Molisch, A.F.; Caire, G.; Zhisheng Niu, "Achievable Rates of FDD Massive MIMO Systems With Spatial Channel Correlation," in Wireless Communications, IEEE Transactions on , vol.14, no.5, pp.2868-2882, May 2015

XI. BIBLIOGRAPHY

REVUES INTERNATIONALES AVEC COMITE DE LECTURE

[J05AW] F. Ferrero, C. Luxey, G. Jacquemod & R. Staraj, «Dual-Band circularly polarized microstrip antenna for satellite applications», IEEE Antennas and Wireless Propagation Letters, vol. 4, 2005, p. 13-15

[J07EL] F. Ferrero, C. Luxey, R. Staraj, G. Jacquemod, V. Fusco, «Compact quasi-lumped hybrid coupler tunable over a large frequency band», Electronic letters, Vol. 43, No. 19, 2007, p.1030-1031

[J09AP] F. Ferrero, C. Luxey, R. Staraj, G. Jacquemod, M. Yedlin, V. Fusco, "A Novel Quad-Polarization Agile Patch Antenna", Antennas and Propagation, IEEE Transactions on , vol.57, no.5, pp.1563-1567, May 2009

[J09MO] F. Ferrero, C. Luxey, R. Staraj, G. Jacquemod, M. Yedlin, V. Fusco, "Theory and design of a tunable quasi-lumped quadrature coupler", MOTL, Vol. 51, No. 9, September 2009

[J09EL] F. Ferrero, C. Luxey, R. Staraj, G. Jacquemod, M. Yedlin, V. Fusco, "Patch antenna with linear polarisation tilt control", Electronic letters, Vol. 45, No. 17, August 2009

[J09MJ] B. Nicolle, R. Khouri, F. Ferrero, W. Tatinian, L. Carpineto, G. Jacquemod, "On the use of behavioral modeling within the RFIC design flow: Satellite receiver case study", Microelectronic Journal, Vol. 40, 2009, 1726-1735.

[J09RE] F. Ferrero, A. Diallo, C. Luxey, B. Derat, P. Hamouz, P. Hazdra, J. Rahola, "Two-Element PIFA Array Structure for Polarization Diversity in UMTS Mobile Phones ", Radioengineering, Vol. 18, N°4, Dec 2009, pp. 407-412.

[J11MO] F. Canneva, F. Ferrero, J. M. Ribero, and R. Staraj, « FREQUENCY RECONFIGURABLE ANTENNA FOR DVB-H APPLICATIONS », MOTL, Vol. 53, No. 8, August 2011.

[J11AW] F. Ferrero, A. Chevalier, J. M. Ribero, R. Staraj, J. L. Mattei, and Y. Queffelec, "A New Magneto-Dielectric Material Loaded, Tunable UHF Antenna for Handheld Devices", IEEE AWPL, Vol. 10, pp. 951-954, Sept. 2011.

[J11MO2] F. Canneva, F. Ferrero, J. M. Ribero, and R. Staraj, « Small reconfigurable PIFA for DVB-H applications », MOTL, Vol. 53, No. 10, October 2011.

[J11TM] J.-L. Mattei, P. Queffelec, L. Huitema, J.-F. Pintos, Ph. Minard, A. Sharaiha; B. Jamnier, F. Ferrero, R. Staraj, D. Souriou, A. Thakur, "Suitability of Ni-Zn Ferrites Ceramics with Controlled Porosity As Granular Substrates for Mobile Handset Miniaturized Antennas", IEEE Trans. On Magnetics., Vol. 47, Iss. 10, pp. 3720-3723, Oct. 2011.

[J12MO] D. Titz, M. Kyrö, F. Ferrero, S. Ranvier, C. Luxey, P. Brachat, G. Jacquemod and P. Vainikainen," Calibration methodology for a 3D radiation pattern set-up of probe-fed millimeter-wave antennas", Microwave and Optical Technology Letters, Volume 54, Issue 5, May 2012, Pages: 1183–1189

[J12MO2]L. Lizzi, F. Ferrero, J. Ribero, and R. Staraj, "Low-Profile Tetra Wire-Patch Antenna For Automotive Applications", Microwave and Optical Technology Letters, Volume 54, Issue 7, July 2012, Pages: 1711–1714.

[J12RE] D.Titz, F. Ben Abdeljelil, S. Jan, F. Ferrero, C. Luxey, P. Brachat, G. Jacquemod, "Design and Characterization of CMOS On-Chip Antennas for 60 GHz Communications", Radioengineering, Vol. 21, N°1, Apr 2012, pp. 324-332.

[J12AW] Titz, D.; Pilard, R.; Gianesello, F.; Ferrero, F.; Luxey, C.; Brachat, P.; Jacquemod, G.; Gloria, D., "Industrial HTCC Antenna-Module SiP for 60-GHz Applications" , IEEE AWPL, Vol. 11, pp. 576-579, 2012.

[J12EL] Trinh L.H, Hoang T.Q.V, Ferret F., Ferrero F., "Improving wake-up receiver's sensitivity by using a novel architecture", Electronics Letters, Vol. 48, Iss. 11, pp. 559-560, May 2012

[J12MO3] Diane Titz, Fabien Ferrero, Romain Debroucke, Romain Pilard,Cyril Luxey ,Frederic Gianesello, Sebastien Jan, Daniel Gloria, and Gilles Jacquemod, "MILLIMETER-WAVE MINIATURIZED HYBRID

COUPLERS INTEGRATED ON ADVANCED BiCMOS TECHNOLOGY", Microwave and Optical Technology Letters, Vol. 54, No. 10, October 2012.

[J12MO4] M. Silva Pimenta, F. Ferrero, R. Staraj and J.M. Ribero, "Low-profile circularly polarized GNSS antenna", Microwave and Optical Technology Letters, Volume 54, Issue 12, December 2012, Pages: 2811–2814

[J12AM] D. Titz, F. Ferrero, C. Luxey, "Development of a Millimeter-Wave Measurement Setup and Dedicated Techniques to Characterize the Matching and Radiation Performance of Probe-Fed Antennas", IEEE Antennas and Propagation Magazine, Vol. 54, Iss. 4, August 2012, pp. 188-203.

[J12AW2] L. Lizzi, F. Ferrero, J. M. Ribero, R. Staraj, "Light and Low-Profile GSM Omnidirectional Antenna", IEEE AWPL, Vol. 11, pp. 1146-1149, 2012.

[J12AW3] D. Titz, F. Ferrero, P. Brachat, G. Jacquemod, C. Luxey, "Efficiency Measurement of Probe-Fed Antennas Operating at Millimeter-Wave Frequencies", IEEE AWPL, Vol. 11, pp. 1194-1197, 2012.

[J13AP] B. Zhang, Y. P. Zhang, D. Titz, F. Ferrero, C. Luxey, "A Circularly-Polarized Array Antenna Using Linearly-Polarized Sub Grid Arrays for Highly-Integrated 60-GHz Radio", IEEE Transactions on Antennas & Propagation, Vol. 61, Iss. 1, pp. 436-439, January 2013.

[J13AP2] Hoang, T.Q.V.; Seguenot, E.; Ferrero, F.; Dubard, J.-L.; Brachat, P.; Desvilles, J.-L., "3D Voltage Pattern Measurement of a 2.45 GHz Rectenna," Antennas and Propagation, IEEE Transactions on , vol.61, no.6, pp.3354,3356, June 2013

[J13CP] Bing Zhang; Titz, D.; Ferrero, F.; Luxey, C.; Yue Ping Zhang, "Integration of Quadruple Linearly-Polarized Microstrip Grid Array Antennas for 60-GHz Antenna-in-Package Applications," Components, Packaging and Manufacturing Technology, IEEE Transactions on , vol.3, no.8, pp.1293,1300, Aug. 2013

[J13EL] Cihangir, A.; Sonnerat, F.; Ferrero, F.; Pilard, R.; Gianesello, F.; Gloria, D.; Brachat, P.; Jacquemod, G.; Luxey, C., "Neutralisation technique applied to two coupling element antennas to cover low LTE and GSM communication standards," Electronics Letters , vol.49, no.13, pp., June 20 2013

[J13MO] Florian Canneva, Fabien Ferrero, Alexis Chevalier, Jean-Marc Ribero, Jean-Luc Mattei, Patrick Queffelec, Robert Staraj, "Miniature Reconfigurable Antenna with Magneto Dielectric Substrate for DVB-H Band", Microwave and Optical Technology Letters, Volume 55, Issue 9, pages 2007–2011, September 2013

[J13EL] Bisognin, A.; Titz, D.; Ferrero, F.; Luxey, C.; Jacquemod, G.; Pilard, R.; Gianesello, F.; Gloria, D.; Brachat, P., "Differential feeding technique for mm-wave series-fed antenna-array," Electronics Letters , Vol.49, No.15, July 18 2013

[J13AP3] Tu Zhihong; Zhang, Y.P.; Luxey, C.; Bisognin, A.; Titz, D.; Ferrero, F., "A Ceramic Antenna for Tri-Band Radio Devices," Antennas and Propagation, IEEE Transactions on , vol.61, no.11, pp.5776,5780, Nov. 2013

[J13AP4] W. Zhang, Y.P Zhang, M. Sun, C. Luxey, D. Titz, F. Ferrero, "A 60-GHz Circularly-Polarized Array Antenna-in-Package in LTCC Technology," Antennas and Propagation, IEEE Transactions on , vol.61, no.12, Dec. 2013

[J13AW] A. Cihangir; W. Whittow, Panagamuwa, C.; Ferrero, F.; Jacquemod, G.; Gianesello, F.; Luxey, C., "Feasibility study of 4G cellular antennas for eyewear communicating devices," Antennas and Wireless Propagation Letters, 2013.

[J14MO] D. Titz, F. Ferrero, R. Debroucke, R. Pilard, C. Luxey, F. Gianesello, S. Jan, D. Gloria, et G. Jacquemod, "Millimeter-Wave Miniaturized Couplers Integrated on BiCMOS Technology", Microwave and Optical Technology Letters, vol. 56, no. 3, pp. 587-590, January 2014.

[J14AW] D. Titz; R. Pilard; F. Ferrero, F. Gianesello; D. Gloria, G. Jacquemod, C. Luxey, "Improved Measurement Accuracy of Probe-Fed mm-Wave Antennas Using the Three Γ Method," Antennas and Wireless Propagation Letters, IEEE , vol.13, no., pp.103,105, 2014

[J14AW2] A. Cihangir; F. Ferrero, G. Jacquemod, P. Brachat, C. Luxey, "Neutralized Coupling Elements for MIMO Operation in 4G Mobile Terminals," Antennas and Wireless Propagation Letters, IEEE , vol.13, pp.141,144, 2014

[J14AW3] Bisognin, A.; Thielleux, J.; Wei, W.; Titz, D.; Ferrero, F.; Brachat, P.; Luxey, C., "Inkjet Coplanar Square Monopole on flexible substrate for 60 GHz applications," Antennas and Wireless Propagation Letters, IEEE , no.99, pp.1,1

[J14CP] Titz, D.; Ferrero, F.; Pilard, R.; Laporte, C.; Jan, S.; Ezzeddine, H.; Gianesello, F.; Gloria, D.; Jacquemod, G.; Luxey, C., "New Wideband Miniature Branchline Coupler on IPD Technology for Beamforming Applications," Components, Packaging and Manufacturing Technology, IEEE Transactions on , vol.4, no.5, pp.911,921, May 2014

[J14MA] Lizzi, Leonardo; Ferrero, Fabien; Ribero, Jean-Marc; Staraj, Robert: 'Simple antenna structure enabling the simultaneous excitation of two different polarisation and radiation modes', IET Microwaves, Antennas & Propagation, 2014

[J14AW] Bisognin, A.; Titz, D.; Ferrero, F.; Jacquemod, G.; Pilard, R.; Gianesello, F.; Gloria, D.; Brachat, P.; Laporte, C.; Ezzeddine, H.; Luxey, C., "PCB Integration of a Vivaldi Antenna on IPD Technology for 60-GHz Communications," Antennas and Wireless Propagation Letters, IEEE , vol.13, no., pp.678,681, 2014

[J14FE] A. Cihangir, F. Ferrero, G. Jacquemod, P. Brachat, C. Luxey "Integration of Resonant and Non-Resonant Antennas for Coverage of 4G LTE Bands in Handheld Terminals", Forum for Electromagnetic Research Methods and Application Technologies (FERMAT), Vol. 3, 2014

[J14EL] Addaci, R.; Hamdiken, N.; Fortaki, T.; Ferrero, F.; Seetharamdoo, D.; Staraj, R., "Simple bandwidth-enhancement technique for miniaturised low-profile UWB antenna design," Electronics Letters , vol.50, no.22, pp.1564,1566, 10 23 2014.

[J15FE] A. Cihangir, F. Sonnerat, F. Ferrero, G. Jacquemod, F. Gianesello, R. Pilard, D. Gloria, P. Brachat, C. Luxey, "LTE/4G Handset Antennas Realized with LDS Technology", Forum for Electromagnetic Research Methods and Application Technologies (FERMAT), Vol. 9, 2015.

[J15AW] Semkin, V.; Ferrero, F.; Bisognin, A.; Ala-Laurinaho, J.; Luxey, C.; Devillers, F.; Raisanen, A.V., "Beam switching conformal antenna array for mm-wave communications," in Antennas and Wireless Propagation Letters, IEEE.

[J15AW2] Chen, Z.; Zhang, Y.; Bisognin, A.; Titz, D.; Ferrero, F.; Luxey, C., "A 94 GHz Dual-Polarized Microstrip Mesh Array Antenna in LTCC Technology," in IEEE Antennas and Wireless Propagation Letters, 2015

[J15AP] Bisognin, A.; Titz, D.; Ferrero, F.; Jacquemod, G.; Pilard, R.; Gianesello, F.; Gloria, D.; Lugara, D.; Lima, E.B.; Costa, J.R.; Fernandes, C.A.; Luxey, C., "Noncollimating MMW Polyethylene Lens Mitigating Dual-Source Offset From a Tx/Rx WiGig Module," in IEEE Transactions on Antennas and Propagation, vol.63, no.12, pp.5908-5913, Dec. 2015

[J15EL] Lizzi, L.; Ferrero, F., "Use of ultra-narrow band miniature antennas for internet-of-things applications," in Electronics Letters , vol.51, no.24, pp.1964-1966, 11 19 2015

[J15AW3] Le Huy Trinh, Fabien Ferrero, Leonardo Lizzi, Jean-Marc Ribero and Robert Staraj, “Reconfigurable Antenna for Future Spectrum Reallocations in 5G Communications”, in IEEE Antennas and Wireless Propagation Letters, November 2015

[J15IJ] Le Huy Trinh, Fabien Ferrero, Leonardo Lizzi, Jean-Marc Ribero and Robert Staraj, “4x4 MIMO MULTIBAND ANTENNA SYSTEM FOR MOBILE HANDSETS" IJAP, International Journal of Antennas and PropagationVolume 2015 (2015), Article ID 857876, 1 November 2015

CONFERENCES INTERNATIONALES A COMITES DE LECTURE SUR INVITATION DANS UNE SESSION SPECIALE OU CONVENUE:

[I07EU] F. Ferrero, C. Luxey, R. Staraj, G. Jacquemod, V. Fusco, «Linearly-Polarized tunable Antenna», European Conference on Antennas and Propagation (EuCAP 2007), November 2007, Edinburgh, UK, ISBN 92-9092-937-5

[I09EU] F. Ferrero, A. Diallo, C. Luxey, B. Derat, "Pattern Diversity versus Polarization Diversity in UMTS Mobile Phones", Proc. Eucap 2009, 3rd European Conference on Antennas & Propagation, 23-27 March 09, Berlin, Germany.

[I09IW] F. Ferrero, A. Diallo, C. Luxey, B. Derat, "Phased Two-Element PIFA for Adaptative Pattern in UMTS Handsets", Proc. IEEE International Workshop on Antenna Technology: "Small Antennas and Novel Metamaterials (IWAT2009), 2-4 March 2009, Santa Monica, California (USA).

[I12EU] Aykut Cihangir, Fabien Ferrero, Cyril Luxey, Gilles Jacquemod, “A Novel Multi-Band Antenna Design with Matching Network for Use in Mobile Terminals”, EUCAP , Pragues, Avril 2012.

[I12EU] Diane Titz, Fabien Ferrero, Cyril Luxey, Gilles Jacquemod, Claire Laporte, Hilal Ezzeddine, “Antenna-in-Package Using PCB and IPD Technologies for 60 GHz Applications”, EUCAP, Pragues, Avril 2012.

[I12LA] Diane Titz, Fabien Ferrero, Gilles Jacquemod, Patrice Brachat, Cyril Luxey, “Measurement System for Mm-wave Integrated and Probe-fed Antennas”, LAPC, Loughborough, Nov 2012.

[I12EU] Bisognin, Aimeric; Titz, Diane; Ferrero, Fabien; Luxey, Cyril; Jacquemod, Gilles; Brachat, Patrice; Laporte, Claire; Ezzeddine, Hilal; Pilard, Romain; Gianesello, Frederic; Gloria, Daniel, "IPD technology for passive circuits and antennas at millimeter-wave frequencies," Antennas and Propagation (EuCAP), 2013 7th European Conference on , vol., no., pp.326,329, 8-12 April 2013

[I13EU] Cihangir, Aykut; Ferrero, Fabien; Luxey, Cyril; Jacquemod, Gilles; Brachat, Patrice, "A bandwidth-enhanced antenna in LDS technology for LTE700 and GSM850/900 standards," Antennas and Propagation (EuCAP), 2013 7th European Conference on , vol., no., pp.2786,2789, 8-12 April 2013

[I13EU] Bisognin, Aimeric; Titz, Diane; Ferrero, Fabien; Luxey, Cyril; Jacquemod, Gilles; Brachat, Patrice; Laporte, Claire; Ezzeddine, Hilal, "D-band Quasi-Yagi antenna in IPD process," Antennas and Propagation (EuCAP), 2013 7th European Conference on , vol., no., pp.330,331, 8-12 April 2013

[I14CA] F. Ferrero, C. Buey, J-M. Fargeas, P. Ratajczak, K. Bashir, L. H. Trinh, "Design of a Dual-Band MIMO Wifi Gateway", IEEE CAMA 2014, November 2014, Antibes, France

[I14CA] L. Lizzi, P. Perrissol, F. Ferrero, P. Le Thuc, R. Staraj, "Experimental Validation of a Miniature Implantable RFID Tag Antenna for Small Animals Monitoring", IEEE CAMA 2014, November 2014, Antibes, France

[I14CA] T. Q. V. Hoang, L. H. Trinh, F. Ferrero, E. Seguenot, T-P. Vuong, J-L. Dubard, "Rectenna Measurement in a Realistic Environment", IEEE CAMA 2014, November 2014, Antibes, France

[C15EU3] L.H. Trinh, Fabien Ferrero, J.M. Ribero, R. Staraj ,"Reconfigurable Antenna for Extension of LTE Operational Mode Over TV White Spaces", Eucap, April 2015, Libon, Portugal

CONGRES INTERNATIONAUX AVEC COMITE DE LECTURE ET ACTES

[C04JI] F. Ferrero, C. Luxey, G. Jacquemod & R. Staraj, «Circularly Polarized Dual-Band Microstrip Antenna», JINA 04, Nice, 2004, p. 472-473,

[C05AC] F. Ferrero, C. Luxey, G. Jacquemod & R. Staraj, «A Circularly Polarized Dual-Band Microstrip Antenna», IEEE/ACES ICWCACE, Honolulu, 2005, p. 942-945,

[C05AN] F. Ferrero, C. Luxey, G. Jacquemod, R. Staraj, G. Kossiavas & V. Fusco, «Reconfigurable phase-arrays based on hybrid couplers in reflection mode», Antem 05, Saint-Malo, 2005, p. 244-245

[C06SA] S. Ranvier, F. Ferrero, C. Luxey, G. Jacquemod, R. Staraj, C. Icheln & P. Vainikainen, «Integrated MIMO Antenna with Directional Diversity in the 60 GHz Band», SAME 06, Sophia Antipolis, 2006

[C06EU] F. Ferrero, C. Luxey, G. Jacquemod, R. Staraj & V. Fusco, «A reconfigurable hybrid coupler circuit for agile polarisation antenna», EuCAP, Nice, 2006, ISBN 92-9092-937-5

[C06IC] F. Ferrero, S. Ranvier, C. Icheln, P. Vainikainen, C. Luxey, R. Staraj & G. Jacquemod, «Integrated MM-Wave MIMO Antenna with Directional Diversity using MEMS Technology», ICECS 06, Nice, 2006, p. 447-450

[C07IW] F. Ferrero, C. Luxey, G. Jacquemod, R. Staraj & V. Fusco, «Polarisation-Reconfigurable Patch Antenna», IWAT, Cambridge, 2007, p. 73-76

[C07IM] F. Ferrero & G. Jacquemod, «A tunable quasi-lumped microstrip coupler and RF applications», IMS, Honolulu, 2007, p. 1197-1200

[C08HS] B. Nicole, F. Ferrero, L. Ferrero, L. Zastrow, Y. Herve, «From the UVA to the lipid chain reaction: archetype of a virtual skin model», HSC'08, Huntsville, Octobre 2008.

[C09EU] Ferrero, F. Diallo, A. Luxey, C. Derat, B. , " Pattern diversity versus polarization diversity in UMTS mobile phones ", Eucap, Berlin, pp. 1522, ISBN 978-1-4577-0250-1, Mars 2009.

[C09AP] F. Ferrero, C. Luxey, M. Yedlin, R. Staraj, G. Jacquemod, «Array-Antenna of Microstrip Patches Fed by a Tunable Quasi-Lumped Hybrid Coupler». Proc. IEEE Antennas and Propagation Society International Symposium (APS 2009), Charleston, June 1-5; 2009.

[C10AP] F. Canneva, F. Ferrero, J-M. Ribero, R. Staraj, «Reconfigurable miniature antenna for DVB-H standard ». Proc. IEEE Antennas and Propagation Society International Symposium (APS 2010), Toronto, July; 2010.

[C10AP2] F. Ferrero, F. Perret, J-M. Ribero, R. Staraj, «Self-Adjustable Circularly Polarized Patch Antenna ». Proc. IEEE Antennas and Propagation Society International Symposium (APS 2010), Toronto, July; 2010.

[C11EU] Canneva, F. Ferrero, F. Chevalier, A. Ribero, J.M. Staraj, R. Mattei, J.L. Queffelec, P., " Miniature reconfigurable antenna with magneto dielectric substrate for DVB-H band", Eucap, pp. 2289, ISBN 978-1-4577-0250-1 , Avril 2011.

[C11EU2] Ferrero, F. Chevalier, A. Ribero, J.M. Staraj, R. Mattei, J.L. Queffelec, P. , "Influence of a magneto-dielectric resonator on DVB-H antenna performances", Eucap, Rome, pp. 2156, ISBN 978-1-4577-0250-1 , Avril 2011.

[C11EU3] Oikonomopoulos-Zachos, C. Titz, D. Martinez-Vazquez, M. Ferrero, F. Luxey, C. Jacquemod, G. , " Accurate characterisation of a 60 GHz antenna on LTCC substrate ", Eucap, Rome, pp. 3117, ISBN 978-1-4577-0250-1, Avril 2011.

[C11NC] Titz, D.; Ferrero, F.; Luxey, C.; Jacquemod, G.; Debroucke, R.; Pilard, R.; Gianesello, F.; Gloria, D., "Reflection-type phase shifter integrated on advanced BiCMOS technology in the 60 GHz band," in *New Circuits and Systems Conference (NEWCAS), 2011 IEEE 9th International* , vol., no., pp.434-437, 26-29 June 2011

[C11AP] Diane Titz, Fabien Ferrero, Cyril Luxey, Gilles Jacquemod, "A Novel Fully-Automatic 3D Radiation Pattern Measurement Setup for 60 GHz Probe-Fed Antennas", IEEE APS, Spokane, July 2011.

[C11AP2] Romain Pilard, Frédéric Gianesello, Daniel Gloria, Diane Titz, Fabien Ferrero, Cyril Luxey, "60 GHz HR SOI CMOS Antenna for a System-on-Chip Integration Scheme Targeting High Data-Rate Kiosk Applications", IEEE APS, Spokane, July 2011.

[C11AP3] Florian Canneva, Fabien Ferrero, Jean-Marc Ribero, Robert Staraj, "New Reconfigurable Small Antenna for DVB-H and GPS Standard", IEEE APS, Spokane, July 2011.

[C11IM] D. Titz, R. Pilard, F. Ferrero, F. Gianesello, D. Gloria, C. Luxey, P. Brachat, G. Jacquemod, "60GHz Antenna Integrated on High Resistivity Silicon Technologies Targeting WHDMI Applications", IMS, Baltimore, June 2011.

[C11LA] Jean-Luc Fournier; Diane Titz; Fabien Ferrero; Cyril Luxey; Eric Dekneuvel; Gilles Jacquemod, "Phased Array Antenna Controlled by Neural Network FGPA", LAPC, Loughborough, Nov 2011.

[C11LA2] Diane Titz; Mikko Kyrö; Fabien Ferrero; Sylvain Ranvier ;Cyril Luxey; Patrice Brachat; Gilles Jacquemod , Pertti Vainikainen, "Measurement Setup and Associated Calibration Methodology for 3D Radiation Pattern of Probe-fed Millimeter-wave Antennas", LAPC, Loughborough, Nov 2011.

[C12IW] Diane Titz, Fabien Ferrero, Cyril Luxey, Patrice Brachat, Gilles Jacquemod, "Radiation Pattern Characterization of Antennas at Millimeter-Wave Frequencies", IWAT 2012, Tucson, March 2012

[C12IW2] Oumy Diop , Fabien Ferrero, Aliou Diallo, Gilles Jacquemod, Claire Laporte, Hilal Ezzeddine, Cyril Luxey, "Planar Antennas on Integrated Passive Device Technology for Biomedical Applications", IWAT 2012, Tucson, March 2012

[C12EU] Marcio Silva Pimenta, Fabien Ferrero, Patrice Brachat, Philippe Ratajczak, Robert Staraj, Jean Marc Ribero, "Textile Artificial Magnetic Conductor for GPS Applications", EUCAP, Pragues, Avril 2012.

[C12EU2] Akiko Kohmura, Jerome Lanteri, Fabien Ferrero, Claire Migliaccio, Philippe Ratajczak, Shunichi Futatsumori, Naruto Yonemoto, "Ka-band Dual Frequency Switchable Reflect array", EUCAP,Pragues, Avril 2012.

[C12AN] Addaci Rafik, Ferrero Fabien, Diallo aliou, Lethuc Philippe, Staraj Robert, Crisan Nicolae, Cremene Ligia, Luxey Cyril, "Design of multi-antenna diversity system dedicated to interrogation in noisy propagation environments", ANTEM, Toulouse, Juin 2012

[C12IM] D. Titz, F. Ferrero, R. Pilard, C. Laporte, S. Jan, H. Ezzeddine, F. Gianesello, D. Gloria, C. Luxey, and G. Jacquemod, "New Wideband Integrated Miniature Branchline Coupler for Beamforming Applications", IEEE IMS, Montreal, Canada, Juin 2012

[C12AP] Leonardo Lizzi, Fabien Ferrero, Jean-Marc Ribero, and Robert Staraj, “Compact Low-Profile Omnidirectional Surface Wave Antenna for UMTS Applications”, IEEE APS, Chicago, Juillet 2012

[C12AP2] Diane Titz, Fabien Ferrero, Cyril Luxey, Gilles Jacquemod, “A Fast and Accurate Method to Measure the Radiation Characteristics of Probe-fed Circularly-Polarized Antennas in Mm-Wave Bands”, IEEE APS, Chicago, Juillet 2012

[C12AP3] F. Ferrero, J.M. Ribero and R. Staraj, “Chassis engineering to enlarge the bandwidth for GSM-450 application”, IEEE APS, Chicago, Juillet 2012

[C12AP4] Jennifer M. Edwards, Gabriel M. Rebeiz, Diane Titz, Fabien Ferrero, Cyril Luxey, “High-Efficiency Elliptical-Slot Silicon RFIC Antenna with Quartz Superstrate”, IEEE APS, Chicago, Juillet 2012

[C12AP5] Diane Titz, Fabien Ferrero, Cyril Luxey, Gilles Jacquemod, Claire Laporte, Hilal Ezzeddine, “Design of a Miniaturized Butler Matrix in IPD Process for 60 GHz Switched-Beam Antenna Arrays”, IEEE APS, Chicago, Juillet 2012

[C12AP6] R. Pilard, D. Titz, F. Gianesello, P. Calascibetta, J.M. Rivière, J. Lopez, R. Coffy, E. Saugier, A. Poulain, F. Ferrero, C. Luxey, P. Brachat, G. Jacquemod and Daniel Gloria, “HDI Organic Technology Integrating Built-In Antennas Dedicated to 60 GHz SiP Solution”, IEEE APS, Chicago, Juillet 2012.

[C12IS] Akiko Kohmura, Jérôme Lanteri, Fabien Ferrero, Claire Migliaccio, Shunichi Futatsumori, Naruto Yonemoto, “Ka-band Beam Switchable Fresnel Reflector”, ISAP 2012, Nagoya, Japan, October 2012.

[C12SA] Oumy Diop, Fabien ferrero, Aliou Diallo, Gilles Jacquemod, Claire Laporte, Hilal Ezzeddine, Cyril Luxey, “ IPD technology for co-integration of balun and miniature antennas at 2.4 GHz ” , Sophia Antipolis Micro-Electronics Conference SAME 2012, 2-3 Octobre 2012, Sophia Antipolis, France.

[C12LA] Aykut Cihangir; Florence Sonnerat; Fabien Ferrero; Cyril Luxey; Romain Pilard; Frederic Gianesello; Gilles Jacquemod, “Design of Traditional and a Novel Space-Efficient Antenna- Coupling Elements for Lower LTE/GSM Mobile Phones”, LAPC, Loughborough, Nov 2012.

[C12LA2] Diane Titz; Bisognin Aimeric; Fabien Ferrero; Cyril Luxey; Gilles Jacquemod; Claire Laporte; Hilal Ezzeddine; Mario Valente; Patrice Brachat, “60 GHz Patch Antenna Using IPD Technology”, LAPC, Loughborough, Nov 2012.

[C12LA3] Florence Sonnerat; Romain Pilard; Frederic Gianesello; Daniel Gloria; François Le Pennec; Christian Person; Aykut Cihangir; Fabien Ferrero; Cyril Luxey; Patrice Brachat, “Wideband LDS Antenna Using Two Radiating Elements”, LAPC, Loughborough, Nov 2012.

[C13JS] Jiashu Chen; Lu Ye; Titz, D.; Gianesello, F.; Pilard, R.; Cathelin, A.; Ferrero, F.; Luxey, C.; Niknejad, A.M., "A digitally modulated mm-Wave cartesian beamforming transmitter with quadrature spatial combining," Solid-State Circuits Conference Digest of Technical Papers (ISSCC), 2013 IEEE International , vol., no., pp.232,233, 17-21 Feb. 2013

[C13IW] Cihangir, A.; Ferrero, F.; Luxey, C.; Jacquemod, G., "A space-efficient coupling element antenna for WWAN applications," Antenna Technology (iWAT), 2013 International Workshop on , pp.55,58, 4-6 March 2013

[C13EU] Semkin, Vasilii; Kyro, Mikko; Kolmonen, Veli-Matti; Luxey, Cyril; Bisognin, Aimeric; Ferrero, Fabien; Happy, Henri; Raisanen, Antti V., "Conformal antenna array for 60 GHz applications," Antennas and Propagation (EuCAP), 2013 7th European Conference on , pp.605,608, 8-12 April 2013

[C13EU2] Lizzi, Leonardo; Ferrero, Fabien; Ribero, Jean-Marc; Staraj, Robert, "Design of light and low-profile antennas for vehicular applications," Antennas and Propagation (EuCAP), 2013 7th European Conference on , pp.1281,1284, 8-12 April 2013.

[C13AP] Bisognin, Aimeric; Luxey, Cyril; Jacquemod, Gilles; Ferrero, Fabien; Titz, Diane; Thielleux, Julien; Wei, Wei; Happy, Henri; Brachat, Patrice, "Antenna on PEN substrate for millimeter-wave applications," Antennas and Propagation Society International Symposium (APSURSI), 2013 IEEE , pp.684,685, 7-13 July 2013.

[C13AP2] Bisognin, Aimeric; Luxey, Cyril; Jacquemod, Gilles; Titz, Diane; Ferrero, Fabien; Pilard, Romain; Gianesello, Frederic; Gloria, Daniel; Brachat, Patrice, "A new symmetric feeding technique for a broadband series-fed antenna-array," Antennas and Propagation Society International Symposium (APSURSI), 2013 IEEE , pp.2183,2184, 7-13 July 2013.

[C13AP3] Lizzi, Leonardo; Ferrero, Fabien; Ribero, Jean-Marc; Staraj, Robert, "Low-profile multimode antenna for vehicular applications," Antennas and Propagation Society International Symposium (APSURSI), 2013 IEEE , pp.2069,2070, 7-13 July 2013

[C13AP4] Trinh, L.H.; Ferrero, F.; Staraj, R.; Ribero, J.-M., "700–960MHz MIMO antenna for picocell applications," Antennas and Propagation Society International Symposium (APSURSI), 2013 IEEE , pp.366,367, 7-13 July 2013

[C13AP5] Cihangir, Aykut; Ferrero, Fabien; Luxey, Cyril; Jacquemod, Gilles; Sonnerat, Florence; Pilard, Romain; Gianesello, Frederic; Gloria, Daniel; Brachat, Patrice, "Combination of two neutralized coupling element antennas for low LTE and GSM mobile phones,"Antennas and Propagation Society International Symposium (APSURSI), 2013 IEEE , pp.2215,2216, 7-13 July 2013

[C13AP6] Bisognin, Aimeric; Luxey, Cyril; Jacquemod, Gilles; Titz, Diane; Ferrero, Fabien; Bisognin, Aimeric; Pilard, Romain; Gianesello, Frederic; Gloria, Daniel; Laporte, Claire; Ezzeddine, Hilal; Brachat, Patrice, "End-fire radiating antenna on IPD technology for 60 GHz communications," Antennas and Propagation Society International Symposium (APSURSI), 2013 IEEE , pp.1830,1831, 7-13 July 2013

[C13LA] Cihangir, Aykut; Ferrero, Fabien; Luxey, Cyril; Jacquemod, Gilles; Larique, Emmanuel; Robin, Renaud; Brachat, Patrice, "Tunable antennas using MEMS switches for LTE mobile terminals," Antennas and Propagation Conference (LAPC), 2013 Loughborough , pp.22,26, 11-12 Nov. 2013.

[C13LA2] Semkin, Vasilii; Kyro, Mikko; Raisanen, Antti V.; Bisognin, Aimeric; Ferrero, Fabien; Luxey, Cyril; Happy, Henri; Thielleux, Julien; Wei, Wei, "Characterization of inkjet patch antenna on different ground planes at millimeter-wave frequencies," Antennas and Propagation Conference (LAPC), 2013 Loughborough , pp.286,288, 11-12 Nov. 2013

[C13AT] L. H. Trinh, F Ferrero, R. Staraj, J-M. Ribero, “Mobile Phone Antenna for 2G, 3G and 4G Standards”, ATC’2013, Ho Chi Minh City, 16-18 October 2013, Vietnam

[C14IW] Aykut Cihangir, Fabien Ferrero, Cyril Luxey,Gilles Jacquemod, Alexandre Reinhardt, Laurent Dussopt, Nicolas Lorphelin, Christophe Pavageau ,Patrice Brachat, "Utilization of Tunable Components for 4G Frequency Reconfigurable Mobile Terminal Antenna", IWAT 2014, Sydney, Australia

[C14EU] Cihangir, Aykut; Ferrero, Fabien; Luxey, Cyril; Jacquemod, Gilles; Reinhardt, Alexandre; Dussopt, Laurent; Lorphelin, Nicolas; Obeid, Nizar; Brachat, Patrice, "Investigation of tunable matching circuits for multiband 4G handsets," Antennas and Propagation (EuCAP), 2014 8th European Conference on , pp.601,604, 6-11 April 2014, The Hague, The Netherlands.

[C14EU2] Bisognin, Aimeric; Titz, Diane; Ferrero, Fabien; Jacquemod, Gilles; Pilard, Romain; Gianesello, Frederic; Gloria, Daniel; Laporte, Claire; Ezzeddine, Hilal; Lugara, Delphine; Luxey, Cyril, "Probe-fed measurement system for F-band antennas," Antennas and Propagation (EuCAP), 2014 8th European Conference on , pp.722,726, 6-11 April 2014, The Hague, The Netherlands.

[C14EU3] Semkin, Vasilii; Jacob, Martin; Kurner, Thomas; Bisognin, Aimeric; Ferrero, Fabien; Luxey, Cyril; Raisanen, Antti V., "Estimation of optimum antenna configurations supported by realistic propagation models at 60 GHz," Antennas and Propagation (EuCAP), 2014 8th European Conference on , pp.3434,3438, 6-11 April 2014, The Hague, The Netherlands.

[C14AP] Cihangir, A; Jacquemod, G.; Luxey, C.; Ferrero, F.; Whittow, W.G.; Panagamuwa, C.J.; Pilard, R.; Gianesello, F., "MIMO antenna concept for 4G electronic eyewear devices," Antennas and Propagation Society International Symposium (APSURSI 2014), Memphis, USA.

[C14AP2] Bisognin, A; Titz, D.; Luxey, C.; Jacquemod, G.; Pilard, R.; Gianesello, F.; Gloria, D.; Ferrero, Fabien; Lugara, Delphine; Costa, Jorge R.; Fernandes, Carlos A, "Comparizon of 3D printed Plastic and micromachined Teflon Lenses for WiGig modules," Antennas and Propagation Society International Symposium (APSURSI), 2014 IEEE , pp.109,110, 6-11 July 2014, Memphis, USA.

[C14AP3] Lizzi, Leonardo; Trinh, Le Huy; Ferrero, Fabien; Pegatoquet, Alain; Ribero, Jean-Marc; Staraj, Robert, "Synthesis of miniature pattern-reconfigurable antennas for smart wireless sensor nodes," Antennas and Propagation Society International Symposium (APSURSI), 2014 IEEE , pp.1443,1444, 6-11 July 2014, Memphis, USA.

[C15EU] Venkatasubramanian, Sathya N.; Li, Linsheng; Icheln, Clemens; Ferrero, Fabien; Luxey, Cyril; Haneda, Katsuyuki, "Impact of neutralization on isolation in co-planar and back-to-back antennas," in Antennas and Propagation (EuCAP), 2015 9th European Conference on , vol., no., pp.1-5, 13-17 April 2015, Lisbon, Portugal

[C15EU2] A. Bisognin Aimeric, F. Ferrero, D. Titz, G. Jacquemod, R. Pilard, F. Gianesello, D. Gloria, C. Laporte and H. Ezzeddine, P. Ratajczak, J.R. Costa, E.B. Lima, C.A. Fernandes, C. Luxey ,"Performance Evaluation of a 120 GHz 3D-Printed Plastic Elliptical Lens Antenna-System", Eucap, April 2015, Lisbon, Portugal

[C15AP] F. Baurreau, R. Staraj, F. Ferrero, L. Lizzi, J. M. Ribero and J. P. Chessel, "Stratospheric platform for telecommunication missions," Antennas and Propagation & USNC/URSI National Radio Science Meeting, 2015 IEEE International Symposium on, Vancouver, BC, 2015, pp. 914-915.

[C15AP2] F. Ferrero and L. Lizzi, "Feasability of an Ultra narrow band antenna for the internet of things," Antennas and Propagation & USNC/URSI National Radio Science Meeting, 2015 IEEE International Symposium on, Vancouver, BC, 2015, pp. 776-777.

[C15AP3] Le Huy Trinh, F. Ferrero, R. Staraj and J. M. Ribero, "Influence of component ESR on a 4G frequency reconfigurable antenna," Antennas and Propagation & USNC/URSI National Radio Science Meeting, 2015 IEEE International Symposium on, Vancouver, BC, 2015, pp. 1136-1137.

[C15AP4] L. Lizzi, Le Huy Trinh, F. Ferrero, J. M. Ribero and R. Staraj, "Transmision line based approach for the synthesis of pattern reconfigurable antennas," Antennas and Propagation & USNC/URSI National Radio Science Meeting, 2015 IEEE International Symposium on, Vancouver, BC, 2015, pp. 2369-2370.

CONGRES NATIONAUX AVEC COMITE DE LECTURE ET ACTES

[C05JN] Ferrero, C. Luxey, G. Jacquemod, R. Staraj, G. Kossiavas & V. Fusco, «Antennes réseaux à déphaseurs actifs», JNM 05, Nantes, 2005

[C07JN] Ferrero, C. Luxey, R. Staraj, G. Jacquemod & V. Fusco, «Coupleur reconfigurable pour antenne à diversité de polarisation», JNM 07, Toulouse, 2007

[C09JN] Ferrero, A. Diallo, C. Luxey, B. Derat, «Système multi-antennes alimenté par déphaseur reconfigurable pour diversité en téléphonie mobile UMTS», Journées Nationales Microondes JNM 09, 27-29 Mai 2009, Grenoble. Présentation orale C. Luxey.

[C09JN2] F. Ferrero, S. Ranvier, C. Luxey, C. Icheln, P. Vainikainen, R. Staraj, G. Jacquemod, «Réseau déphaseur à base de commutateurs MEMS pour antennes millimétriques intégrées agiles en rayonnement» , Journées Nationales Microondes JNM2009, 27-29 Mai 2009, Grenoble.

[C11JN] M. Silva Pimenta, F. Ferrero, J. M. Ribero, R. Staraj, " Antenne à polarisation circulaire pour les standards GPS-Galileo ", Journées Nationales Microondes JNM2011, Mai 2011, Brest.

[C11JN2] Diane Titz, Fahd Ben Abdeljelil, Sébastien Jan, Fabien Ferrero, Cyril Luxey, Patrice Brachat, Gilles Jacquemod" Antennes Intégrées pour des Communications à 60 GHz, Journées Nationales Microondes JNM2011, Mai 2011, Brest.

[C11JN3] Diane Titz, Fabien Ferrero, Romain Debroucke, Romain Pilard, Cyril Luxey, Frédéric Gianesello, Daniel Gloria, Gilles Jacquemod, " Miniaturisation de coupleurs sur Substrat Silicium pour Applications en bande Millimétrique ", Journées Nationales Microondes JNM2011, Mai 2011, Brest.

[C11JN4] F. Canneva, F. Ferrero, J.-M. Ribero, R. Staraj, “ Antenne miniature reconfigurable en fréquence pour les standards DVB-H et GPS”, GDR Ondes, Nice, Oct. 2011.

[C11JN5] Marcio Silva Pimenta, F. Ferrero, P. Ratajzack, P. Brachat, R. Staraj, J. M. Ribero, “ Conducteur Magnétique Artificiel sur substrat textile pour le standard GPS”, GDR Ondes, Nice, Oct. 2011.

[C11JN6] L.H. Trinh, T.Q.V. Hoang, F. Perret, F.Ferrero, “ Conception d'une rectenna à 433 mhz pour réseau de capteurs”, GDR Ondes, Nice, Oct. 2011.

[C13JN] Bisognin Aimeric, Titz Diane, Ferrero Fabien, Luxey Cyril, Jacquemod Gilles, Pilard Romain, Gianesello Fréderic, Gloria Daniel, Brachat Patrice, « Banc de caractérisation d'antennes intégrées alimentées sous pointes pour bandes de fréquences millimétriques », Journées Nationales Microondes JNM2013, Mai 2013, Paris.

[C13JN2] Bisognin Aimeric, Titz Diane, Ferrero Fabien, Luxey Cyril, Jacquemod Gilles, Pilard Romain, Gianesello Fréderic, Gloria Daniel, Laporte Claire, Ezzeddine Hilal, Valente Mario, Brachat Patrice, « Patch en technologie IPD reporté sur substrat organique pour des transferts de données courte portée à 60 GHz », Journées Nationales Microondes JNM2013, Mai 2013, Paris.

[C13JN3] Bisognin Aimeric, Titz Diane, Ferrero Fabien, Luxey, Cyril, Jacquemod Gilles, Pilard Romain, Gianesello, Fréderic, Gloria Daniel, Brachat Patrice, « Nouvelle technique d'alimentation symétrique pour réseaux d'antennes en bandes millimétriques », Journées Nationales Microondes JNM2013, Mai 2013, Paris.

[C13JN4] Bisognin Aimeric, Titz Diane, Ferrero Fabien, Luxey Cyril, Jacquemod Gilles, Pilard Romain, Gianesello Fréderic, Gloria Daniel, Laporte Claire, Ezzeddine Hilal, Brachat Patrice, « Antenne-in-package à rayonnement longitudinal pour standard WiGig », Journées Nationales Microondes JNM2013, Mai 2013, Paris.

[C13JN5] Bisognin Aimeric, Titz Diane, Ferrero Fabien, Luxey, Cyril, Jacquemod Gilles, Pilard Romain, Gianesello Fréderic, Gloria Daniel, Laporte Claire, Ezzeddine, Hilal, Brachat Patrice, « Conception et caractérisation d'antennes à 120 GHz en technologie IPD ™ », Journées Nationales Microondes JNM2013, Mai 2013, Paris.

[C13JN6] Bisognin Aimeric, Titz Diane, Thielleux Julien, Wei Wei, Happy Henri, Ferrero Fabien, Luxey Cyril, Jacquemod Gilles, Brachat Patrice, « Conception et mesure d'une antenne à 60 GHz imprimée par jet d'encre sur un substrat souple PEN », Journées Nationales Microondes JNM2013, Mai 2013, Paris.

[C13JN7] Ferrero Fabien, Diallo Aliou, Luxey Cyril, Derat Benoit, Hamouz Pavel, Hazdra Pavel, Rahola Jussi, « Excitation des modes caractéristiques d'un PCB de téléphone mobile pour diversité de polarisation aux fréquences UMTS », Journées Nationales Microondes JNM2013, Mai 2013, Paris.

[C13JN8] Cihangir Aykut, Ferrero Fabien, Luxey Cyril, Jacquemod Gilles, Brachat Patrice, « Conception d'un nouvel élément antennaire de couplage pour terminaux mobiles LTE/UMTS/GSM », Journées Nationales Microondes JNM2013, Mai 2013, Paris.

[C13JN9] Diane Titz, Ferrero Fabien, Cyril Luxey, Gilles Jacquemod, Romain Pilard, Fréderic Gianesello, Claire Laporte, Hilal Ezzedine, Daniel Gloria, « Matrice de Butler en technologie IPD' pour formation de faisceau à 60 GHz », Journées Nationales Microondes JNM2013, Mai 2013, Paris.

[C13JN10] Lizzi Leonardo, Ferrero Fabien, Ribero Jean-Marc, Staraj Robert, « Antenne multi-bandes multimodes pour applications sur véhicules », Journées Nationales Microondes JNM2013, Mai 2013, Paris.

[C13JN11] Titz Diane, Ferrero Fabien, Luxey Cyril, Jacquemod Gilles, Pilard Romain, Gianesello Fréderic, Gloria Daniel, « Coupleurs hybrides miniatures large bande en technologie BiCMOS pour circuits fonctionnant à 60 GHz », Journées Nationales Microondes JNM2013, Mai 2013, Paris.

[C13JN12] Le Huy Trinh, Emmanuel Le Guen, Fabien Ferrero, R. Staraj, Jean-Marc Ribero, Jean-Luc Mattei, « Miniaturisation d'antenne IFA avec un matériau magnéto-diélectrique pour application LTE 700-GSM dans une picocell », Journées Nationales Microondes JNM2013, Mai 2013, Paris.

[C13JN13] Aykut Cihangir, Florence Sonnerat, Fabien Ferrero, Romain Pilard, Frédéric Gianesello, Daniel Gloria, Cyril Luxey, Gilles Jacquemod, Patrice Brachat, « Antenne en technologie LDS pour terminaux mobiles LTE700 et GSM850/900 », Journées Nationales Microondes JNM2013, Mai 2013, Paris.

CONFERENCE D'ORDRE PEDAGOGIQUE

[C09JN] R. Staraj, S. Ranvier, F. Ferrero, P. Panaia, Ph. Le Thuc, C. Luxey, G. Jacquemod, P. Vainikainen, "Reconfiguration dynamique d'antennes imprimées et composants radiofréquences micro-électromécaniques MEMS RF", 16èmes Journées Nationales Microondes 2009, Journée thématique "De la RF au millimétrique sur Silicium", 26 Mai 2009, Grenoble.

[C09JP] Fabien.Ferrero, Cyril.Luxey, Gregory. Sauder, Philippe. Lorenzini, Gilles. Jacquemod, " Radar doppler hyperfrequences pour détection de vitesse ", JPCNFM, St Malo, Octobre 2009.

[C12JP] Stéphane MEILLÈRE, Fabien FERRERO, Philippe PANNIER, Gilles JACQUEMOD, " Réseaux de Capteurs Intelligents RECAIN / WSN", JPCNFM, St Malo, Novembre 2012.

[C14JP] Miguel Angel García Pérez, Yves Leduc, Fabien Ferrero, " Re-imaginons les travaux pratiques pour la formation ingénieurs en électronique ", JPCNFM, St Malo, Novembre 2014.

JOURNAL D'ORDRE PEDAGOGIQUE

[J15J3] Miguel Ángel García Pérez, Yves Leduc et Fabien Ferrero, "Re-imaginons les travaux pratiques pour la formation des ingénieurs en électronique", 7 août 2015, J3eA, Vol. 14, HORS SÉRIE 2 (2015).

PATENTS

[B09IM] BR36810/EP/GD, F. Ferrero, "Antenne multi-services à bande ultralarge incorporée dans un véhicule", IMRA EUROPE SAS, Mars 2009

[B09IM2] BR37414/EP/GD/TM , F. Ferrero, "Antenne multi-services à bande ultra-large miniature", IMRA EUROPE SAS, Juillet 2009